The University of Sydney

School of Civil Engineering
Sydney NSW 2006
AUSTRALIA

http://www.civil.usyd.edu.au/

Centre for Advanced Structural Engineering

Experimental Study of High Strength Cold-Formed Stiffened Web Steel Sections

Research Report No R889

Derrick C Y Yap BE
Gregory J Hancock BSc BE PhD DEng

January 2008

ISSN 1833-2781

The University of Sydney

School of Civil Engineering
Centre for Advanced Structural Engineering
http://www.civil.usyd.edu.au/

Experimental Study of High Strength Cold-Formed Stiffened Web Steel Sections

Research Report No R889

Derrick C Y Yap, BE
Gregory J Hancock, BSc, BE, PhD, DEng

January 2008

Abstract:

High strength cold-formed steel sections are commonly used in a variety of applications including residential construction. These steel sections typically have a nominal yield stress of 550 MPa and the use of such high strength material allows for a reduction in thicknesses. With this reduction in thickness, the high strength steel can be manufactured into complex shapes including stiffeners. Such complex shapes exhibit structural instabilities such as local, distortional and flexural-torsional buckling modes, and in some cases, interaction of the local and distortional buckling modes may occur.

This paper describes the design and testing of web-stiffened high strength steel cold-formed lipped channel columns. In order to be able to apply the Direct Strength Method in Section 7 of the Australian Standard AS/NZS 4600:2005 to design, the steel sections must be pre-qualified as a compression member. The section chosen is pre-qualified and has nearly coincidental local buckling and distortional buckling loads as well as a flexural-torsional mode which varies with length.

A series of compression tests was carried out in a 300 kN capacity SINTEC testing machine over a range of lengths with fixed ended conditions. The varying lengths were chosen so as to observe the buckling modes and the possibility of interaction between them. The effect of the different type of failure modes is also discussed in this paper. The experimental results are then compared with design methods in the existing design standards. The methods include the Effective Width Method (EWM) and the Direct Strength Method (DSM) as described in the Australian Cold-Formed Steel Structures Standard AS/NZS 4600. It is shown that the existing standards are unconservative and new proposals for dealing with this are made.

Keywords:

Cold-formed; high strength steel; local buckling; distortional buckling; interaction buckling; postbuckling behaviour; intermediately stiffened section

Copyright Notice

School of Civil Engineering, Research Report R889

Experimental Study of High Strength Cold-Formed Stiffened Web Steel Sections

Email: D.Yap@usyd.edu.au
hancock@eng.usyd.edu.au

ISSN 1833-2781

Published by:
School of Civil Engineering
The University of Sydney
Sydney NSW 2006
AUSTRALIA

January 2008

This report and other Research Reports published by The School of Civil Engineering are available on the Internet:

http://www.civil.usyd.edu.au

TABLE OF CONTENTS

1 INTRODUCTION

High strength cold-formed steel sections are commonly used in a variety of applications including residential construction. These steel sections typically have a nominal yield stress of 550 MPa and the use of such high strength material allows for a reduction in thicknesses. With this reduction in thickness, the high strength steel can be manufactured into complex shapes including stiffeners. Such complex shapes exhibit structural instabilities such as local, distortional and flexural-torsional buckling modes, and in some cases, interaction of the local and distortional buckling modes may occur.

The short half-wavelength local buckling mode has been well researched over the years and it is known that a locally buckled element has significant postbuckling reserve strength, while the long half-wavelength flexural-torsional buckling mode has been shown to have little postbuckling reserve strength. The intermediate half-wavelength distortional buckling mode has been researched and its postbuckling behaviour is somewhat in between the other two modes. The distortional buckling mode has postbuckling reserve strength, but is generally less than that of the local buckling. In a previous research carried out by Yap and Hancock (2006a), the stress distribution in a simple lipped channel column was analysed for a section undergoing distortional buckling in the postbuckling range. In that analysis, the effect of the interaction of local and distortional buckling in the postbuckling range was presented. It was shown that for thin sections, where the thickness is approximately 1 mm and the critical local and distortional buckling loads are approximately similar, the interaction of local and distortional buckling modes in the postbuckling range caused the stresses at the flange-web junction to increase, causing a premature failure of the column.

The main objective in this report is to further extend this understanding of the stress distributions to a section that would demonstrate the effects of the interaction of local and distortional buckling modes. This report describes the design and testing of high strength cold-formed stiffened-web lipped channel columns. In order to be able to apply the Direct Strength Method in Section 7 of the Australian Standard AS/NZS 4600:2005 to design, the steel sections must be pre-qualified as a compression member. The tests are compared to design rules in the 2005 Australian Standard and the 2001 North American Specifications (AISI 2001) and its 2004 supplement (AISI 2004), which includes the Direct Strength Method. Proposals to the interaction of local and distortional buckling are presented.

2 PREVIOUS TESTS ON THIN-WALLED HIGH STRENGTH STEEL SECTION

Tests were conducted by Yang and Hancock (2004) on intermediate stiffened lipped channels, brake-pressed from high strength aluminium/zinc-coated Grade G550 structural steel to Australia Standard AS 1397 (1993) with thickness 0.42 mm and a nominal yield stress of 550 MPa. The length of the columns ranged from 360 mm to 2000 mm. The tests showed the interaction of local and distortional buckling modes for very thin sections. They noted that at intermediate column lengths, the interaction of local and distortional modes induced a premature failure of the intermediately stiffened channel columns. Failure occurred at loads lower than the predicted distortional buckling strength, which was itself

lower than the local buckling strength. Yap and Hancock (2006b) studied the interaction of local and distortional buckling modes for an innovative stiffened cross-shaped open section column. The length of the columns ranged from 110 mm to 2000 mm. The 110 mm specimens were used to compare the Direct Strength Method for local buckling and the predicted results were found to be unconservative. The remaining specimens were used to analyse two different types of distortional buckling modes, namely the short half-wavelength and the long half-wavelength distortional buckling modes. The test results for the intermediate and long specimens were found to be unconservative when compared to both the Effective Width Method and the Direct Strength Method for distortional buckling. This is because the interaction of buckling modes is not accounted for by these design codes. However it is relatively difficult to understand how the interaction caused the unconservative results as the design of the section was too complicated.

Hence the aim of the experiments in this report is to design a simpler and new stiffened-web open section column and to test and observe any possible interaction of buckling modes. The main objective here is to understand the interactions observed by Yang and Hancock (2004) and Yap and Hancock (2006b) in a simpler designed section, and to verify and enhance the proposed design equations.

A thicker section (1.0 mm) has been chosen than used in the earlier tests.

3 TEST SPECIMEN

3.1 Design of Open-Section Shape Column

Tests conducted by Yap and Hancock (2006b) on stiffened cross-shape section columns, brake-pressed from high strength aluminium/zinc-coated Grade G550 structural steel to Australia Standard AS 1397 (1993) with thickness 0.42 mm and a nominal yield stress of 550 MPa, showed the interaction of local and distortional buckling modes occurring in very thin sections. This interaction of buckling modes resulted in unconservative results when compared to the Australian Standard AS/NZS 4600:2005.

To further investigate the interaction of local and distortional buckling modes, a new open-section shape column was designed. The new stiffened web section, as shown in Fig. 1, was based on the design limits of the lipped channel with web stiffener as listed in Table 7.1.1 of AS/NZS 4600:2005 for pre-qualified compress members. Two different finite strip methods were used to analyse the buckling half-wavelengths and corresponding buckling stresses of the new stiffened web section. These methods are the semi-analytical finite strip method (SAFSM) (Cheung, 1976), which assumes simply supported ends and the spline finite strip method (SFSM) (Lau and Hancock, 1986), which assumes fixed-end conditions. Finite strip buckling analysis softwares (THINWALL) (Papangelis and Hancock, 1995) and BFPLATE (Lau and Hancock, 1986) were used to analyse the open-section shape column.

3.1.1 Semi-Analytical Finite Strip Method (SAFSM)

The semi-analytical finite strip method of buckling analysis of thin-walled sections (Cheung, 1976) is a very efficient tool for investigating the buckling behaviour of cold-formed members in compression and bending. SAFSM assumes thin-walled sections buckle with simple supported ends free to warp but with section distortion prevented at the ends. The buckling stress for each buckling mode is plotted against the buckle half-wavelength and is shown as the solid line in Fig 2.

It can be observed that local buckling (L(1)) occurred at very short buckle half-wavelengths of approximately 60 mm with an elastic buckling stress of approximately 210.8 MPa. It can be noted that local buckling occurs in all wide plate elements. The distortional buckling mode (D(1)) occurred at an intermediate buckle half-wavelength of approximately 700 mm with an elastic buckling stress of approximately 130.4 MPa, and it can be noted that the distortional buckling mode has rotations about the flange-web junctions. A Young's Modulus value of 200 MPa has been used for these analyses. The elastic local and distortional buckling stresses are summarised in Table 1a.

3.1.2 Spline Finite Strip Method (SFSM)

The spline finite strip method (Lau and Hancock, 1986) of buckling analysis, defined by the circle and dashed line in Fig. 2, assumes fixed-ended boundary conditions. This method is more powerful than the SAFSM as it is able to account for different boundary conditions other than simply supported (Cheung, 1976). The SAFSM analysis gives the elastic local and distortional buckling stresses at a given half-wavelength, whereas the SFSM determines the buckling mode and stress at a given length between two fixed ends. The section was constructed with 29 nodal strips and 30 spline sections longitudinally. At long half-wavelengths of 5000 mm, the section displayed only flexural-torsional buckling modes (FT(1)).

Local buckling from the SFSM analysis occurs at column lengths 60 mm to 800 mm and is associated with increasing numbers of local buckle half-waves. It has a similar buckle half-wavelength (60 mm) and buckling stress (213.8 MPa) as the SAFSM analysis. However, at a column length of 700 mm, local and distortional buckling modes appeared simultaneously. The corresponding buckling stress (208.4 MPa) is much higher than the distortional buckling minima (130.4 MPa) of the SAFSM analysis due to the effect of end conditions. With the effect of fixed ends, the local and distortional buckling modes have relatively similar buckling stresses along a column length up to approximately 1000 mm. Therefore interaction of local and distortional buckling modes may occur at intermediate lengths since both buckling modes have similar buckling stresses for the fixed-ended sections.

The elastic buckling stress and corresponding buckling mode for the chosen specimen lengths are summarised in Table 1b. The buckling stresses and modes for Eigenmodes 2 and 3 are also given in Table 1b. It can be seen that the higher modes generally consist of increasing number of local buckles at slightly higher stresses, although at longer lengths, the distortional mode with one half-wavelength occurs before the local buckles.

3.2 Length of Column

The objective of the test program was to investigate the interaction of local and distortional buckling modes. Analysis of the section was performed to determine the distortional buckling stresses and buckle half-wavelengths using the above-mentioned methods, SAFSM and SFSM. A short column length of 350 mm was chosen to test the section undergoing local buckling only. A series of intermediate lengths were chosen to investigate distortional buckling. The chosen lengths were 700, 1000, 1300 and 2000 mm. The length of 2000 mm was chosen to be the longest as it was at the maximum range of the test machine.

3.3 Material Properties

The steel sheets were produced using a process called cold reduction, whereby the material's strength and hardness is increased. This method also allows the material's thickness to be formed accurately. Initially the sheet steels are rolled to size in a hot strip mill with finishing and coiling temperatures of 940 °C and 670 °C respectively. The hot worked coil of steel, typically 2.5 mm thickness with a minimum specified 300 MPa yield stress, is uncoiled and cleaned in an acid solution to remove surface oxides and scale. The uncoiled steel is then trimmed to size and fed into a cold reduction mill, which may contain up to six sets of stands. High compressive force in the stands and strip tension systematically reduce the thickness of the steel sheet until the desired dimension is reached.

The milling process causes the grain structure of cold reduced steels to elongate in the rolling direction, whereby there is an increase in material strength and a decrease in material ductility. The effects of cold working are cumulative, i.e. grain distortion increases with further cold working, however it is possible to change the distorted grain structure and control the steel properties through heat treatment. Various types of heat treatment exist and are used for different steel products. G550 sheet steels are stress relief annealed, whereby recrystallisation does not occur. Stress relief annealing involves heating the steel to below the recrystallisation temperature, holding the temperature until the temperature is constant throughout the thickness and then cooling slowly.

Mild sheet steels of similar thicknesses are annealed to a greater extent in comparison with G550 sheet steels, and hence recover their ductile behaviour. Annealing is carried out in the hot dip coating line prior to application of either zinc or aluminium/zinc coating. Upon cooling the sheet steel may be further processed through a tension levelling mill, e.g. 0.35% extension, to improve the finish quality and flatness of the coil (BHP, 1992). The G550 sheet steels must be differentiated from other sheet steels whose high yield stress and ultimate strength values are obtained by means of an alloying process, i.e. high strength low alloy (HSLA) steels.

The material property requirements for G550 or Grade E sheet steels are specified in Australia by AS 1397 (1993) and in North America by the following ASTM standards, A653 (2000), A792 (1999), A875 (1999) and A1039 (2004).

3.3.1 Material Thickness

The thickness of the steel sheet has to be accurately measured in order to determine the buckling stress of the section. A layer of corrosion protection coating was applied to the steel sheet during the manufacturing process. Since the thickness of the steel sheet is very thin, this coating may allow the steel to carry more load, hence the base metal thickness of the virgin material had to be determined.

The coating was removed to expose the virgin (base) material by acid etching. The base metal thickness was measured using a micrometer. The average thickness for the steel sheet is 1.065 mm as shown in Table 2.

3.3.2 Tensile Coupons and Testing Results

Tensile coupons are used to determine the material properties. The coupon dimensions conformed to the Australian Standard AS 1391 (1991) for the tensile testing of metals using 12.5 mm wide coupons with gauge length 50 mm. Rogers and Hancock (1996) noted that a larger radius (55 mm) was required to have a gradual change of cross section from the constant gauge width to the grip in order for the coupon to fail in the middle portion of the constant gauge width. Five tensile coupons were tested whereby strain gauges were used for three of the coupons (1A, 2A and 3A) and an extensometer was used for the other two coupons (1B and 2B).

The tests were carried out using the Sintech/MTS-300 kN testing machine. The coupons were secured in a pair of vice-grips and an extensometer was used to record the elongation. The yield stress F_y was obtained as the 0.2 % nominal proof stress as no distinct yield point occurred. The stress was the load measured divided by the initial cross-sectional area of the coupon. The measured 0.2 % proof stress is shown in Table 2 and ranged from 628.5 MPa to 639.5 MPa. The calculated mean value of F_y is approximately 634 MPa. This yield stress is higher than the "pre-qualified" value of 593 MPa as shown in Table 7.1.1 of AS/NZS 4600:2005.

The Young's modulus of elasticity (E) was also calculated from the stress-strain curves. The calculated mean value of the Young's modulus of elasticity was 216.9 GPa and is also shown in Table 2.

3.4 Labelling

The test specimens were labelled such that the end conditions, type of test, nominal length of specimen and specimen number were expressed by the label.

For example, the label "SWC350_1" defines the following specimen:

- "SWC" indicates that the section is a stiffened-web channel
- "350" indicates the nominal length of the column was 350 mm

- "_1" indicates the specimen number at a specific length (alternatively "_2" and "_3")

3.5 Geometric Imperfection Measurements

Geometric imperfections were measured for all of the test specimens with lasers attached to a guide to measure the readings along the specimen length. The main components included consisted of a guide frame, two laser sensors, a Datataker data logger and a synchronous motor. The lasers were attached to individual movable seats, so that they could be adjusted onto the flanges' and web's centreline. The seats were drawn by a synchronous motor in order to keep the sensor moving smoothly and at a constant rate.

Each specimen was positioned horizontally across the lasers and was clamped to ensure stability during the testing. The readings were recorded at a rate of 0.5 mm/sec along the specimen length and the maximum imperfections are shown in Table 3. The lasers were positioned around the specimen and the flanges and webs were recorded in a counter-clockwise manner from the top edge-stiffened flange to the bottom edge-stiffened flange as L1 to L4 as shown in Fig. 3. Only the maximum deflections along the specimen length are shown. The positive and negative signs indicate outwards and inwards deflections respectively. In addition to the laser measurements, the flanges and the lips were also measured and the detailed results are provided in Appendix A.

4 COLUMN TESTS

4.1 General

A total of fourteen specimens were tested with various column lengths of 350 mm, 700 mm, 1000 mm, 1300 mm and 2000 mm. The test rig consisted of a 300 kN capacity MTS SINTECH 65/G displacement controlled testing machine with fixed-ended bearings was used for the column tests. The bottom bearing was adjustable so that it could orientate the specimens vertically with the ends flat on the plates before the bearing was secured for testing. Specially designed end plates were filled with Pattern-stone to ensure a fixed end boundary condition. The plates also ensured uniform compression and prevented the top and bottom edges from localized failure (Yap and Hancock, 2006b). Load and axial shortening were recorded using the SINTECH data acquisition system at a compressive deformation rate of 0.1 mm/min.

Lateral deflections were measured using three LVDT transducers positioned at fixed locations around the specimen and located at both edge-stiffened flanges and on the web elements at the rear flange. This was carried out at fixed locations along the length of each specimen at the quarter, mid and three-quarter height positions. A transducer was positioned to measure the axial defection (stroke) of the crosshead to minimise errors with the elasticity of the testing machine. The transducers were measured by connecting to a Vishay System 5000 data acquisition system.

4.2 Discussion and Analysis of Results

The results of the compression tests for the stiffened-cross sections are shown in Table 4 and all but one specimen (SWC2000_3) was performed. The LVDT measurements for all the tests have been detailed in Appendix B. The combined results for all test specimens are shown in Figs. 4a and 4b to allow for comparison.

For the test specimens of column lengths 350 mm, the failure modes were observed to be purely local buckling and with failure occurring in all flanges as shown in Fig. 5. The average failure load is approximately 89.76 kN.

For specimens with column length 700 mm, all specimens failed in the distortional buckling mode with an average failure load of 71.41 kN. Simultaneous elastic local buckling and distortional buckling was observed along the flanges for an inward lip deflection with the column under compressive load is as shown in Fig. 6a. Fig. 6b shows the failure mode for a 700 mm specimen with outward lip deflection.

Specimens SWC700_1 and SWC700_3 failed with both flanges deflecting outwards (O-O) with failure occurring in the flange-web junctions. In can also be seen from Table 3 that the maximum imperfection values at the flanges (L1 and L4) were positive, indicating an outward deflection. For both these specimens, the lips on the flanges were observed to have inelastically locally buckled prior to the failure in the flange-web junctions.

Specimen SWC700_2 failed with both flanges deflecting inwards (I-I) with failure occurring across the flanges. The maximum imperfection values of L1 and L4 from Table 3 were negative, indicating an inward deflection. It can be noted that the specimens that failed with flanges deflecting outwards have higher failure loads (75.6 kN, 73.46 kN) compared to the specimen that failed with the flanges deflecting inwards (65.18 kN), which is most likely due to the difference in failure modes and stress redistribution (Yap and Hancock 2006a).

For specimens with column length 1000 mm, all specimens failed in the distortional buckling mode with an average failure load of 58.75 kN. Elastic local buckles were seen to occur along the length of the inwards deflecting flanges as shown in Fig. 7a. All specimens failed with both flanges deflecting inwards (I-I) with failure occurring across the flanges as shown in Fig. 7b. The maximum imperfection values of L1 and L4 from Table 3 for all 3 specimens were negative, indicating an inward lip deflection.

For specimens with column length 1300 mm, all specimens failed in the distortional buckling mode with an average failure load of 56.47 kN. The specimens displayed 2 buckle half-waves along the specimen length when the column was subjected to compressive loads as shown in Fig. 8a. Specimen SWC1300_1 failed with one flange deflecting inwards, while the other flange remained straight as it only deflected inward elastically. Specimens SWC1300_2 and SWC1300_3 failed with both flanges deflecting inwards (I-I) with failure occurring across the flanges as shown in Fig. 8b. Elastic local buckles were seen to occur along the length of the inwards deflecting flanges as previously described. The maximum imperfection values of L1 and L4 from Table 3 for all 3 specimens were negative, indicating an inward lip deflection.

For specimens with column length 2000 mm, all specimens failed in the distortional buckling mode with an average failure load of 47.68 kN. The specimens displayed 3 buckle half-

waves along the specimen length when the column is subjected to compressive loads as shown in Fig. 9a. Both specimens failed with both flanges deflecting inwards (I-I) with failure occurring across the flanges as shown in Fig. 9b. Elastic local buckles were seen to occur along the length of the inwards deflecting flanges as previously described. The maximum imperfection values of L1 and L4 from Table 3 for both specimens were negative, indicating an inward deflection. SWC2000_2 had larger maximum imperfections compared to SWC2000_1, hence failed with a lower failure load.

4.2.1 Effect of Inward and Outward Deflection Cases on Section Strength

Specimens with column length 700 mm had two failure modes where the flanges deflected outward (O-O) and one failure mode with inwards (I-I) deflections of the flanges. Fig. 10 shows the inward and outward lip deflection of specimens SWC700_1 and SWC700_2 plotted against load. The failure loads of the specimens with the outward (O-O) deflection (75.6 kN, 73.46 kN) were approximately 14.3% higher than the specimen with the inwards (I-I) deflection (65.18 kN). This effect of inwards and outward deflection on section strength is consistent with the analysis carried out by Yap and Hancock (2006a) where the failure load for the outward deflection mode of a thin section was higher than the inward deflection mode, as more stress was distributed to the flange-web junction of the inward deflection. This effect is also consistent with the previous tests on the complex cross-shaped section carried out by Yap and Hancock (2006b).

5 DESIGN METHODS COMPARED WITH TEST RESULTS

5.1 General

Two design methods can be used to predict the member compression capacity: the Effective Width Method (EWM) and the Direct Strength Method (DSM). The EWM accounts for postbuckling of plate elements by using the effective width at the design stress (von Karman et al. 1932). However as sections are designed with more complex shapes, the calculation of effective widths becomes more complicated and may be less accurate. The DSM was developed by Schafer and Pekoz (1998) to overcome this problem by using elastic buckling stress for a whole section rather than individual plate elements. Both methods were used to predict the nominal member capacity of this open-section column and the strength curves are compared in this report.

The test results are plotted against the effective length of the column and are compared to the design strength curves as detailed below. The effective lengths are taken as one half the test lengths due to the fully fixed ends.

5.2 Nominal Member Capacity N_c to Clause 3.4 (AS/NZS 4600:2005)

5.2.1 Local and Overall Buckling N_c (Clause 3.4.1)

The nominal member capacity N_c (Effective Width Method (EWM)) is based on Eq. 3.4.1 (2) of AS/NZS 4600:2005 and uses the effective width formula and conventional column design curve. It allows for interaction of local and overall buckling only. It is represented by (—△—) line in Fig. 11. It intersects the vertical axis at an effective length of zero at a section capacity, N_s, which is shown by a solid line (——) in Fig. 11.

The section capacity N_s was obtained using the EWM and was approximately 94.54 kN, which was slightly higher than the average ultimate test strength of 89.76 kN for the specimens with column length 350 mm. The strength curves and test results have been plotted against an effective length, l_e, which is half of the column length to allow for the fixed ends. From Fig. 11, the test results showed that the average ultimate test strengths for all longer length specimens were much lower than the predicted member capacity. The reason for the unconservative results at longer lengths is believed to be distortional buckling as well as the interaction of local and distortional buckling.

5.2.2 Distortional Buckling N_{cd} (Clause 3.4.6)

Two values are shown for this strength curve, which is based on the Cl 3.4.6 of AS/NZS 4600:2005. The equations are shown below.

N_{cd} (Clause 3.4.6):

$$\text{For } f_{od} > \frac{f_y}{2}, \qquad N_{cd} = Af_y\left(1-\frac{f_y}{4f_{od}}\right) \tag{1}$$

$$\text{For } \frac{f_y}{13} \le f_{od} \le \frac{f_y}{2}, \qquad N_{cd} = Af_y\left[0.055\left(\sqrt{\frac{f_y}{f_{od}}}-3.6\right)^2+0.237\right] \tag{2}$$

These are the distortional buckling strength curves, where the elastic distortional buckling stresses (f_{od}) are based on the SAFSM and SFSM values as seen in Table 1a and 1b. They are shown by (—○—) and (—☆—) lines respectively in Fig. 11 and form a cutoff at lower slenderness for N_c (Clause 3.4.1). The values of N_{cd} based on elastic distortional buckling stresses of SAFSM and SFSM are as shown in Table 4.

Design based on the AS/NZS 4600:2005 Clause 3.4 methodology with distortional buckling stress based on the SAFSM value, the strength curve predicts conservatively for specimens with column length 700 mm, but is unconservative for specimens with column lengths 1000 mm, 1300 mm and 2000 mm by approximately 4.6 %, 8.3 % and 22.6 % respectively.

If the elastic distortional buckling stress (f_{od}) used in these calculations are based on the SFSM value, then the strength curve is unconservative for specimens with column lengths 700 mm, 1000 mm, 1300 mm and 2000 mm by approximately 6.4 %, 23.0 %, 26.0 % and 32.2 % respectively. Clearly, the AS/NZS 4600:2005 Clause 3.4 does not appear to adequately predict the interaction of local and distortional buckling.

5.3 Nominal Member Capacity N_c to Clause 7 (Direct Strength Method)

5.3.1 Local and Overall Buckling N_{cl} (DSM)

The equation to predict N_{cl} (DSM) is based on Cl 7.2.1.3 of AS/NZS 4600:2005. It requires N_{ce} (DSM), which is based on Cl 7.2.1.2 of AS/NZS 4600:2005. The equations are as shown below.

N_{ce} (DSM):

$$\text{For } \lambda_c \le 1.5, \qquad N_{ce} = \left(0.658^{\lambda_c^2}\right) N_y \tag{3}$$

$$\text{For } \lambda_c > 1.5, \qquad N_{ce} = \left(\frac{0.877}{\lambda_c^{\,2}}\right) N_y \tag{4}$$

where,

λ_c = non - dimensional slenderness used to determine N_{ce}

$= \sqrt{N_y / N_{oc}}$

N_{oc} = least of the elastic compression member buckling load in flexural, torsional and flexural - torsional buckling

$= \mathrm{A} f_{oc}$

N_y = nominal yield capacity of the member in compression

$= A f_y$

Nominal axial capacity for local buckling (N_{cl}):

$$\text{For } \lambda_l \le 0.776, \qquad N_{cl} = N_{ce} \tag{5}$$

$$\text{For } \lambda_l > 0.776, \qquad N_{cl} = \left[1 - 0.15\left(\frac{N_{ol}}{N_{ce}}\right)^{0.4}\right]\left(\frac{N_{ol}}{N_{ce}}\right)^{0.4} N_{ce} \tag{6}$$

where,

λ_l = non - dimensional slenderness used to determine N_{cl}

$= \sqrt{N_{ce} / N_{ol}}$

N_{ol} = elastic member local buckling load in compression

$= Af_{ol}$

This curve is shown by the diamond line (—◇—) in Fig. 12 and is higher than N_c (Clause 3.4.1) as a result of the fact that N_s, on which N_c (Clause 3.4.1) is based, includes some distortional buckling of the edge stiffened elements in Cl 2.4 with a consequent reduction in the *k* value (Table 2.4.2) of AS/NZS 4600:2005 and the fact that inelastic local failure occurred on all elements of the specimen, which does not appear to be adequately accounted for by Equation 6 with a 0.4 exponent in place of the 0.5 exponent in the Winter formula used in the EWM. The average value of the test results for specimens with column length 350 mm was observed to be approximately 13 % lower than the predicted value of the strength curve.

5.3.2 Distortional Buckling N_{cd} (DSM)

The equations to predict N_{cd} (DSM) are as shown:

For $\lambda_d \le 0.561$, $$N_{cd} = N_y \quad (7)$$

For $\lambda_d > 0.561$, $$N_{cd} = \left[1 - 0.25\left(\frac{N_{od}}{N_y}\right)^{0.6}\right]\left(\frac{N_{od}}{N_y}\right)^{0.6} N_y \quad (8)$$

where,

λ_d = non - dimensional slenderness used to determine N_{cd}

$= \sqrt{N_y / N_{od}}$

N_{od} = elastic distortional compression member buckling load

$= Af_{od}$

Two values are shown for this strength, which is based on Cl 7.2.1.4 of AS/NZS 4600:2005. These are for distortional buckling strength curves, where the elastic distortional buckling stresses (f_{od}) are based on the SAFSM and SFSM values as seen in Table 1a and 1b. They are shown by dashed-line (- - -) and dash-dot line (- · - ·) lines respectively in Fig. 12 and form a cutoff at low slenderness for N_{cl} (DSM). The values of N_{cd} based on elastic distortional buckling stresses of SAFSM and SFSM are as shown in Table 4.

The distortional strength curve based on the SAFSM value was conservative for specimens with column length 700 mm at approximately 62.6 kN. However the distortional strength curve was unconservative having higher values of approximately 6.1 %, 9.8 % and 23.8 % for specimens with column lengths 1000 mm, 1300 mm and 2000 mm respectively. This was most likely due to the interaction of local and distortional buckling modes not being accounted for by AS/NZS 4600:2005.

If the elastic distortional buckling stresses (f_{od}) used in these calculations are based on the SFSM values as seen in Table 1b for distortional buckling, then the strength curve is raised

higher to approximately 80.0 kN. This means that the 700 mm results are now also unconservative, together with the specimens with column lengths 1000 mm, 1300 mm and 2000 mm by approximately 10.8 %, 26.6 %, 29.4 % and 38.5 % respectively. As with the EWM, it is clear that the DSM does not adequately account for local and distortional buckling interaction.

6 COMPARISON OF TEST RESULTS TO NON-DIMENSIONALISED STRENGTH CURVES

When test results are plotted against effective lengths as shown in Figs. 11 and 12, the results indicate how the specimens prematurely fail when compared to the strength curves for a particular section design. In order to further understand the effect of the interaction of buckling modes, the test results have to be plotted in non-dimensional format cumulatively against the existing strength curves also in non-dimensional format.

The test results of both the stiffened web column (SWC) and the stiffened cross-shaped column (SCR) specimens (Yap and Hancock 2006b) that failed in the local buckling mode have been non-dimensionalised by dividing the ultimate failure load (N_{test}) with the overall buckling strength (N_{ce}) and plotted against the non-dimensional local slenderness $\lambda_l = \sqrt{N_{ce}/N_{ol}}$ defined in the DSM. Test conducted by Yang and Hancock (2004) on a web and flange stiffened open section column that failed in the local buckling mode are also non-dimensionalised and plotted against the non-dimensional local slenderness λ_l. The non-dimensionalised SWC, SCR and Yang and Hancock test results are plotted as the square (□), triangle (Δ) and diamond (◊) points respectively, as shown in Fig. 13. The average non-dimensionalised SWC, SCR and Yang and Hancock test results are approximately 0.51, 0.44 and 0.38 respectively, as summarised in Table 5. The test results are compared against the non-dimensional slenderness of the local DSM strength curve, as shown in Fig. 13 as the solid line with cross (x) points. The non-dimensional slenderness of the local DSM strength curve was calculated based on the SFSM values of the elastic local buckling stresses for all the test specimens. The local DSM strength curve is generally unconservative and predicts higher values by approximately 12.6 %, 13.7 % when compared to the SWC and SCR test results respectively and predicts accurately when compared to the Yang and Hancock test results, as shown in Table 5. The reasons for this were discussed earlier in Section 5.3.1 and relate to the exponent of 0.4 in the DSM local strength curve.

The test results of both the SWC and SCR specimens that failed in the distortional buckling mode have been non-dimensionalised by dividing the ultimate failure load (N_{test}) with the yield load (N_y) and plotted against the non-dimensional distortional slenderness $\lambda_d = \sqrt{N_y/N_{od}}$ defined in the DSM. The non-dimensionalised SWC and SCR test results are plotted as the square (□) and triangle (Δ) points respectively, as shown in Fig. 14. Tests conducted by Yang and Hancock that failed in the distortional buckling mode are also non-dimensionalised and are plotted as diamond (◊) points as shown in Fig. 14. Tests conducted by Kwon and Hancock (1992) on a section shape similar to the SWC specimens and failing in the distortional buckling mode are also non-dimensionalised and are plotted as asterisks (✳) points as also shown in Fig. 14. The average non-dimensionalised test results are summarised in Table 6. The test results are compared against the non-dimensional slenderness of the

distortional DSM strength curve, as shown in Fig. 14 as the solid line with starred (☆) points. The non-dimensional slenderness of the distortional DSM strength curve was calculated based on the SFSM values of the elastic distortional buckling stresses for all the test specimens.

The SWC, SCR and Yang and Hancock (2004) test results, when plotted against the non-dimensionalised slenderness, can be seen to be decreasing over a very narrow slenderness range. This is due to the elastic local and distortional buckling stresses being relatively similar for a range of lengths of the test shape. There was a spread in the Kwon and Hancock (1992) results across a range of non-dimensional distortional slenderness because of the change in the lip sizes, allowing for an increase in the elastic buckling stresses. This spread of results allowed the calibration of the original distortional DSM strength curve in design standards.

For the specimens failing in the distortional mode, the average non-dimensionalised SWC test results are predicted unconservatively by the distortional DSM strength curve with higher values of approximately between 10.7 % and 29 %. The average SCR test results are also predicted unconservatively by the distortional DSM strength curve with higher values of approximately between 1.8 % and 23.9 %. The Yang and Hancock average test results are predicted unconservatively by the distortional DSM strength curve with higher values of approximately between 7.4 % and 21.7 %. The Kwon and Hancock average test results are predicted by the distortional DSM strength curve to have values that were both conservative and unconservative. The predicted values ranged from approximately 18.9 % below the test results to 10.1 % higher than the test results. This was a consequence of the test results spread across a range of non-dimensional distortional slenderness as previously mentioned. The results are summarised in Table 6. Since most of the chosen test specimens failed with the interaction of local and distortional buckling modes, therefore it can be seen that the distortional DSM strength curve is inadequate to account for specimens that exhibit such interaction of local and distortional buckling modes.

7 PROPOSED DESIGN METHODS TO DIRECT STRENGTH METHOD

7.1 General

As described previously for local and overall buckling N_{cl} (DSM), the Direct Strength Method does not predict the member capacity accurately when the column fails by local buckling only. The design method was unconservative when a column fails in all flange elements. A proposed method is required to account for the local strength curve. At longer length specimens, the design method was significantly unconservative as it does not account for the interactions of local and distortional buckling modes. Three new design methods are proposed to account for the interaction buckling.

7.2 Proposed Method for Local/Overall Buckling

When the Direct Strength Method was used to predict the local strength curve, it predicted unconservatively when compared to the test results. This unconservative prediction is most likely due to the fact that inelastic local failure occurred on all elements of the specimen, which is not adequately accounted for by Equation 6. Equation 6 has an exponential of 0.4, which is lower than the 0.5 in the Winter formula for a single element, and most likely assumes that all elements of the section do not fail at the same time. If this is the case, the exponential in Equation 6 should be 0.5 to match the Winter formula.

The proposed nominal axial capacity for local buckling ($N_{cl0.5}$):

$$\text{For } \lambda_{l0.5} \le 0.673, \qquad N_{cl0.5} = N_{ce} \tag{9}$$

$$\text{For } \lambda_{l0.5} > 0.673, \qquad N_{cl0.5} = \left[1 - 0.22\left(\frac{N_{ol}}{N_{ce}}\right)^{0.5}\right]\left(\frac{N_{ol}}{N_{ce}}\right)^{0.5} N_{ce} \tag{10}$$

where,

$\lambda_{l0.5}$ = non-dimensional slenderness used to determine $N_{cl0.5}$

$= \sqrt{N_{ce}/N_{ol}}$

N_{ol} = elastic member local buckling load in compression

$= Af_{ol}$

The proposed nominal axial capacity for local buckling, $N_{cl0.5}$, for the stiffened web channel column (SWC) is shown as the starred line (—✲—) in Fig. 15 and is approximately 89.4 kN at column length 350 mm. The average failure load for the specimens failing in the local buckling mode is approximately 89.8 kN. This proposed method is shown to predict the specimens failing in the local buckling mode relatively accurately. The elastic local buckling stress used was based on the SAFSM value in Table 1a.

When the SWC test results were non-dimensionalised by dividing the results by the overall buckling strength (N_{ce}) and plotted against the proposed local/overall buckling strength curve as the square (□) points shown in Fig 16, the proposed strength curve predicts the average SWC results conservatively with a lower value by approximately 0.9 %, as shown in Table 7.

When the SCR test results were non-dimensionalised by dividing the results by the overall buckling strength (N_{ce}) and plotted against the proposed local/overall buckling strength curve as the triangle (Δ) points shown in Fig 16, the proposed strength curve predicts the average SCR results slightly conservatively with a lower value by approximately 2.4 %, as shown in Table 7.

The Yang and Hancock test results for specimens failing in the local buckling mode are non-dimensionalised and plotted against the proposed local/overall buckling strength curve as the diamond (◇) points shown in Fig 16. The proposed strength curve predicts the average Yang and Hancock results very conservatively with a lower value by approximately 25.0 %, as shown in Table 7. This is most likely due to the specimens not failing in all flange elements but at the lips (Yang and Hancock 2004).

The average ratio of test results to design for this proposed strength curve is 1.094, as shown in Table 7, compared to 0.911, as shown in Table 5, of the original DSM local strength curve. This indicates that the proposed strength curve is conservative however the scatter is slightly wider, 0.135 compared to 0.074. Therefore when compared to both test programs and Yang and Hancock results, the proposed local/overall buckling strength curve is shown to be relatively accurate in predicting the axial capacity of compression members when the section fails in all flange elements.

7.3 Proposed Method for Distortional Buckling

The new proposed design methods for the distortional DSM strength curve are in conjunction with the proposed design methods discussed in Yap and Hancock (2006b). Yap and Hancock (2006b) presented three design methods for a stiffened cross-shape (SCR) section with multiple distortional buckling modes, with proposed design Method 1 accounting for multiple distortional buckling modes. Since the SWC section does not have multiple distortional buckling modes, Method 1 is not described here.

7.3.1 Method 2 – Distortional Buckling Interacting with Overall Buckling

It should be noted that the N_{cd} in Cl 7.2.1.4 of AS/NZS 4600:2005 assumes no interaction of distortional and overall buckling. To observe interaction of the distortional and overall buckling modes, N_y in Equations 7 and 8 is replaced with the overall buckling strength, N_{ce}, of the full section.

The proposed nominal axial capacity for distortional buckling interacting with overall buckling (N_{c_de}):

$$\text{For } \lambda_{d2} \le 0.561, \qquad N_{c\_de} = N_{ce} \tag{11}$$

$$\text{For } \lambda_{d2} > 0.561, \qquad N_{c\_de} = \left[1 - 0.25\left(\frac{N_{od}}{N_{ce}}\right)^{0.6}\right]\left(\frac{N_{od}}{N_{ce}}\right)^{0.6} N_{ce} \tag{12}$$

where,

λ_{d2} = non-dimensional slenderness used to determine N_{c_de}

$= \sqrt{N_{ce}/N_{od}}$

N_{od} = elastic distortional compression member buckling load

$= Af_{od}$

For the SWC columns, the proposed strength curve was analysed with elastic distortional buckling stress based on both SAFSM and SFSM values. However, only the proposed strength curve based on SFSM is plotted in Fig. 15.

When the elastic distortional buckling stress f_{od} is based on the SAFSM value in Table 1a, this proposed strength curve (not shown) predicts conservatively for SWC specimens with column length 700 mm and is slightly unconservative for specimens with column lengths 1000 mm, 1300 mm and 2000 mm with higher values by approximately 1 %, 1.2 % and 5.4 % respectively.

When the elastic distortional buckling stress f_{od} used is based on the SFSM value in Table 1b, the strength curve is pushed up much higher as shown as the diamond line (−◇··) in Fig. 15. This caused the strength curve to predict unconservatively for specimens with column lengths 700 mm, 1000 mm, 1300 mm and 2000 mm by approximately 8.3 %, 22.3 %, 22.4 % and 25.0 % respectively.

When the SWC test results are non-dimensionalised by dividing the results by the overall buckling strength (N_{ce}), the results are plotted against the proposed distortional buckling strength curve (Method 2) as the square (□) points shown in Fig 17. Note that the horizontal axis is now λ_{d2} given by Equations 11 and 12 and not λ_d as defined in the DSM. The average non-dimensionalised SWC test results are predicted unconservatively by the proposed distortional DSM strength curve with higher values by approximately between 8.1 % and 20.7 %, as shown in Table 8.

When the SCR test results are non-dimensionalised by dividing the results by the overall buckling strength (N_{ce}), the results are plotted against the proposed distortional buckling strength curve (Method 2) as the triangle (Δ) points shown in Fig 17. Note that the horizontal axis is now λ_{d2} given by Equations 11 and 12. The average non-dimensionalised SCR test results are predicted slightly conservatively by the proposed distortional DSM strength curve for the 600 mm specimens with a lower value of approximately 0.3 % and unconservatively for the longer length specimens with higher values approximately between 3.8 % and 6.2 % as shown in Table 8.

The Yang and Hancock test results for specimens failing in the distortional buckling mode are non-dimensionalised and plotted against the proposed distortional strength curve as the diamond (◊) points shown in Fig 17. The proposed strength curve predicts the average Yang and Hancock results unconservatively with higher values up to approximately 14.7 %, as shown in Table 8.

The average ratio of test results to design for this proposed distortional strength curve is 0.92, as shown in Table 8, compared to 0.9, as shown in Table 6, of the original DSM distortional strength curve. This indicates that the proposed strength curve is slightly more accurate than the original DSM distortional strength curve, and the scatter is much improved, 0.067 compared to 0.139. Therefore when compared to both test programs and Yang and Hancock results, the proposed distortional buckling strength curve is shown to be relatively accurate and reliable in predicting the design strength of compression members that exhibit interaction of buckling modes. The accuracy of this proposed strength curve can be improved by increasing the exponential value of 0.6 in Equation 12 to 0.65.

7.3.1.1 Adjusted Method 2 - Distortional buckling interacting with overall buckling

It has been shown that proposed design Method 2 is relatively accurate and reliable, and this accuracy can be improved by increasing the exponential value of 0.6 in Equation 12 to 0.65.

In this section, the exponential value has been increased and the results are discussed as below.

The proposed nominal axial capacity for the interaction of distortional buckling and overall buckling (N_{c_de}):

$$\text{For } \lambda_{d2} \le 0.587, \qquad N_{c\_de} = N_{ce} \tag{13}$$

$$\text{For } \lambda_{d2} > 0.587, \qquad N_{c\_de} = \left[1 - 0.25\left(\frac{N_{od}}{N_{ce}}\right)^{0.65}\right]\left(\frac{N_{od}}{N_{ce}}\right)^{0.65} N_{ce} \tag{14}$$

where,

λ_{d2} = non-dimensional slenderness used to determine N_{c_de}

$= \sqrt{N_{ce}/N_{od}}$

N_{od} = elastic distortional compression member buckling load

$= Af_{od}$

When the SWC test results are non-dimensionalised by dividing the results by the overall buckling strength (N_{ce}), the results are plotted against the proposed distortional buckling strength curve (Adjusted Method 2) as the square (□) points shown in Fig. 18. Note that the horizontal axis is now λ_{d2} given by Equations 13 and 14. The average non-dimensionalised SWC test results are predicted unconservatively by the proposed distortional DSM strength curve with higher values by approximately between 3.9 % and 17.2 %, as shown in Table 9.

When the SCR test results are non-dimensionalised by dividing the results by the overall buckling strength (N_{ce}), the results are plotted against the proposed distortional buckling strength curve (Adjusted Method 2) as the triangle (Δ) points shown in Fig. 18. Note that the horizontal axis is now λ_{d2} given by Equations 13 and 14. The average non-dimensionalised SCR test results are predicted conservatively by the proposed distortional DSM strength curve for the 600 mm and 1200 specimens with a lower value of approximately 6.9 % and 2.0 % and slightly unconservatively for the 1600 mm and 2000 mm specimens with higher values approximately between 1.2 % and 0.2 % as shown in Table 9.

The Yang and Hancock test results for specimens failing in the distortional buckling mode are non-dimensionalised and plotted against the proposed distortional strength curve as the diamond (◊) points shown in Fig. 18. The average non-dimensionalised Yang and Hancock test results are predicted conservatively by the proposed distortional DSM strength curve for the 800 mm and 2000 mm specimens with lower values by approximately 5.8 % and 9.3 % respectively and unconservatively for the 1300 mm specimens with a higher value of approximately 6.3 %, as shown in Table 9.

The average ratio of test results to design for this proposed distortional strength curve is 0.979, as shown in Table 9, compared to 0.9, as shown in Table 6, of the original DSM distortional strength curve. This indicates that the proposed strength curve (Adjusted Method 2) is much more accurate than the original DSM distortional strength curve, and the scatter is also lower, 0.08 compared to 0.139. Therefore when compared to both test programs and Yang and Hancock results, the proposed distortional buckling strength curve (Adjusted Method 2) is shown to be highly accurate and reliable in predicting the design strength of compression members that exhibit interaction of buckling modes.

7.3.2 Method 3 – Interaction of Local and Distortional Buckling Modes

A strength curve that considers the interaction of local and distortional buckling modes is most likely necessary. To account for the interaction of local and distortional modes, the Kwon and Hancock (1992) strength curve, N_{kh}, which is the same as the DSM distortional strength (N_{cd}) given in Equations 7 and 8, is adopted as the compressive member design strength, N_{ce} in Equations 5 and 6 and is shown below.

The proposed nominal axial capacity for interaction of local and distortional buckling modes (N_{c_ld}):

$$\text{For } \lambda_d \le 0.561, \qquad N_{kh} = N_y \tag{15}$$

$$\text{For } \lambda_d > 0.561, \qquad N_{kh} = \left[1 - 0.25\left(\frac{N_{od}}{N_y}\right)^{0.6}\right]\left(\frac{N_{od}}{N_y}\right)^{0.6} N_y \tag{16}$$

where,

λ_d = non-dimensional slenderness used to determine N_{kh}
$= \sqrt{N_y / N_{od}}$

N_{od} = elastic distortional compression member buckling load
$= Af_{od}$

$$\text{For } \lambda_{l3} \le 0.776, \qquad N_{c\_ld} = N_{kh} \tag{17}$$

$$\text{For } \lambda_{l3} > 0.776, \qquad N_{c\_ld} = \left[1 - 0.15\left(\frac{N_{ol}}{N_{kh}}\right)^{0.4}\right]\left(\frac{N_{ol}}{N_{kh}}\right)^{0.4} N_{kh} \tag{18}$$

where,

λ_{l3} = non-dimensional slenderness used to determine N_{c_ld}
$= \sqrt{N_{kh} / N_{ol}}$

N_{ol} = elastic member local buckling load in compression
$= Af_{ol}$

For the SWC columns, the proposed strength curve was analysed with the elastic distortional buckling stress based on both SAFSM and SFSM values. However, only the proposed strength curve based on SFSM is plotted in Fig. 15.

When the elastic buckling stresses f_{ol} and f_{od} are based on the SAFSM values in Table 1a for the local and distortional buckling modes respectively, the proposed distortional strength curve (not shown) now predicts conservatively for the specimens up to column length 1300 mm and slightly unconservative for specimens with column length 2000 mm by approximately 8.9 %. The proposed strength curve N_{c_ld} forms a cutoff at lower slenderness at $N_{cl0.5}$ of the proposed local/overall strength curve.

When the elastic distortional buckling stress f_{od} is based on the SFSM value in Table 1b, the proposed distortional buckling strength curve for the SWC section, shown by the dashed-circle line (–⊖··) in Fig. 15, predicts conservatively for specimens with column length 700 mm and is slightly unconservative for specimens with column lengths 1000 mm and 1300 mm by approximately 4.6 % and 8.3% respectively and very unconservatively for specimens with column length 2000 mm by approximately 22.6 %. When interaction of local and distortional buckling modes is considered, the strength curve predicts a more conservative curve to the test results than when no interaction is considered. However this method does not seem to be able to predict accurately at longer specimen lengths, hence a new method is required to allow for the interaction of local, distortional and overall buckling modes.

When the SWC test results are non-dimensionalised by dividing the results by the Kwon and Hancock strength (N_{kh}) from Equations 15 and 16, the results are plotted against the proposed distortional buckling strength curve (Method 3) as the square (□) points shown in Fig 19. The average non-dimensionalised SWC test results are predicted conservatively by the proposed distortional DSM strength curve for the 700 mm specimens with a lower value of approximately 16.1 % and unconservatively for the longer length specimens with higher values approximately between 2.4 % and 13.0 % as shown in Table 10.

When the SCR test results are non-dimensionalised by dividing the results by the Kwon and Hancock strength (N_{kh}) from Equations 15 and 16, the results are plotted against the proposed distortional buckling strength curve (Method 3) as the triangle (Δ) points shown in Fig 19. The average non-dimensionalised SCR test results are predicted conservatively for all column lengths by the proposed distortional DSM strength curve with lower values of approximately between 4.4 % and 35.6 % as shown in Table 10.

In addition to both the test results, the test results of the Yang and Hancock (2004) specimens that failed in the distortional buckling mode are also non-dimensionalised and plotted as the diamond (◊) points as shown in Fig. 19. The average non-dimensionalised Yang and Hancock test results are predicted conservatively for all column lengths by the proposed distortional DSM strength curve with lower values of approximately between 22.6 % and 44.7 % as shown in Table 10.

The average ratio of test results to design for this proposed distortional strength curve is 1.147, as shown in Table 10, compared to 0.9, as shown in Table 6, of the original DSM

distortional strength curve. This indicates that the proposed strength curve is much more conservative than the original DSM distortional strength curve, however the scatter is wider, 0.174 compared to 0.139. Therefore when compared to both test programs and Yang and Hancock results, the proposed distortional buckling strength curve is shown to be conservative and generally predicts reasonably well the specimens subjected to interaction of buckling modes. This proposed strength curve, when taken with the proposed local/overall buckling strength curve, generally produces safe designs.

7.3.3 Method 4 – Interaction of Local, Distortional and Overall Buckling Modes

A strength curve that considers the interaction of all local, distortional and overall buckling modes is most likely necessary to safely account for the SWC specimens at longer lengths. To account for the interaction of local, distortional and overall buckling modes, the proposed strength curve for the interaction of distortional and overall modes, N_{c_de} from Equations 11 and 12, is adopted as the overall buckling strength, N_{ce} in Equations 9 and 10 and is shown below.

The proposed nominal axial capacity for the interaction of local, distortional and overall buckling ($N_{c\_lde0.5}$):

$$\text{For } \lambda_{l4} \le 0.673, \qquad N_{c\_lde0.5} = N_{c\_de} \tag{19}$$

$$\text{For } \lambda_{l4} > 0.673, \qquad N_{c\_lde0.5} = \left[1 - 0.22\left(\frac{N_{ol}}{N_{c\_de}}\right)^{0.5}\right]\left(\frac{N_{ol}}{N_{c\_de}}\right)^{0.5} N_{c\_de} \tag{20}$$

where,

λ_{l4} = non-dimensional slenderness used to determine $N_{c\_lde0.5}$

$= \sqrt{N_{c\_de}/N_{ol}}$

N_{ol} = elastic member local buckling load in compression

$= Af_{ol}$

For the SWC columns, the proposed strength curve was analysed with the elastic distortional buckling stress based on both SAFSM and SFSM values. However, only the proposed strength curve based on SFSM is plotted in Fig. 15.

When the elastic buckling stresses f_{ol} and f_{od} are based on the SAFSM values in Table 1a for the local and distortional buckling modes respectively, the proposed distortional buckling strength curve for the SWC section (not shown) now predicts conservatively for all column lengths by approximately between 14.4 % and 51.5 %. The proposed strength curve N_{c_ld} forms a cutoff at lower slenderness at $N_{cl0.5}$ of the proposed local strength curve.

When the elastic distortional buckling stress f_{od} is based on the SFSM values in Table 1b for the distortional buckling mode in N_{c_de}, the proposed distortional strength curve for the SWC section, shown by the dotted line (….) in Fig. 15, appears to predict conservatively the test results, even at longer specimen lengths.

When the SWC test results are non-dimensionalised by dividing the results by the strength proposed in Method 2 (N_{c_de}) from Equations 11 and 12, the results are plotted against the proposed distortional buckling strength curve (Method 4) as the square (□) points shown in Fig 20. The average non-dimensionalised SWC test results are now predicted conservatively by the proposed distortional DSM strength curve with lower values approximately between 9.6 % and 30.1 % as shown in Table 11. As a comparison, the SCR and Yang and Hancock test results are also non-dimensionalised and plotted as the triangle (Δ) and diamond (◊) points in Fig. 20. The average non-dimensionalised SCR test results are predicted very conservatively by the proposed distortional DSM strength curve with lower values approximately between 33.3 % and 52.6 % as shown in Table 11. The average non-dimensionalised Yang and Hancock test results are also predicted very conservatively by the proposed distortional DSM strength curve with lower values approximately between 46.4 % and 67.3 % as shown in Table 11. Hence, this proposed method can produce conservative results at longer lengths.

The average ratio of test results to design for this proposed distortional strength curve is 1.362, as shown in Table 11, compared to 0.9, as shown in Table 6, of the original DSM distortional strength curve. This indicates that the proposed strength curve always produces safe design values, though the design capacities are very much lower. The scatter of the results is much higher, 0.194 compared to 0.139, when compared to the original DSM distortional strength curve.

8 APPLICABILITY OF PROPOSED DESIGN METHODS

The application of the DSM for design has been clearly outlined in the Australian Standard for cold-formed steel structures, where the design of a compression member is restrained by pre-qualification criteria. This pre-qualification criteria was necessary as it allowed designers to create section designs that would most likely fail in either the local or distortional buckling modes, hence providing an alternative approach to calculate the member capacity by applying the DSM. However, the DSM approach is inadequate to account for sections, such as the stiffened web channel column (SWC), failing with interaction of local and distortional buckling modes, even when designed to the pre-qualification criteria. Several design method proposals have been discussed to improve the DSM local and distortional strength curves, and a range of applicability is required to find out in what circumstances the proposed design methods can be applied.

The proposed local/overall DSM strength curve can be applied when analyses or experiments indicate that local buckling failure occurred in all the flange elements in the section.

The two test programs carried out in this research and the Yang and Hancock (2004) test results can be observed to have one thing in common, nearly coincident elastic local and distortional buckling stresses. When the sections were analysed using the semi-analytical finite strip method (SAFSM), the elastic local and distortional buckling stresses did not appear nearly coincident. In fact, the ratio of elastic distortional buckling stress to local buckling stress (F_{od}/F_{ol}) is $0.52 \le F_{od}/F_{ol} \le 0.94$, as shown in Table 12, for this range of test programs. However, with fixed-end boundary conditions, the sections were analysed with

the spline finite strip method (SFSM), and the elastic local and distortional buckling stresses are noted to be nearly coincident. The ratio of elastic distortional buckling stress to local buckling stress (F_{od}/F_{ol}), for this range of test programs, is $0.72 \le F_{od}/F_{ol} \le 1.02$ as shown in Table 12. Sections having nearly coincident elastic buckling stresses are definitely an indication that interaction of local and distortional buckling stresses most likely will occur, as previously demonstrated in the test programs.

A parametric study was carried out by Silvestre et al. (2007) on six "basic" pre-qualified compression members that exhibited such local and distortional buckling modes interaction. The authors noted that though the sections were pre-qualified, interaction of local and distortional buckling occurred for slender columns with nearly coincident elastic local and distortional buckling stresses. The authors also noted the importance of the ratio of the critical distortional buckle half-wavelength (L_{crd}) to the critical local buckle half-wavelength (L_{crl}). It was noted that as the ratio increased, the column ultimate strength decreased. The authors also noted when the non-dimensional distortional slenderness (λ_d) was less than 1.4, the sections had no interaction of local and distortional buckling. When $\lambda_d > 1.4$, interaction buckling occurs and the test results generally lie below the non-dimensionalised DSM distortional strength curve.

With the current test programs carried out, there was insufficient data to confirm and verify the effect of the ratio of critical buckle half-wavelengths (L_{crd}/L_{crl}) on column ultimate strength. When $\lambda_d > 1.4$, the test results carried out in this work do indicate the sections failing with interaction buckling when compared to the non-dimensionalised DSM distortional strength curve in Fig. 14. However, there is no data available from the test programs to indicate that no interaction buckling occurs when $\lambda_d < 1.4$. Therefore both of these indicators cannot be confirmed by this work.

Although design proposal Methods 3 and 4 predict more conservatively, they have considerable scatter over a range of test lengths and will probably lead to more unreliable designs. Therefore the proposed distortional strength curve (Adjusted Method 2) can be applied when the ratio of elastic distortional buckling stress to local buckling stress (F_{od}/F_{ol}) for a fixed-ended section is $0.72 \le F_{od}/F_{ol} \le 1.02$.

9 CONCLUSION

A new stiffened-web cold-formed high strength steel section was designed based on the limits of a pre-qualified compression member as stated in the Australian Standard for cold-formed steel structures AS/NZS 4600:2005. This section shape was designed using both the semi-analytical finite strip method (SAFSM) and the spline finite strip (SFSM) method. With the SFSM analysis of the section, interaction of local and distortional buckling mode was observed at intermediate lengths.

The material used for the test specimens was G550 high strength steel, with a thickness of 1 mm. Compression tests were carried to investigate the effects of local and distortional buckling modes and the possible interaction of these modes. The effect of different failure modes, inwards or outwards flange deflections, was also discussed. The Effective Width

Method (EWM) and Direct Strength Method (DSM) were employed to analyse the nominal capacity of the columns and were used to compare against the test results. The local buckling DSM strength curve was found to be unconservative when compared to the specimens that failed in the local buckling mode. The distortional buckling DSM strength curve was also found to be unconservative when compared to the test specimens that failed in the distortional buckling mode.

A design method is proposed to improve the prediction of the local buckling DSM strength curve and at the same time, design methods are proposed to improve the distortional buckling DSM strength curve by accounting for the interaction of local, distortional and overall buckling modes.

For sections failing in all flange elements, the DSM local buckling strength curve predicts unconservatively when compared against the test results. A proposed DSM local/overall strength curve, based on the Winter strength formula, was presented and discussed. The proposed strength curve was generally conservative when compared to the test results.

For section failing in the distortional mode and subjected to the interaction of local and distortional buckling modes, the test results showed that the sections failed prematurely and the DSM distortional strength curve was inadequate to account for such interactions. Design proposals to the DSM distortional strength curve were presented and discussed.

DSM design proposal Method 1 accounts for sections with multiple distortional buckling modes, taking the elastic buckling stress of the longer half-wavelength distortional mode to calculate the member capacity and has been discussed by Yap and Hancock (2008). Since the SWC section does not have multiple distortional buckling modes, this design method was not discussed for this section.

DSM design proposal Method 2 accounts for the interaction of distortional and overall buckling modes by replacing the yield strength N_y, of the DSM distortional strength curve, with the overall buckling strength N_{ce} of the full section. The proposed strength curve can be quite a good predictor of the member capacity as it is shown to be relatively accurate and reliable for the two test programs and the Yang and Hancock (2004) test results. When the exponential value was adjusted, the new design proposal (Adjusted Method 2) is now even more accurate and reliable, and is the recommended design proposal to account for the interaction of local and distortional buckling modes.

DSM design proposal Method 3 accounts for the interaction of local and distortional buckling modes by replacing the overall buckling strength N_{ce}, of the DSM local strength curve, with the N_{kh}, which is same as the DSM distortional strength curve. This method produces conservative results when compared to the two test programs and Yang and Hancock test results. However, the proposed strength curve is not reliable as the scatter is relatively high.

DSM design proposal Method 4 accounts for the interaction of local, distortional and overall buckling modes by replacing the overall bucking strength N_{ce}, of the proposed local strength curve, with the design strength N_{c_de} of proposal Method 2. This proposed strength curve is very conservative and always produces very safe predictions when compared to the two test programs and Yang and Hancock tests results. However, the proposed strength curve is not reliable as the scatter is relatively high.

With the proposed design methods for the DSM distortional strength curves, designers would require to know when it should be applied as it has been presented and discussed that pre-qualified compression members are subjected to such interaction buckling. A good measure for the applicability of the proposed method is to observe the ratio of elastic distortional buckling stress to local buckling stress (F_{od}/F_{ol}) of fixed ended sections. Interaction of local and distortional buckling occurs when there is nearly coincident elastic buckling stresses. Therefore the range of applicability for the proposed DSM distortional method is $0.72 \le F_{od}/F_{ol} \le 1.02$ for the two test programs and Yang and Hancock test results carried out in this research.

ACKNOWLEDGEMENTS

This report forms part of an ARC research project entitled "Interaction of local and distortional buckling modes in cold-formed high strength steel" being carried out at the School of Civil Engineering at the University of Sydney. The authors would like to thank the Australian Research Council and the Centre of Advance Structural Engineering (CASE) of the University of Sydney for the financial support provided.

REFERENCES

AISI (2001) *North American Specification for the Design of Cold-Formed Steel Structural Members,* American Iron and Steel Institute, Washington, D.C., USA.

AISI (2004) *Supplement 2004 to the North American Specification for the Design of Cold-Formed Steel Structural Members, 2001 Edition,* American Iron and Steel Institute, Washington, D.C., USA.

ASTM A653/A653M-05A (2000) *Standard Specification for Steel Sheet, Zinc-Coated (Galvanized) or Zinc-Iron Alloy-Coated (Galvannealed) by the Hot-Dip Process,* ASTM International.

ASTM A792/A792M-05 (1999) *Standard Specification for Steel Sheet, 55 % Aluminium-Zinc Alloy-Coated by the Hot-Dip Process,* ASTM International.

ASTM A875/A875M-05 (1999) *Standard Specification for Steel Sheet, Zinc-5% Aluminium Alloy-Coated by the Hot-Dip Process,* ASTM International.

ASTM A1039/A1039M-04 (2004) *Standard Specification for Steel, Sheet, Hot Rolled, Carbon, Commercial and Structural, Produced by the Twin-Toll Casting Process,* ASTM International.

BHP (1992) *The Making of Iron and Steel,* BHP Steel Group, Melbourne.

CHEUNG, Y. K. (1976) *Finite Strip Method in Structural Analysis,* Pergamon Press, New York.

KWON, Y. B. & HANCOCK, G. J. (1992) 'Tests of Cold-Formed Channels with Local and Distortional Buckling', *Journal of Structural Engineering,* 118, 7**,** p. 1786-1803.

LAU, S. C. W. & HANCOCK, G. J. (1986) 'Buckling of Thin Flat-Walled Structures by a Spline Finite Strip Method', *Thin-Walled Structures,* 4, 4**,** p. 269-294.

PAPANGELIS, J. P. & HANCOCK, G. J. (1995) 'Computer Analysis of Thin-Walled Structural Members', *Computers & Structures,* 56, 1**,** p. 157-176.

ROGERS, C. A. & HANCOCK, G. J. (1996) 'Ductility of G550 Sheet Steels in Tension-Elongation Measurements and Perforated Tests', *Research Report R735*, Department of Civil Engineering, University of Sydney, Sydney.

SCHAFER, B. W. & PEKOZ, T. (1998) 'Direct Strength Prediction of Cold-Formed Steel Members Using Numerical Elastic Buckling Solutions', *Fourteenth International Specialty Conference on Cold-Formed Steel Structures*, St. Louis, MO, United States, University of Missouri-Rolla, Rolla, MO, United States, p. 69-76.

SILVESTRE, N., CAMOTIM, D. & DINIS, P. B. (2007) 'DSM Design of Fixed Lipped Channel Columns against Local-Plate/Distortional Interactive Buckling', *Proceedings ISCAS '07*, Oxford, Brookes University, p. 752-759.

STANDARDS AUSTRALIA (1991) *AS1391: Methods for Tensile Testing of Metals,* Standards Australia, Sydney, NSW, Australia.

STANDARDS AUSTRALIA (1993) *AS1397: Steel Sheet and Strip - Hot-Dipped Zinc-Coated or Aluminium/Zinc-Coated,* Standards Australia, Sydney, NSW, Australia.

STANDARDS AUSTRALIA (2005) *AS/NZS4600: Cold-Formed Steel Structures,* Standards Australia, Sydney, NSW, Australia.

VON KARMAN, T., SECHLER, E. F. & DONNELL, L. H. (1932) 'Strength of Thin Plates in Compression', *American Society of Mechanical Engineers -- Transactions -- Applied Mechanics,* 54, 2**,** p. 53-56.

WINTER, G. (1947) 'Strength of Thin Steel Compression Flanges', *Transaction, ASCE,* 112, 2305**,** p. 525-576.

YANG, D. & HANCOCK, G. J. (2004) 'Compression Tests of High Strength Steel Channel Columns with Interaction between Local and Distortional Buckling', *Journal of Structural Engineering,* 130, 12**,** p. 1954-1963.

YAP, D. C. Y. & HANCOCK, G. J. (2006b) 'Compression Tests of High Strength Cold-Formed Cross-Shaped Steel Columns', *Research Report R869*, School of Civil Engineering, University of Sydney, Sydney, NSW, Australia.

YAP, D. C. Y. & HANCOCK, G. J. (2006a) 'Interaction Buckling and Postbuckling in the Distortional Mode of Thin-Walled Section', *Research Report R870*, School of Civil Engineering, University of Sydney, Sydney, NSW, Australia.

NOTATIONS

The following symbols are used in this paper:

A = Cross-sectional area (mm^2)

b = Width of element (mm)

b_e = Effective width of element (mm)

E = Young's modulus (GPa)

f_{od} = Elastic distortional buckling stress (MPa)

f_{ol} = Elastic local buckling stress (MPa)

f_y = Yield stress (MPa)

l_e = Effective length (mm)

N_c = Nominal member compression capacity (kN)

N_{cd} = Nominal axial capacity for distortional buckling

N_{c_de} = Proposed nominal axial capacity for interaction of distortional and overall buckling

N_{ce} = Nominal axial capacity for overall failure mode

N_{cl} = Nominal axial capacity for local buckling

$N_{cl0.5}$ = Proposed nominal axial capacity for local buckling

N_{c_ld} = Proposed nominal axial capacity for interaction of local and distortional buckling

$N_{c\_lde0.5}$ = Proposed nominal axial capacity for interaction of local, distortional and overall buckling

N_{kh} = Nominal axial capacity based on Kwon and Hancock strength equations

N_l = Theoretical local buckling load (kN)

N_d = Theoretical distortional buckling load (kN)

N_{od} = Elastic distortional buckling load (kN)

N_{ol} = Elastic local buckling load (kN)

N_s = Nominal section compression capacity (kN)

N_y = Squash load (kN)

t = Thickness (mm)

TABLES

Table 1a Elastic buckling stress of stiffened-web section using Semi-Analytical Finite Strip Method

SEMI-ANALYTICAL FINITE STRIP METHOD (SAFSM)		
Buckling mode	Buckle half-wavelength (mm)	Elastic buckling stress (MPa)
Local buckling	60	210.8
Distortional buckling	700	130.4
Flexural-torsional buckling (FT)	2700	82.89

Table 1b Elastic buckling stresses and modes of stiffened-web section using Spline Finite Strip Method

Specimen length (mm)	SPLINE FINITE STRIP METHOD (SFSM)					
	Elastic buckling stress (MPa)	Eigenmode 1	Elastic buckling stress (MPa)	Eigenmode 2	Elastic buckling stress (MPa)	Eigenmode 3
350	208.6	L(6)	208.8	L(6)	213.0	L(7)
700	208.4	L(11) + D(1)	208.6	L(12)	209.2	L(11)
1000	201.1	D(1)	209.1	L(17)	209.3	L(17)
1300	174.5	D(2)	195.3	D(1)	211.0	L(20)
2000	149.1	D(3)	155.1	D(2)	203.3	D(4)

Table 2 Results of tensile coupon tests

Specimen	b (mm)	t (mm)	0.2% Proof Stress F_y (MPa)	E (GPa)
1A	12.6	1.068	633.5	217.5
2A	12.7	1.065	633.4	217.8
3A	12.6	1.064	628.5	215.9
1B	12.7	1.064	639.5	211.0
2B	12.7	1.061	635.3	221.0
Mean	**12.67**	**1.065**	**634.0**	**216.9**

Table 3 Maximum geometric imperfection measurements of specimens

Specimen	L1 (mm)	L2 (mm)	L3 (mm)	L4 (mm)
SWC350_1	0.22	0.13	0.22	0.17
SWC350_2	0.23	0.20	0.10	0.18
SWC350_3	0.15	0.14	0.22	-0.23
SWC700_1	0.40	0.16	0.21	0.39
SWC700_2	-0.33	0.29	0.59	-0.23
SWC700_3	0.46	0.24	0.25	0.45
SWC1000_1	-0.57	0.25	0.30	-0.89
SWC1000_2	-0.58	0.19	0.15	-0.47
SWC1000_3	-0.32	-0.19	0.28	-0.38
SWC1300_1	-0.34	0.31	0.32	-0.31
SWC1300_2	-0.30	0.17	0.32	-0.32
SWC1300_3	-0.49	0.47	0.28	-0.44
SWC2000_1	-1.18	-0.33	-0.28	-1.15
SWC2000_2	-1.81	1.09	0.76	-1.32

Table 4 Summary of results for stiffened-web column (SWC)

Specimen	Area (mm^2)	P_u (kN)	F_u (MPa)	N_l (kN)	Effective Width Method		Direct Strength Method	
					SAFSM N_{cd} (kN)	SFSM N_{cd} (kN)	SAFSM N_{cd} (kN)	SFSM N_{cd} (kN)
SWC350_1	280.50	95.98	342.17	59.51	61.57	76.31	62.58	80.03
SWC350_2	281.47	82.35	292.57	59.51	61.57	76.31	62.58	80.03
SWC350_3	280.99	90.96	323.71	59.51	61.57	76.31	62.58	80.03
SWC700_1	282.26	75.60	267.84	59.51	61.57	76.31	62.58	80.03
SWC700_2	281.48	65.18	231.56	59.51	61.57	76.31	62.58	80.03
SWC700_3	282.00	73.46	260.50	59.51	61.57	76.31	62.58	80.03
SWC1000_1	282.19	58.37	206.85	59.51	61.57	76.31	62.58	80.03
SWC1000_2	281.67	58.65	208.22	59.51	61.57	76.31	62.58	80.03
SWC1000_3	281.03	59.24	210.80	59.51	61.57	76.31	62.58	80.03
SWC1300_1	281.94	53.59	190.08	59.51	61.57	76.31	62.58	80.03
SWC1300_2	281.85	57.45	203.83	59.51	61.57	76.31	62.58	80.03
SWC1300_3	281.61	58.36	207.24	59.51	61.57	76.31	62.58	80.03
SWC2000_1	282.32	49.00	173.56	59.51	61.57	76.31	62.58	80.03
SWC2000_2	281.47	46.37	164.74	59.51	61.57	76.31	62.58	80.03

Table 5 Summary of non-dimensionalised test results compared with local DSM strength curve

	Average $\frac{N_{test}}{N_{ce}}$	Predicted design value	% Difference when test results compared to design	Ratio of average test results to design
SWC350 specimens	0.511	0.585	-12.57	0.874
SCR110 specimens	0.440	0.510	-13.68	0.863
Yang and Hancock (2004b) 360mm specimens	0.381	0.382	-0.39	0.996
			Average	**0.911**
			St. Dev.	**0.074**

Table 6 Summary of non-dimensionalised test results compared with distortional DSM strength curve

	Average $\frac{N_{test}}{N_y}$	Predicted design value	% Difference when test results compared to design	Ratio of average test results to design
SWC700 specimens	0.400	0.447	-10.66	0.893
SWC1000 specimens	0.329	0.439	-25.05	0.750
SWC1300 specimens	0.316	0.408	-22.53	0.775
SWC2000 specimens	0.267	0.376	-28.97	0.710
SCR600 specimens	0.363	0.370	-1.75	0.983
SCR1200 specimens	0.327	0.368	-11.24	0.888
SCR1600 specimens	0.296	0.365	-18.82	0.812
SCR2000 specimens	0.277	0.364	-23.95	0.760
Yang and Hancock (2004b) 800mm specimens	0.225	0.244	-7.41	0.926
Yang and Hancock (2004b) 1300mm specimens	0.192	0.245	-21.72	0.783
Yang and Hancock (2004b) 2000mm specimens	0.183	0.224	-18.42	0.816
Kwon and Hancock (1992) CH2-7-800	0.336	0.292	15.22	1.152
Kwon and Hancock (1992) CH2-7-1000	0.327	0.276	18.86	1.189
Kwon and Hancock (1992) CH2-8-1000	0.326	0.306	6.33	1.063
Kwon and Hancock (1992) CH2-10-1000	0.343	0.347	-1.32	0.987
Kwon and Hancock (1992) CH2-12-1000	0.349	0.384	-9.01	0.910
Kwon and Hancock (1992) CH2-14-1000	0.363	0.404	-10.01	0.900
			Average	**0.900**
			St. Dev.	**0.139**

Table 7 Summary of non-dimensionalised test results compared with proposed local strength curve

	Average $\frac{N_{test}}{N_{ce}}$	Predicted design value	% Difference when test results compared to design	Ratio of average test results to design
SWC350 specimens	0.511	0.507	0.90	1.009
SCR110 specimens	0.440	0.429	2.44	1.024
Yang and Hancock (2004b) 360mm specimens	0.381	0.304	25.01	1.250
			Average	**1.094**
			St. Dev.	**0.135**

Table 8 Summary of non-dimensionalised test results compared with proposed distortional strength curve (Method 2)

	Average $\frac{N_{test}}{N_{ce}}$	Predicted design value	% Difference when test results compared to design	Ratio of average test results to design
SWC700 specimens	0.423	0.460	-8.14	0.919
SWC1000 specimens	0.369	0.465	-20.71	0.793
SWC1300 specimens	0.384	0.451	-14.90	0.851
SWC2000 specimens	0.421	0.476	-11.52	0.885
SCR600 specimens	0.379	0.378	0.27	1.003
SCR1200 specimens	0.388	0.403	-3.76	0.962
SCR1600 specimens	0.401	0.428	-6.21	0.938
SCR2000 specimens	0.445	0.466	-4.48	0.955
Yang and Hancock (2004b) 800mm specimens	0.243	0.254	-4.33	0.957
Yang and Hancock (2004b) 1300mm specimens	0.233	0.273	-14.68	0.853
Yang and Hancock (2004b) 2000mm specimens	0.289	0.289	-0.04	1.000
			Average	**0.920**
			St. Dev.	**0.067**

Table 9 Summary of non-dimensionalised test results compared with proposed distortional strength curve (Adjusted Method 2)

	Average $\frac{N_{test}}{N_{ce}}$	Predicted design value	% Difference when test results compared to design	Ratio of average test results to design
SWC700 specimens	0.423	0.4399	-3.93	0.961
SWC1000 specimens	0.369	0.4454	-17.15	0.829
SWC1300 specimens	0.384	0.43	-10.80	0.892
SWC2000 specimens	0.421	0.4563	-7.74	0.923
SCR600 specimens	0.379	0.3548	6.85	1.069
SCR1200 specimens	0.388	0.3801	1.97	1.020
SCR1600 specimens	0.401	0.4062	-1.22	0.988
SCR2000 specimens	0.445	0.4457	-0.19	0.998
Yang and Hancock (2004b) 800mm specimens	0.243	0.2293	5.81	1.058
Yang and Hancock (2004b) 1300mm specimens	0.233	0.2485	-6.27	0.937
Yang and Hancock (2004b) 2000mm specimens	0.289	0.2645	9.26	1.093
			Average	**0.979**
			St. Dev.	**0.080**

Table 10 Summary of non-dimensionalised test results compared with proposed distortional strength curve (Method 3)

	Average $\frac{N_{test}}{N_{kh}}$	Predicted design value	% Difference when test results compared to design	Ratio of average test results to design
SWC700 specimens	0.894	0.770	16.09	1.161
SWC1000 specimens	0.749	0.774	-3.21	0.968
SWC1300 specimens	0.775	0.794	-2.40	0.976
SWC2000 specimens	0.710	0.816	-12.99	0.870
SCR600 specimens	0.983	0.725	35.57	1.356
SCR1200 specimens	0.888	0.726	22.26	1.223
SCR1600 specimens	0.812	0.728	11.50	1.115
SCR2000 specimens	0.761	0.729	4.37	1.044
Yang and Hancock (2004b) 800mm specimens	0.926	0.640	44.65	1.446
Yang and Hancock (2004b) 1300mm specimens	0.783	0.639	22.59	1.226
Yang and Hancock (2004b) 2000mm specimens	0.816	0.659	23.77	1.238
			Average	**1.147**
			St. Dev.	**0.174**

Table 11 Summary of non-dimensionalised test results compared with proposed distortional strength curve (Method 4)

	Average $\frac{N_{test}}{N_{c\_de}}$	Predicted design value	% Difference when test results compared to design	Ratio of average test results to design
SWC700 specimens	0.918	0.706	30.10	1.301
SWC1000 specimens	0.793	0.719	10.27	1.103
SWC1300 specimens	0.851	0.749	13.57	1.136
SWC2000 specimens	0.885	0.808	9.58	1.096
SCR600 specimens	1.003	0.657	52.57	1.526
SCR1200 specimens	0.962	0.674	42.70	1.427
SCR1600 specimens	0.938	0.694	35.24	1.352
SCR2000 specimens	0.955	0.717	33.32	1.333
Yang and Hancock (2004b) 800mm specimens	0.956	0.572	67.30	1.673
Yang and Hancock (2004b) 1300mm specimens	0.853	0.583	46.36	1.464
Yang and Hancock (2004b) 2000mm specimens	1.000	0.634	57.69	1.577
			Average	**1.362**
			St. Dev.	**0.194**

Table 12 Summary of test results to determine DSM proposal range of applicability

	SFSM				SAFSM		
	λ_d	F_{od} (MPa)	F_{ol} (MPa)	$\frac{F_{od}}{F_{ol}}$	F_{od} (MPa)	F_{ol} (MPa)	$\frac{F_{od}}{F_{ol}}$
SWC700 specimens	1.744	208.4	208.6	**0.99**	130.4	210.8	0.62
SWC1000 specimens	1.776	201.1		**0.96**			
SWC1300 specimens	1.906	174.5		**0.84**			
SWC2000 specimens	2.062	149.1		**0.72**			
SCR600 specimens	2.093	153.6	153.4	**1.00**	145.9 (SWD)	154.9	0.94
SCR1200 specimens	2.102	152.3		**0.99**			
SCR1600 specimens	2.120	149.7		**0.98**	95.8 (LWD)	154.9	0.62
SCR2000 specimens	2.125	149.0		**0.97**			
Yang and Hancock (2004b) 800mm specimens	3.0681	73.3	73.0	**1.00**	38.1	73.2	0.52
Yang and Hancock (2004b) 1300mm specimens	3.050	74.2		**1.02**			
Yang and Hancock (2004b) 2000mm specimens	3.304	63.2		**0.87**			

FIGURES

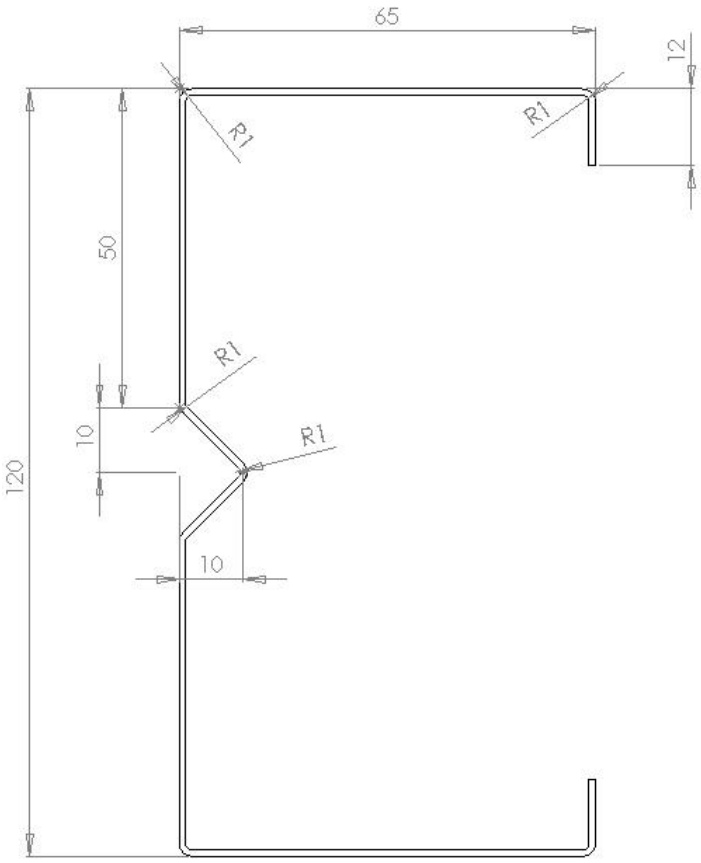

Fig. 1 Design and dimensions of stiffened-web open-shape section

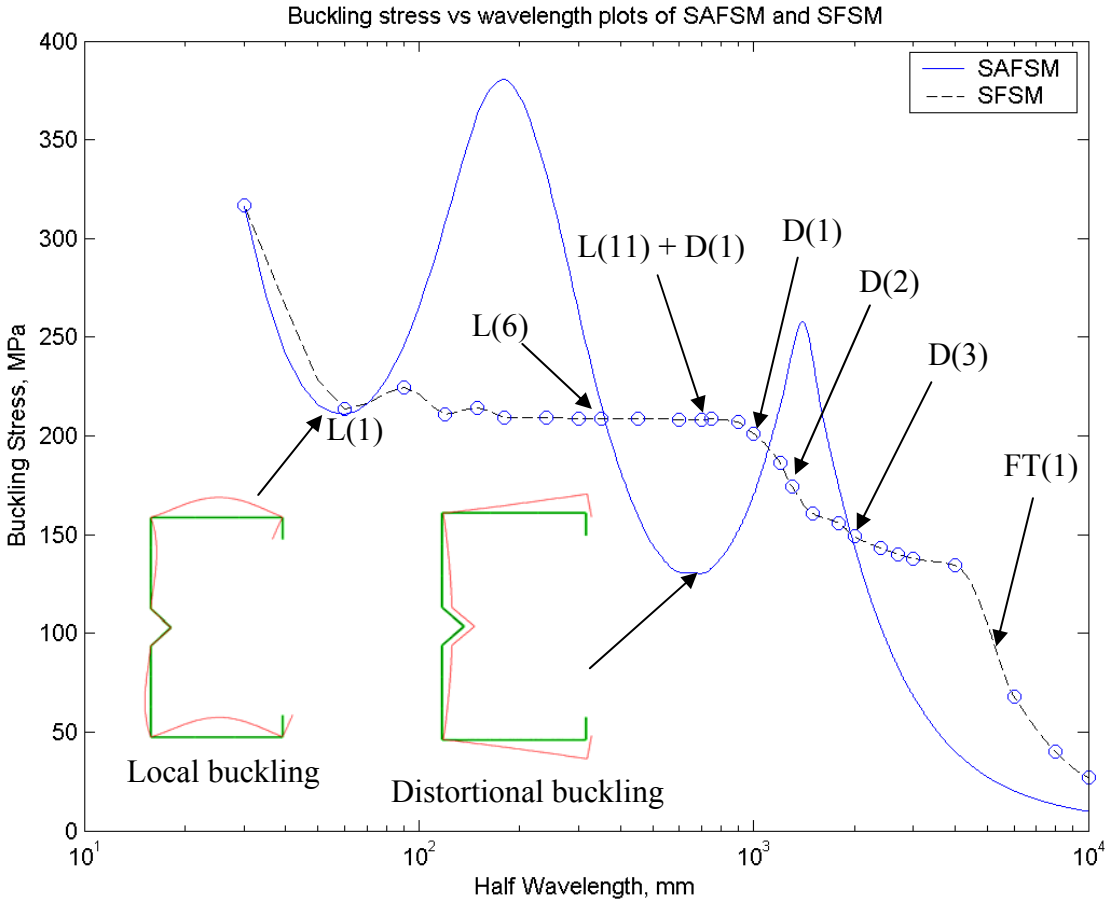

Fig. 2 Buckling stresses and modes for stiffened-web section

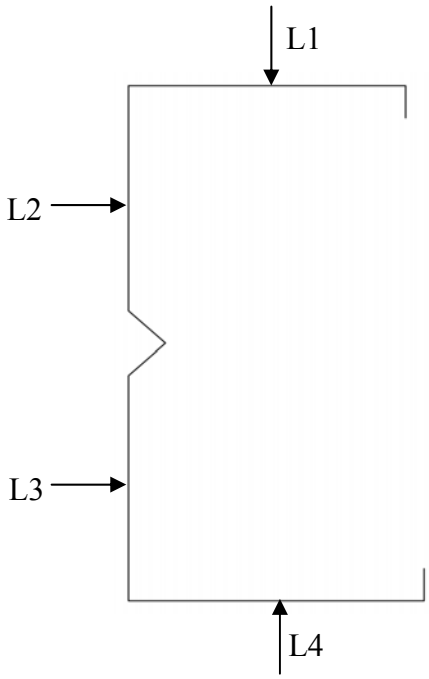

Fig. 3 Positions for laser measurements

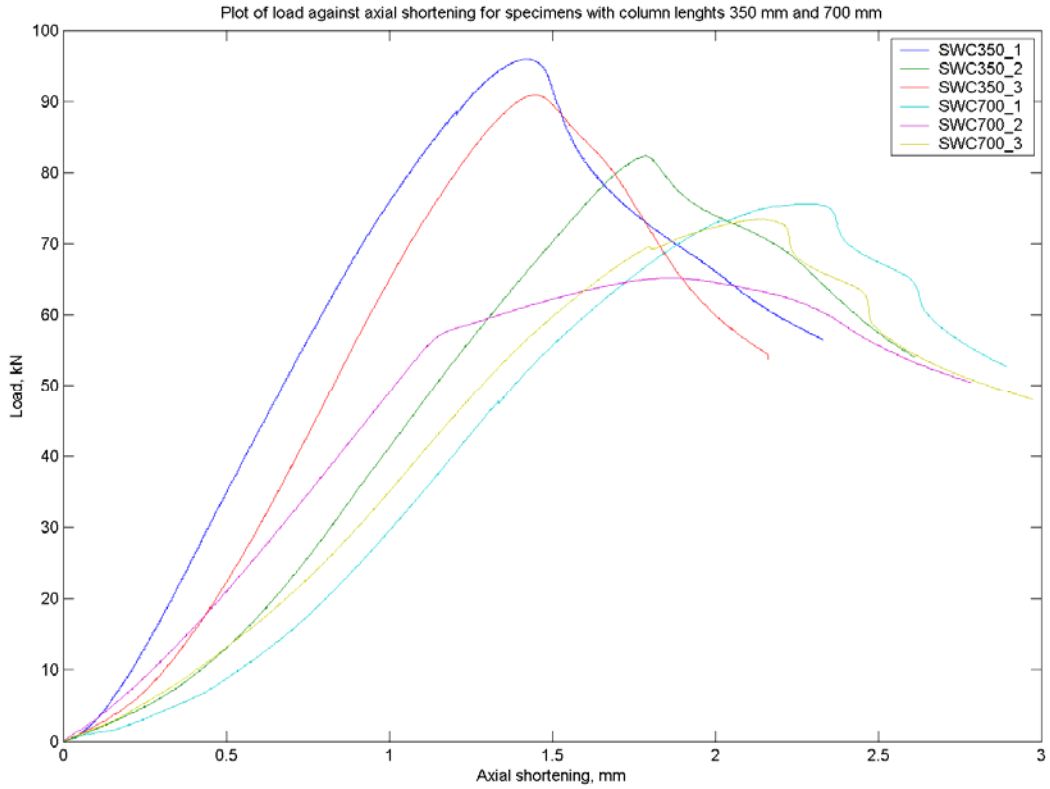

Fig. 4a Load vs axial shortening for specimens with column lengths 350 mm and 700 mm

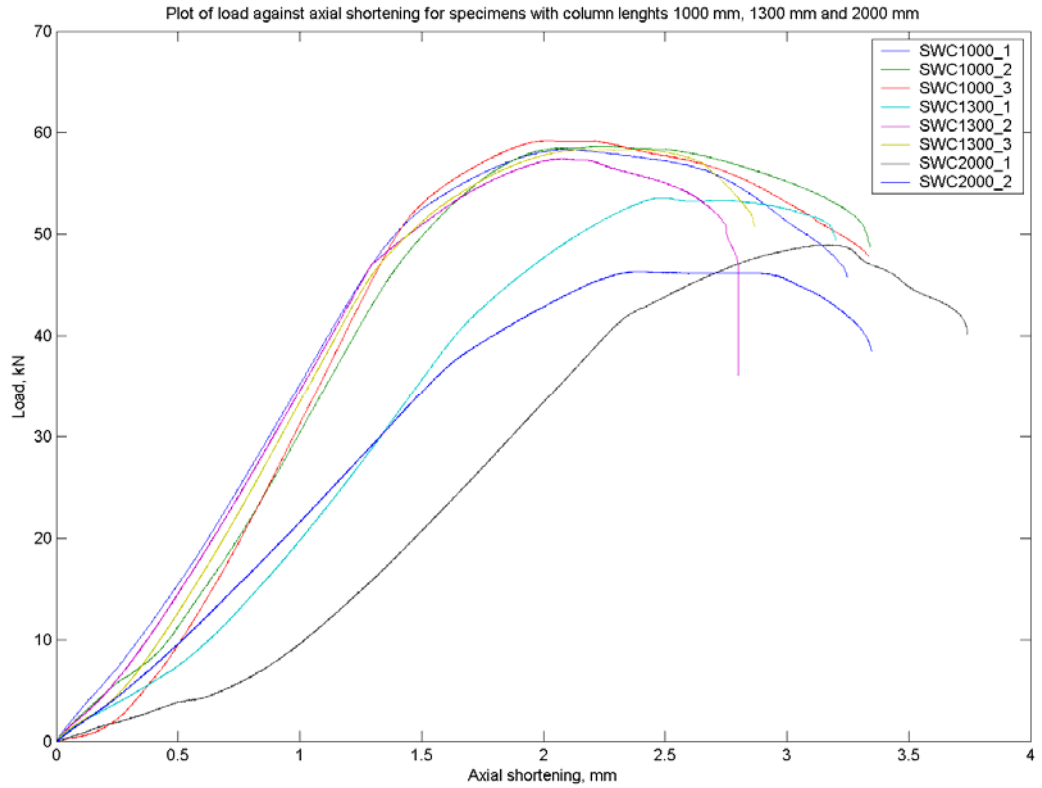

Fig. 4b Load vs axial shortening for specimens with column lengths 1000 mm, 1300 mm and 2000 mm

Fig. 5 Inelastic local buckling occurring in all flanges for 350 mm specimen

Fig. 6a Elastic local buckling occurring along flange with inward lip deflection of 700 mm column

Fig. 6b Outward lip deflection failure mode of 700 mm column

Fig. 7a Elastic local buckling occurring along flange with inward lip deflection of 1000 mm column

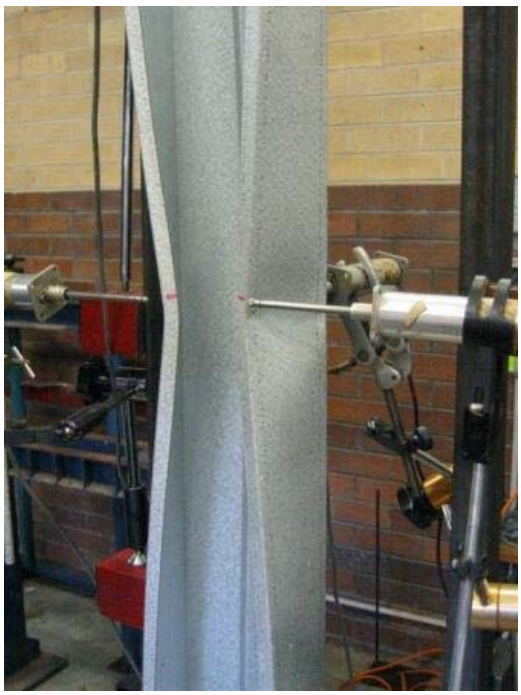

Fig. 7b Inward lip deflection failure mode of 1000 mm column

Fig. 8a Elastic distortion buckling with 2 buckle half-waves for 1300 mm column

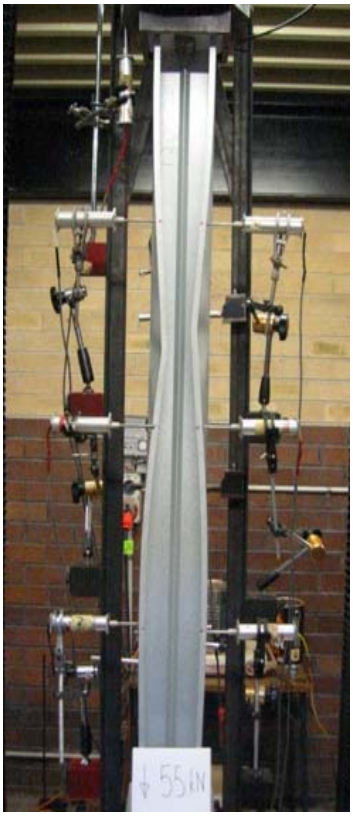

Fig. 8b Inward lip deflection failure mode of 1300 mm column

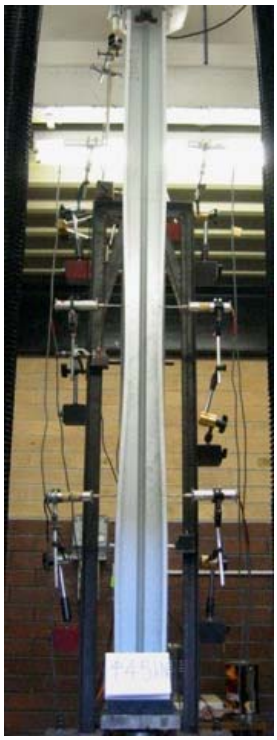

Fig. 9a Elastic distortion buckling with 3 buckle half-waves for 2000 mm column

Fig. 9b Inward lip deflection failure mode of 2000 mm column

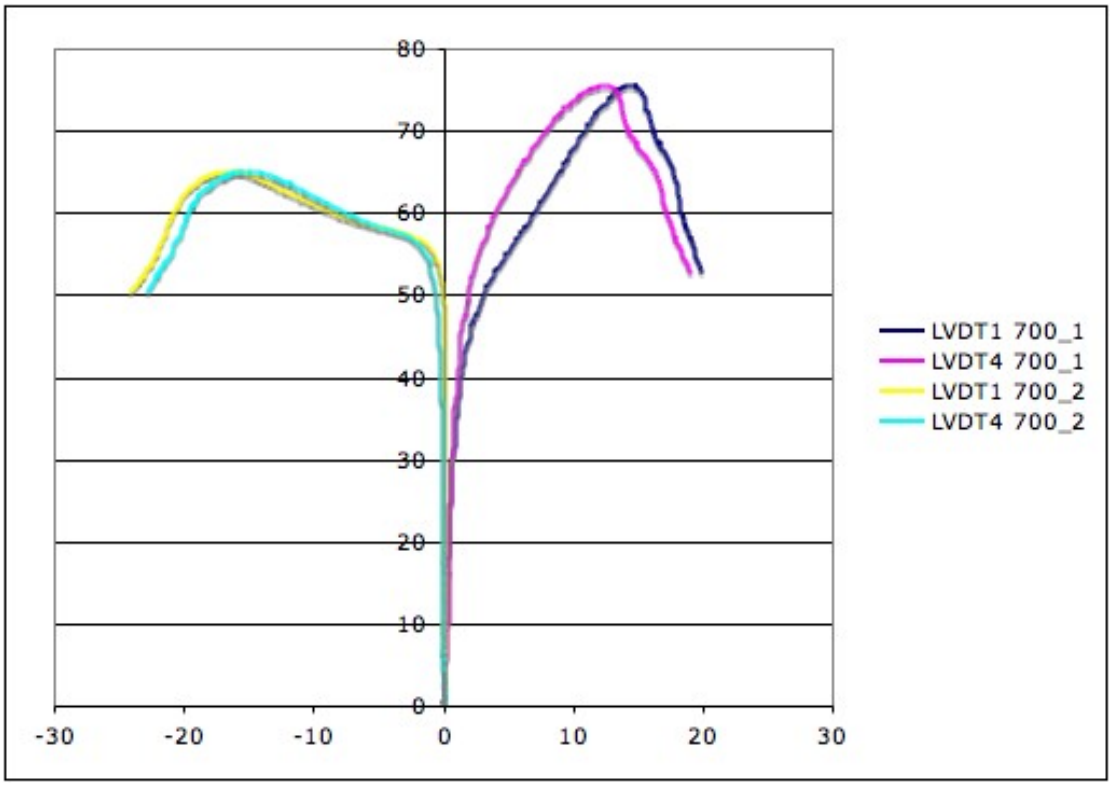

Fig. 10 Plot of load vs lip deflections for inward and outward deflection modes

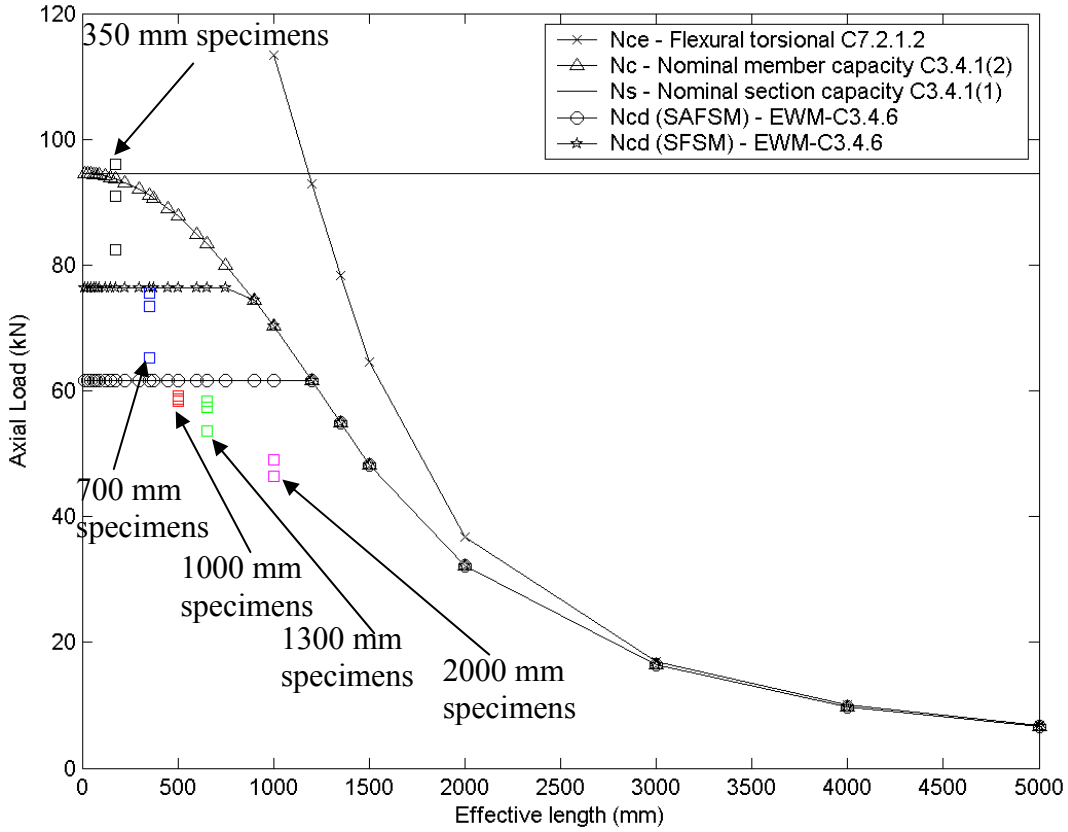

Fig. 11 Comparison of EWM design strength curves and test results

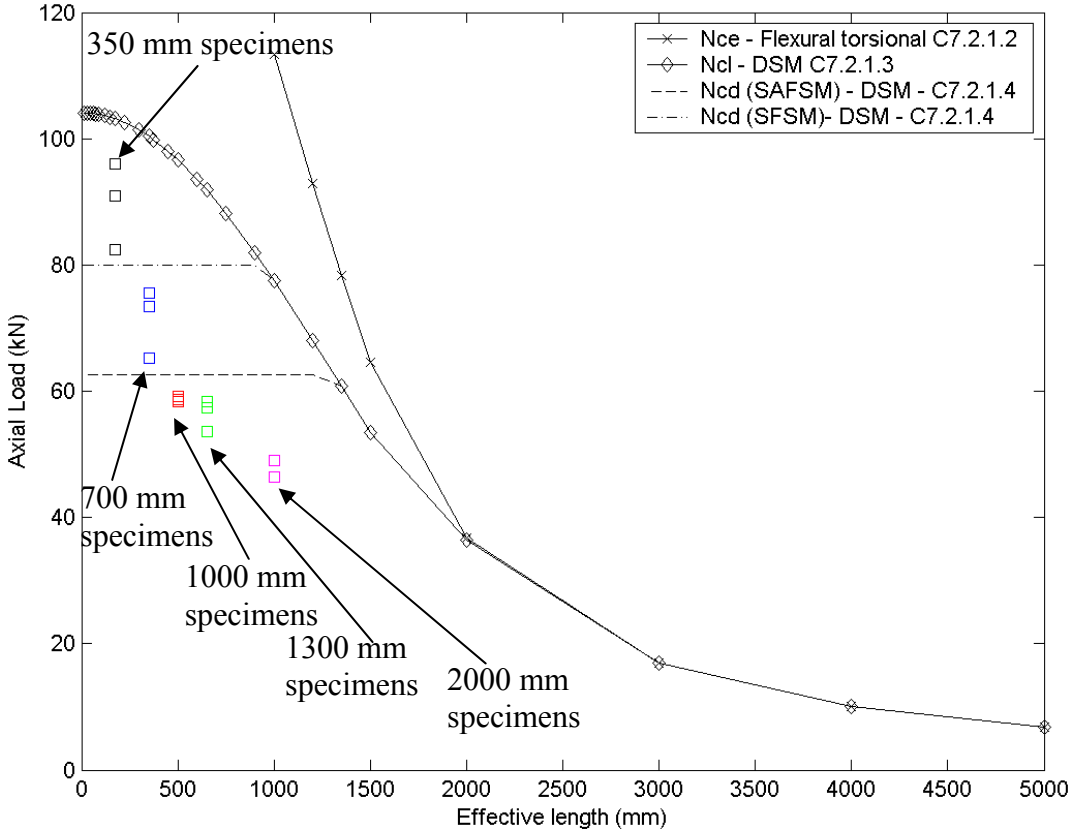

Fig. 12 Comparison of DSM design strength curves and test results

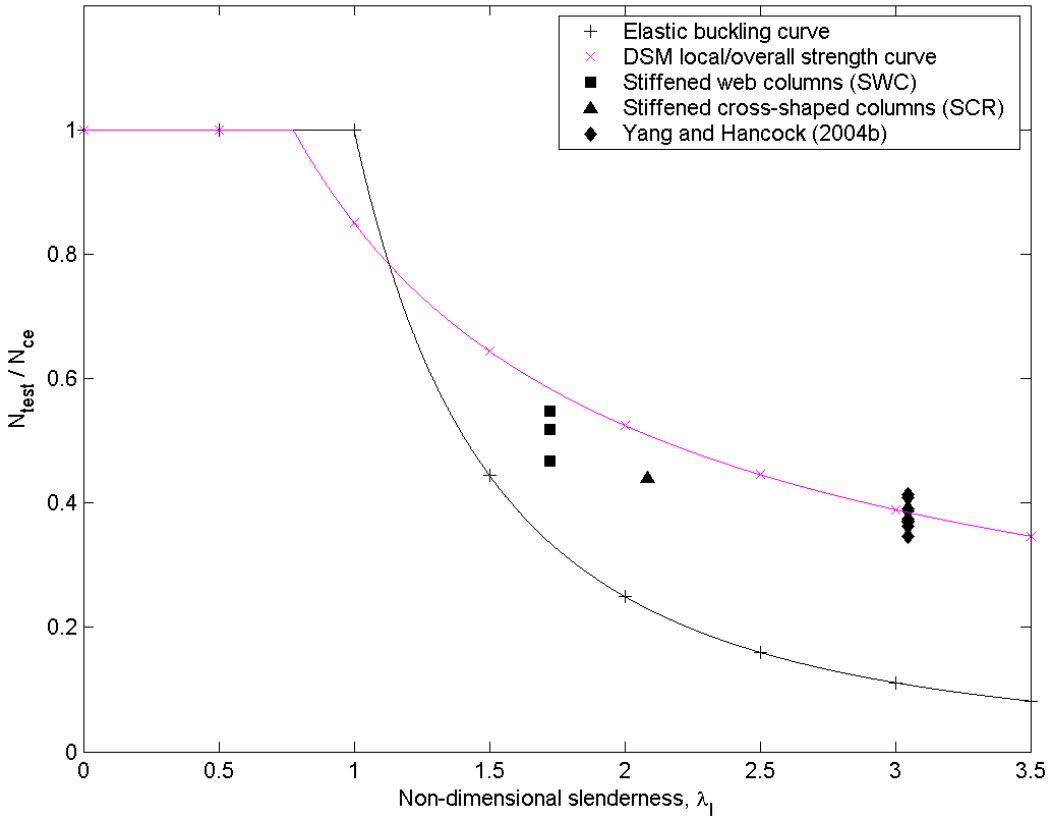

Fig. 13 Test results compared to non-dimensionalised local DSM strength curve

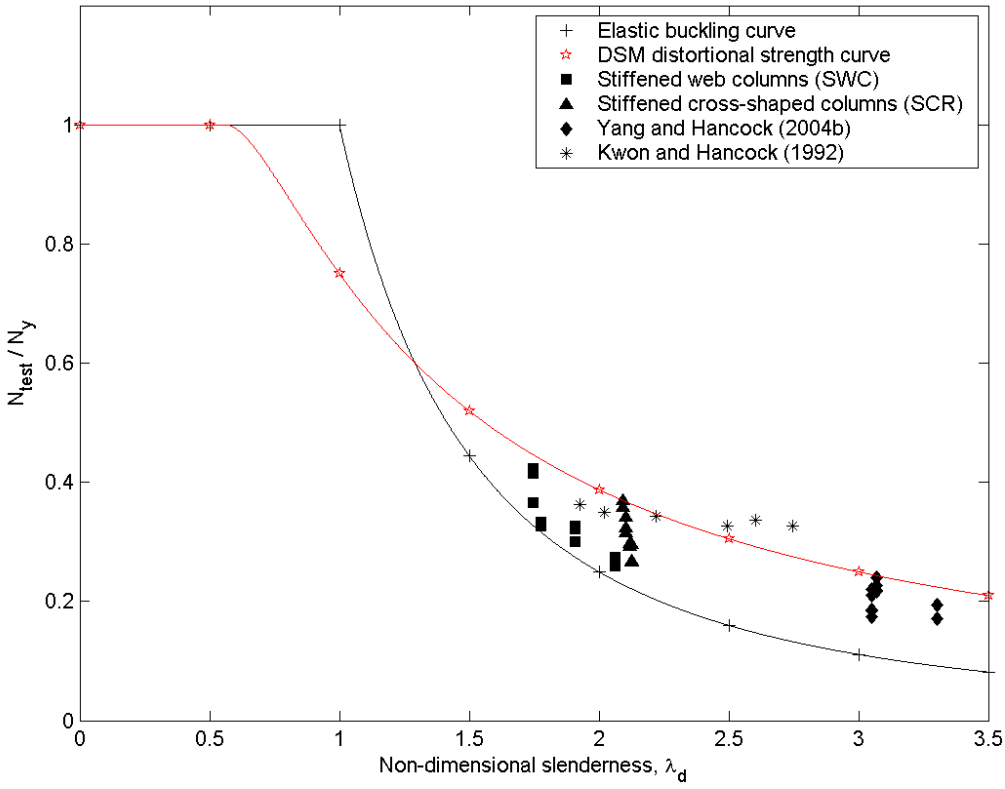

Fig. 14 Test results compared to non-dimensionalised distortional DSM strength curve

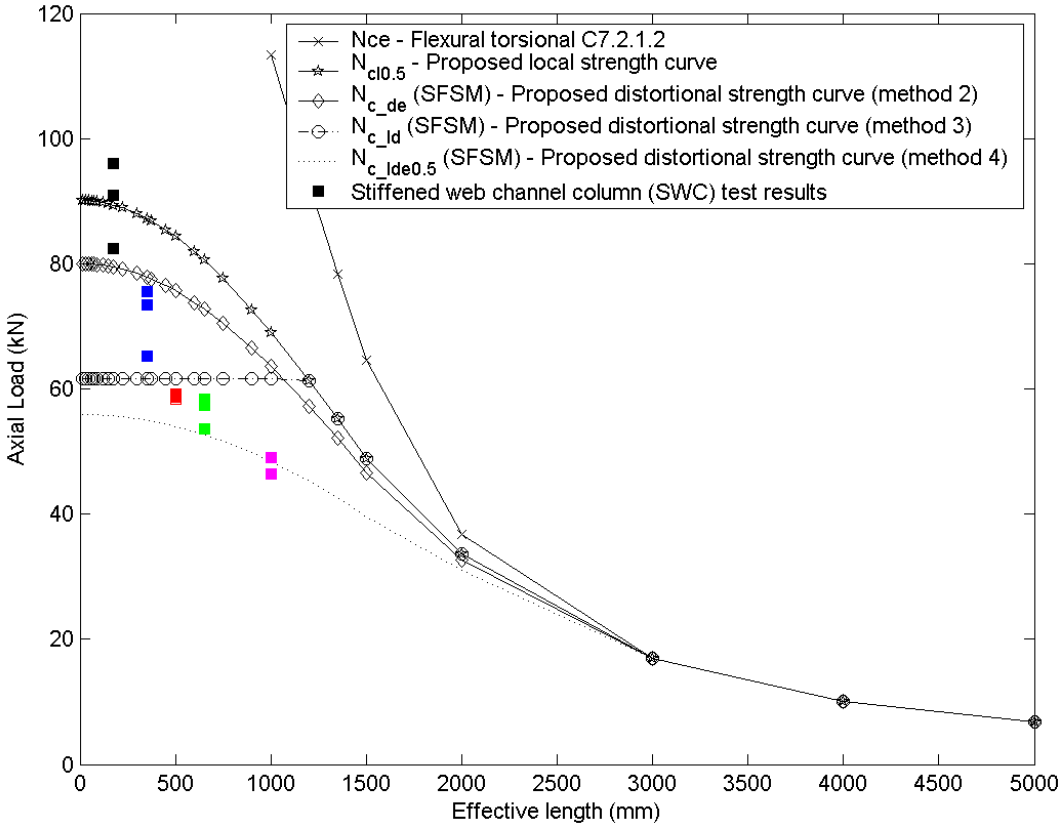

Fig. 15 Comparison of proposed design method and test results

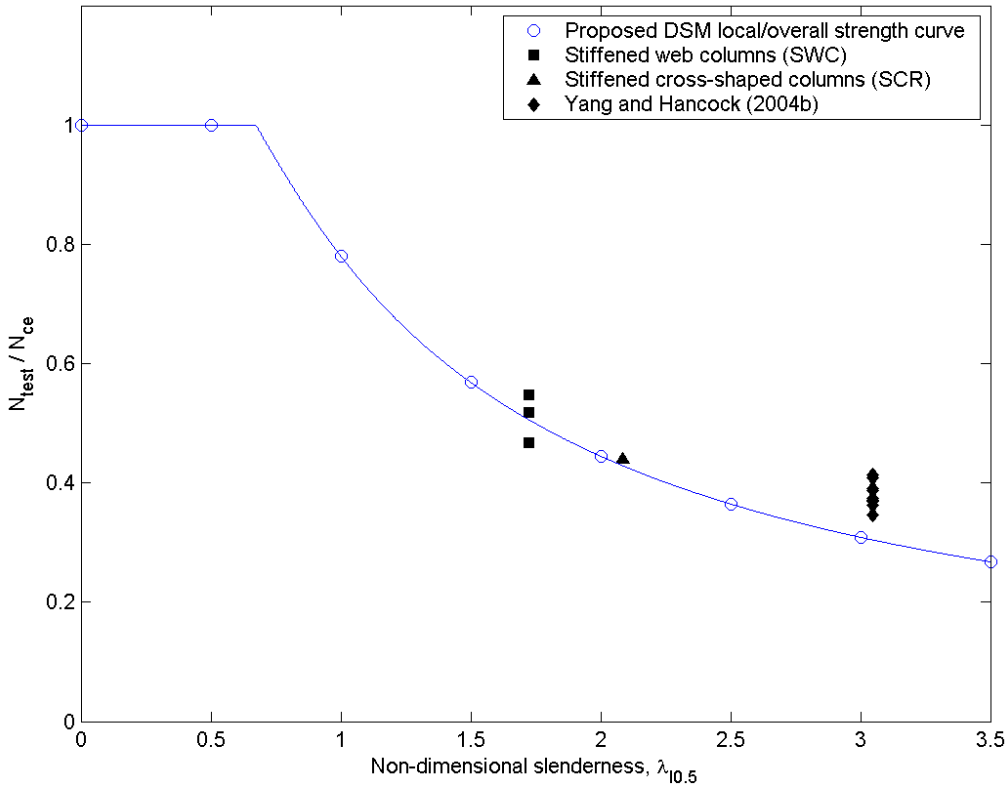

Fig. 16 Test results compared to proposed local/overall DSM strength curve

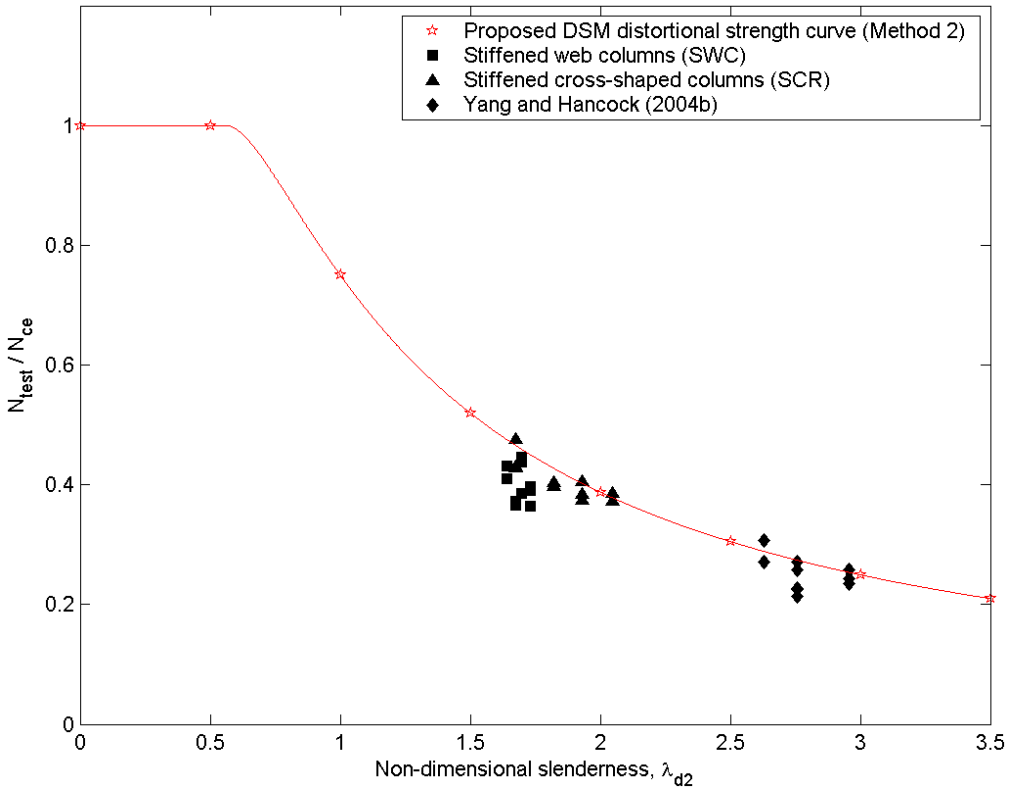

Fig. 17 Test results compared to proposed distortional DSM strength curve (Method 2)

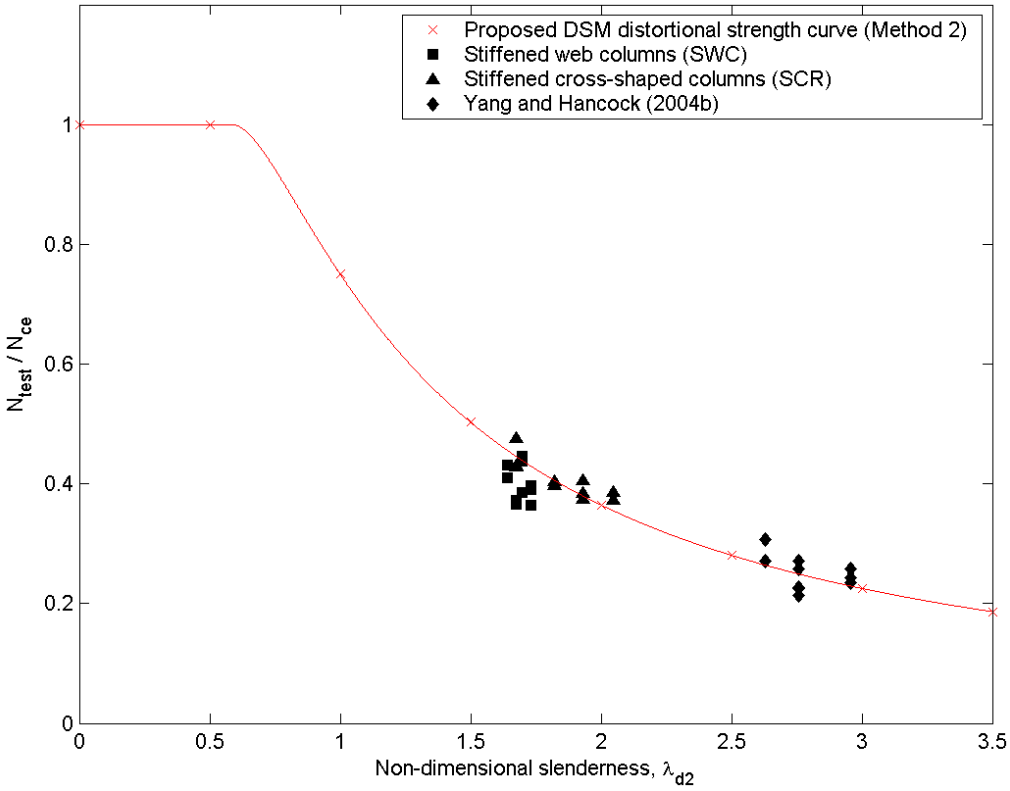

Fig. 18 Test results compared to proposed distortional DSM strength curve (Adjusted Method 2)

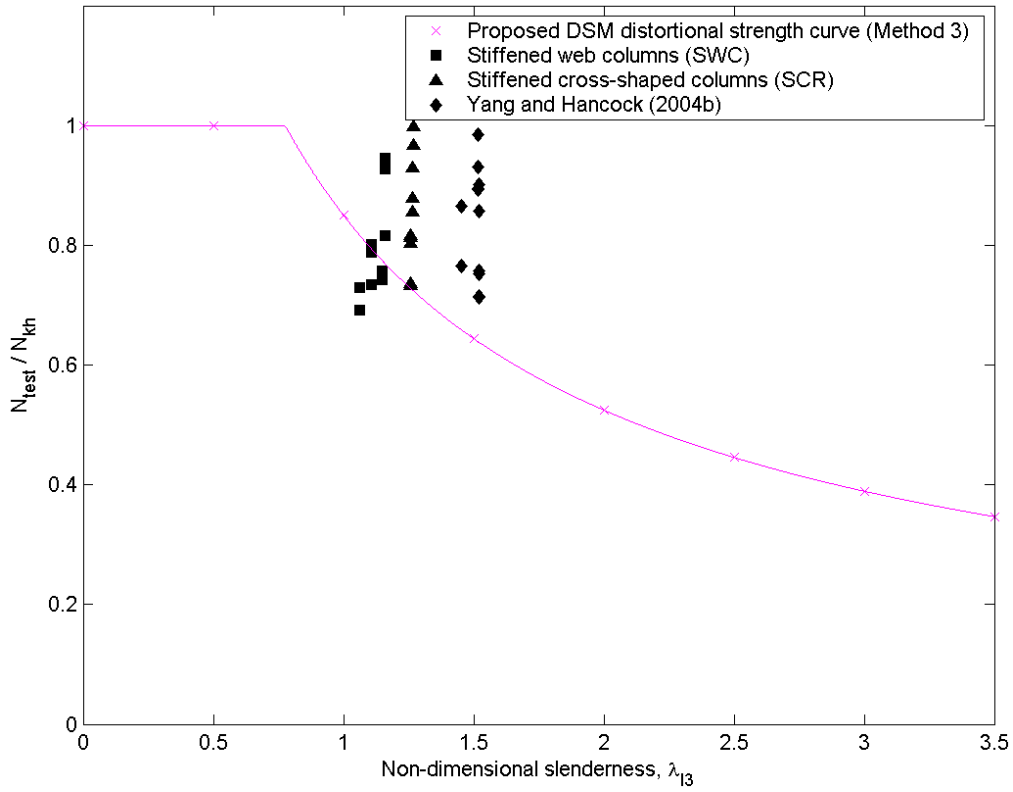

Fig. 19 Test results compared to proposed distortional DSM strength curve (Method 3)

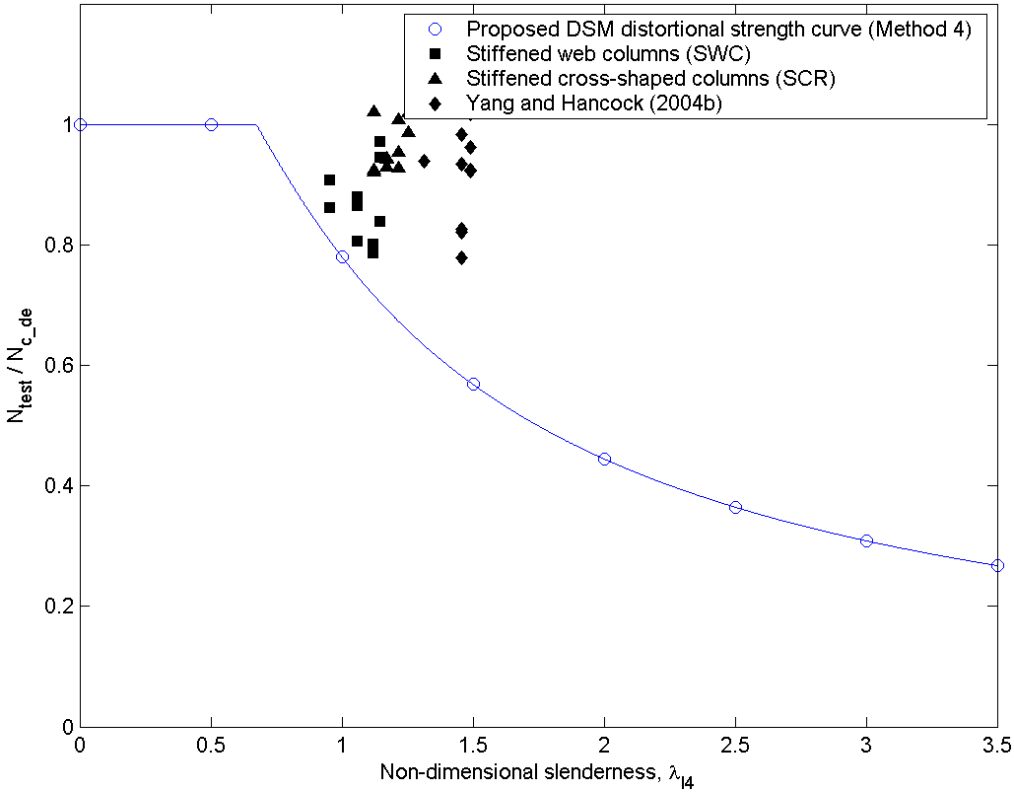

Fig. 20 Test results compared to proposed distortional DSM strength curve (Method 4)

APPENDIX A

Geometric and Imperfection Measurements

Appendix A contains the measured geometric imperfections for the stiffened-web channel column section specimens. This includes the measured geometries of each of the specimens, with the flanges labelled 'F' and the depth measured as 'Δ'. The imperfection measurements for each specimen are also included and the locations of the measurements are indicated by the arrows on the figure provided.

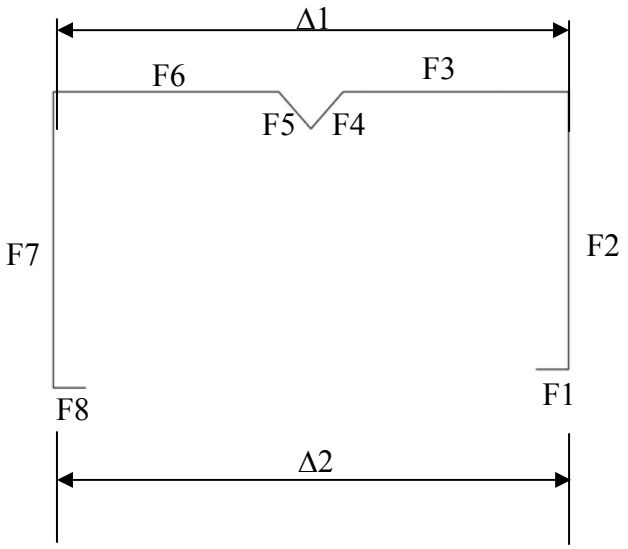

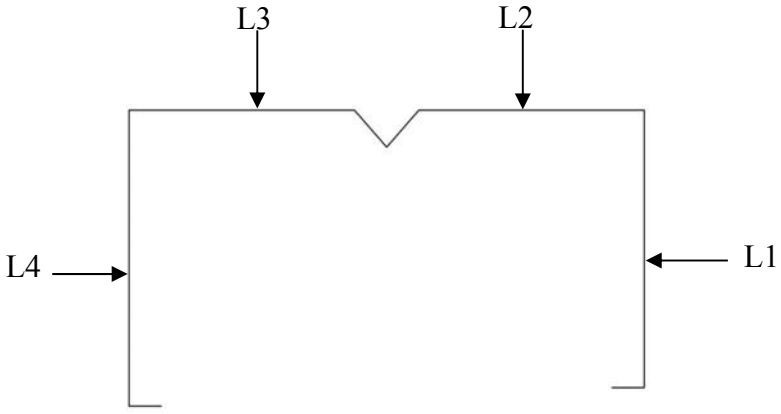

Table A 1 Geometric measurements of SWC 350 mm specimens

	F1	F2	F3	F4	F5	F6	F7	F8	Δ1	Δ2
350_1 (top)	12.05	64.73	49.07	14.05	14.1	49.36	64.64	12.0	119.3	119.51
350_1 (bot)	12.11	64.7	49.27	14.3	14.7	49.27	64.54	12.11	119.34	118.3
350_1 (avg)	12.08	64.72	49.17	14.18	14.4	49.32	64.59	12.06	119.32	118.91
350_2 (top)	12.15	64.67	49.53	14.3	14.46	49.7	64.51	12	119.5	117.41
350_2 (bot)	12.02	64.69	49.67	14.29	14.57	49.79	64.52	12.06	119.43	118.67
350_2 (avg)	12.09	64.68	49.6	14.30	14.52	49.74	64.51	12.03	119.47	118.04
350_3 (top)	12.11	64.65	49.7	14.07	14.29	49.6	64.51	11.99	119.25	117.52
350_3 (bot)	12.09	64.68	49.34	14.27	14.03	50.02	64.6	12.03	119.33	113.81
350_3 (avg)	12.1	64.66	49.52	14.17	14.16	49.81	64.55	12.01	119.29	115.67

(All dimensions are in mm)

Table A 2 Geometric measurements of SWC 700 mm specimens

	F1	F2	F3	F4	F5	F6	F7	F8	Δ1	Δ2
700_1 (top)	11.87	64.38	50.09	15.1	14.14	49.93	64.63	12.05	119.83	119.86
700_1 (bot)	12.16	64.66	49.81	14.86	14.6	50.03	64.4	11.81	119.76	120.64
700_1 (avg)	12.02	64.52	49.95	14.98	14.37	49.98	64.52	11.93	119.80	120.25
700_2 (top)	11.8	64.43	50.21	14.4	14.1	49.59	64.67	12.1	119.75	118.48
700_2 (bot)	12.1	64.68	50.05	14.21	14.38	50.04	64.4	11.8	119.54	118.0
700_2 (avg)	11.95	64.56	50.13	14.31	14.24	49.82	64.54	11.95	119.65	118.24
700_3 (top)	11.81	64.4	49.99	15.15	14.11	49.93	64.71	12.15	119.85	119.67
700_3 (bot)	12.18	64.63	49.95	14.35	14.3	50.02	64.47	11.85	119.36	120.69
700_3 (avg)	12.0	64.52	49.97	14.75	14.21	49.98	64.59	12.0	119.61	120.18

(All dimensions are in mm)

Table A 3 Geometric measurements of SWC 1000 mm specimens

	F1	F2	F3	F4	F5	F6	F7	F8	Δ1	Δ2
1000_1 (top)	11.66	64.13	50.16	15.31	14.55	49.95	64.64	12.05	121.55	123.91
1000_1 (bot)	12.06	64.56	49.62	14.6	15.17	50.21	64.31	11.41	121.3	122.11
1000_1 (avg)	11.86	64.35	49.89	14.96	14.86	50.08	64.48	11.73	121.43	123.01
1000_2 (top)	11.78	64.46	50.46	14.05	15.02	50.01	64.37	12.08	120.41	122.33
1000_2 (bot)	11.93	64.4	49.78	13.98	14.81	50.03	64.39	11.8	120.02	117.08
1000_2 (avg)	11.86	64.43	50.12	14.02	14.92	50.02	64.38	11.94	120.22	119.71
1000_3 (top)	11.98	64.38	49.8	14.06	14.65	49.69	64.37	11.83	120.01	115.87
1000_3 (bot)	12.1	64.47	49.63	13.99	14.77	50.19	64.34	11.8	120.19	119.68
1000_3 (avg)	12.04	64.43	49.72	14.03	14.71	49.94	64.36	11.82	120.1	117.78

(All dimensions are in mm)

Table A 4 Geometric measurements of SWC 1300 mm specimens

	F1	F2	F3	F4	F5	F6	F7	F8	Δ1	Δ2
1300_1 (top)	11.67	64.26	50.57	14.92	13.98	49.7	64.76	12.07	120.07	119.86
1300_1 (bot)	12.13	64.56	49.74	14.57	14.58	50.08	64.43	11.86	120.02	119.53
1300_1 (avg)	11.9	64.41	50.16	14.75	14.28	49.89	64.60	11.97	120.05	119.70
1300_2 (top)	11.71	64.15	50.49	14.29	14.23	50.41	64.61	12.01	120.17	118.43
1300_2 (bot)	11.99	64.53	49.98	13.74	15.24	50.41	64.13	11.78	120.39	118.1
1300_2 (avg)	11.85	64.34	50.24	14.02	14.74	50.41	64.37	11.90	120.28	118.27
1300_3 (top)	11.71	64.33	50.29	14.39	14.51	49.63	64.4	12.5	120.01	120.91
1300_3 (bot)	11.93	64.35	50.29	13.87	14.98	50.1	64.24	11.69	120.47	119.42
1300_3 (avg)	11.82	64.34	50.29	14.13	14.75	49.87	64.32	12.10	120.24	120.17

(All dimensions are in mm)

Table A 5 Geometric measurements of SWC 2000 mm specimens

	F1	F2	F3	F4	F5	F6	F7	F8	Δ1	Δ2
2000_1 (top)	11.84	64.34	50.08	14.7	15.11	49.83	64.62	12.22	120.22	119.53
2000_1 (bot)	12.06	64.36	49.71	14.79	14.19	50.11	64.64	12.03	119.93	121.62
2000_1 (avg)	11.95	64.35	49.90	14.75	14.65	49.97	64.63	12.13	120.08	120.58
2000_2 (top)	12.1	64.62	50	14.3	14.77	49.48	64.56	12.01	119.88	126.29
2000_2 (bot)	11.77	64.56	49.32	14.16	15.15	49.93	64.32	11.89	120.33	122.98
2000_2 (avg)	11.94	64.59	49.66	14.23	14.96	49.71	64.44	11.95	120.11	124.64

(All dimensions are in mm)

A.1 Stiffened-web channel section with length 350 mm

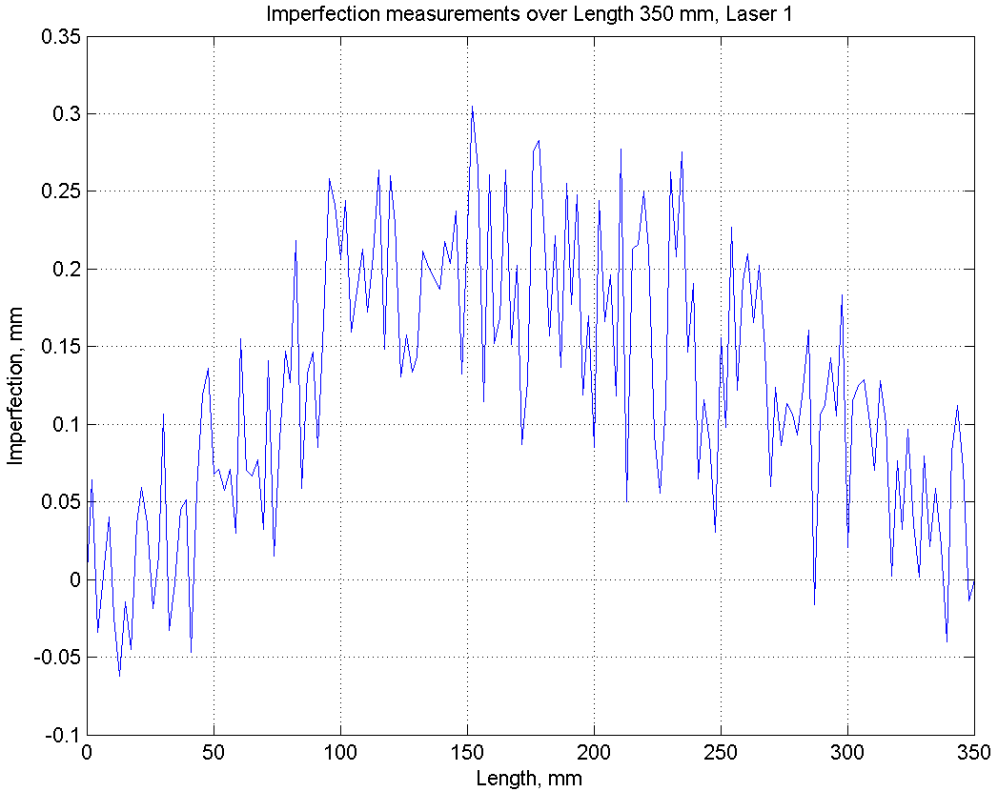

Figure A - 1 Imperfection measurement of SWC350_1 (Right flange)

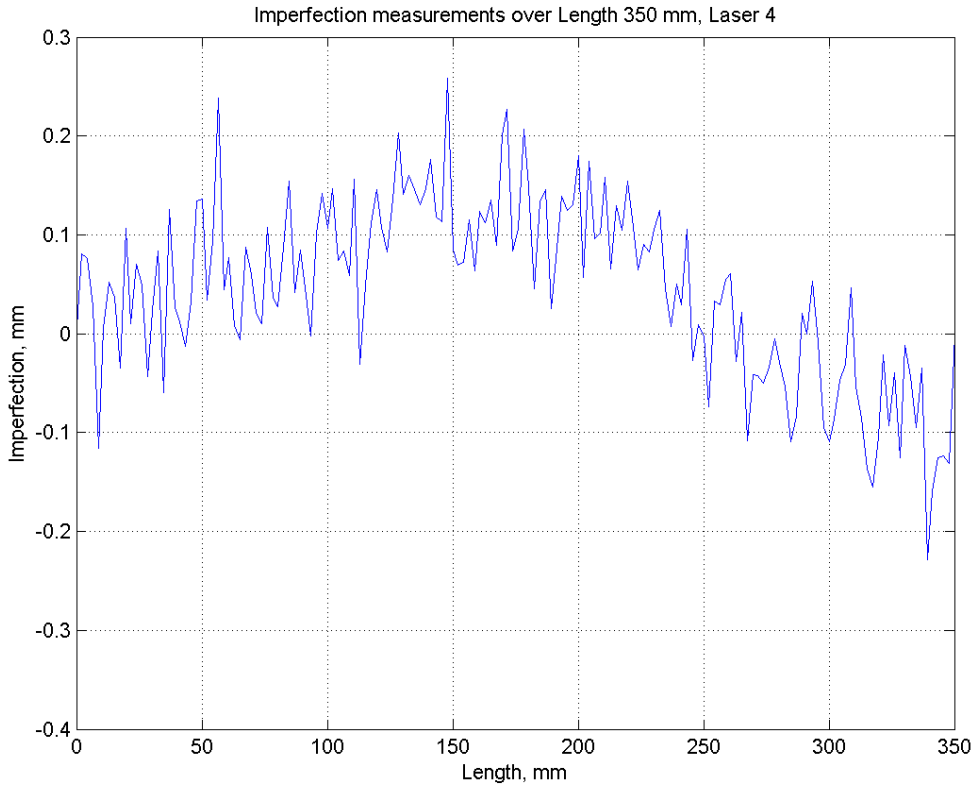

Figure A - 2 Imperfection measurement of SWC350_1 (Left flange)

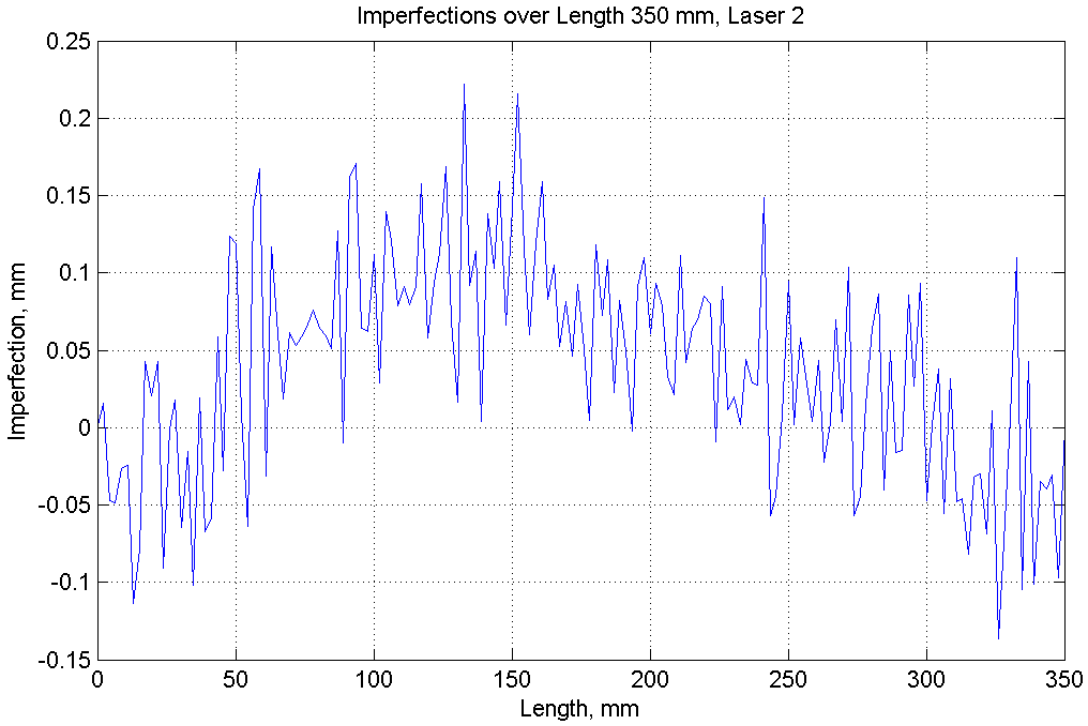

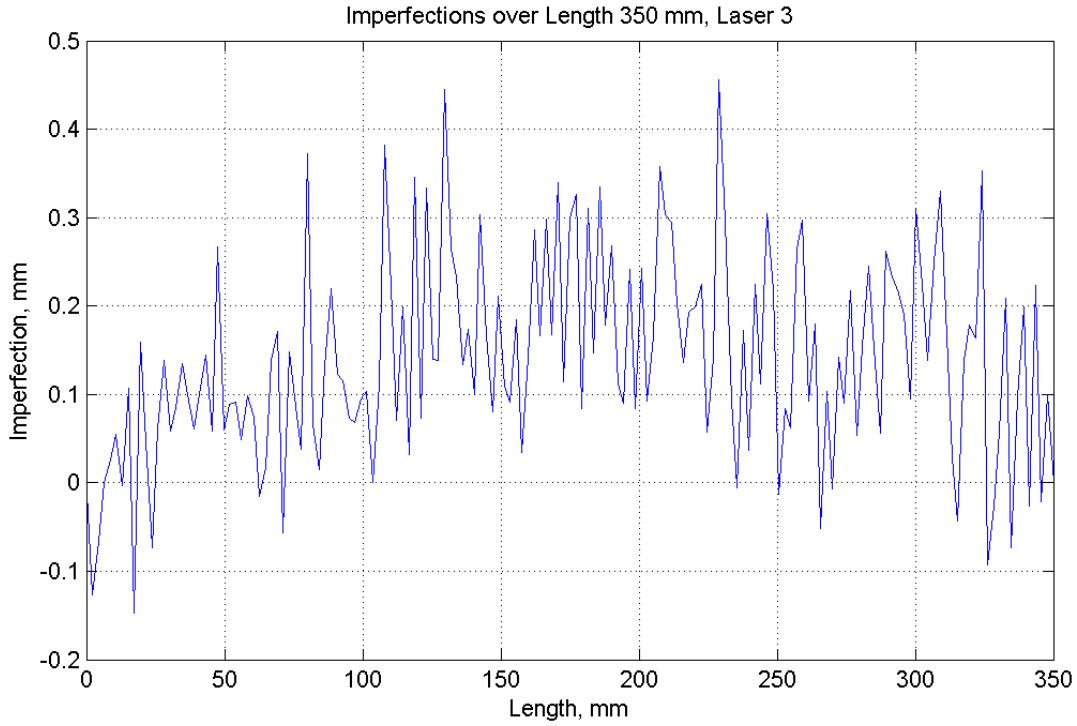

Figure A - 3 Imperfection measurement of SWC350_1 (Web)

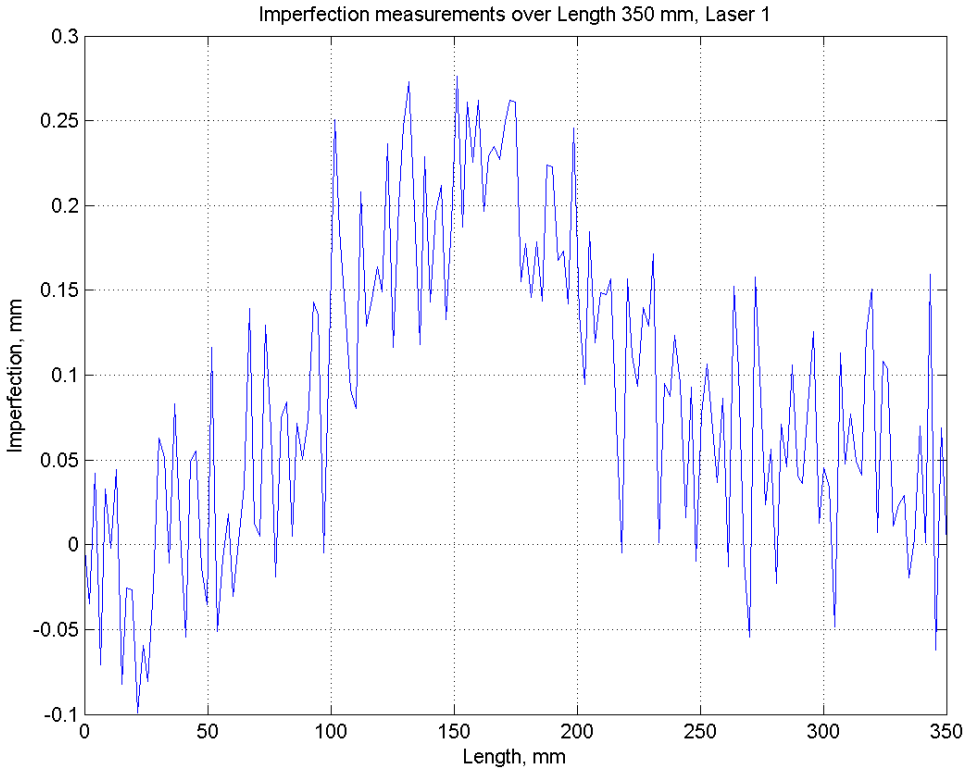

Figure A - 4 Imperfection measurement of SWC350_2 (Right flange)

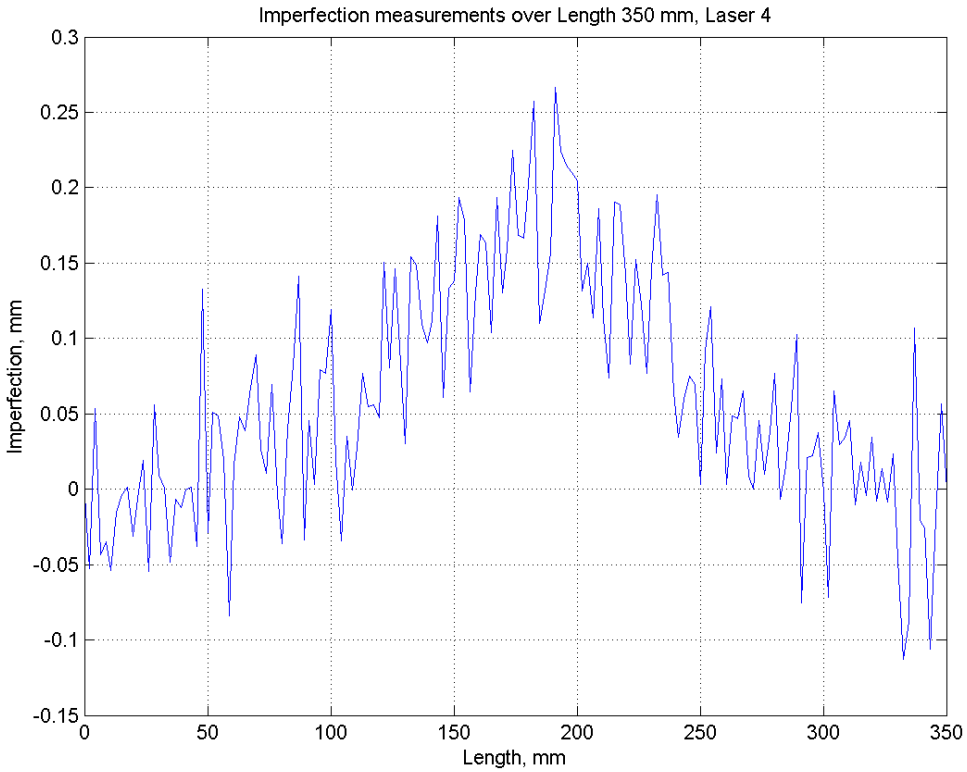

Figure A - 5 Imperfection measurement of SWC350_2 (Left flange)

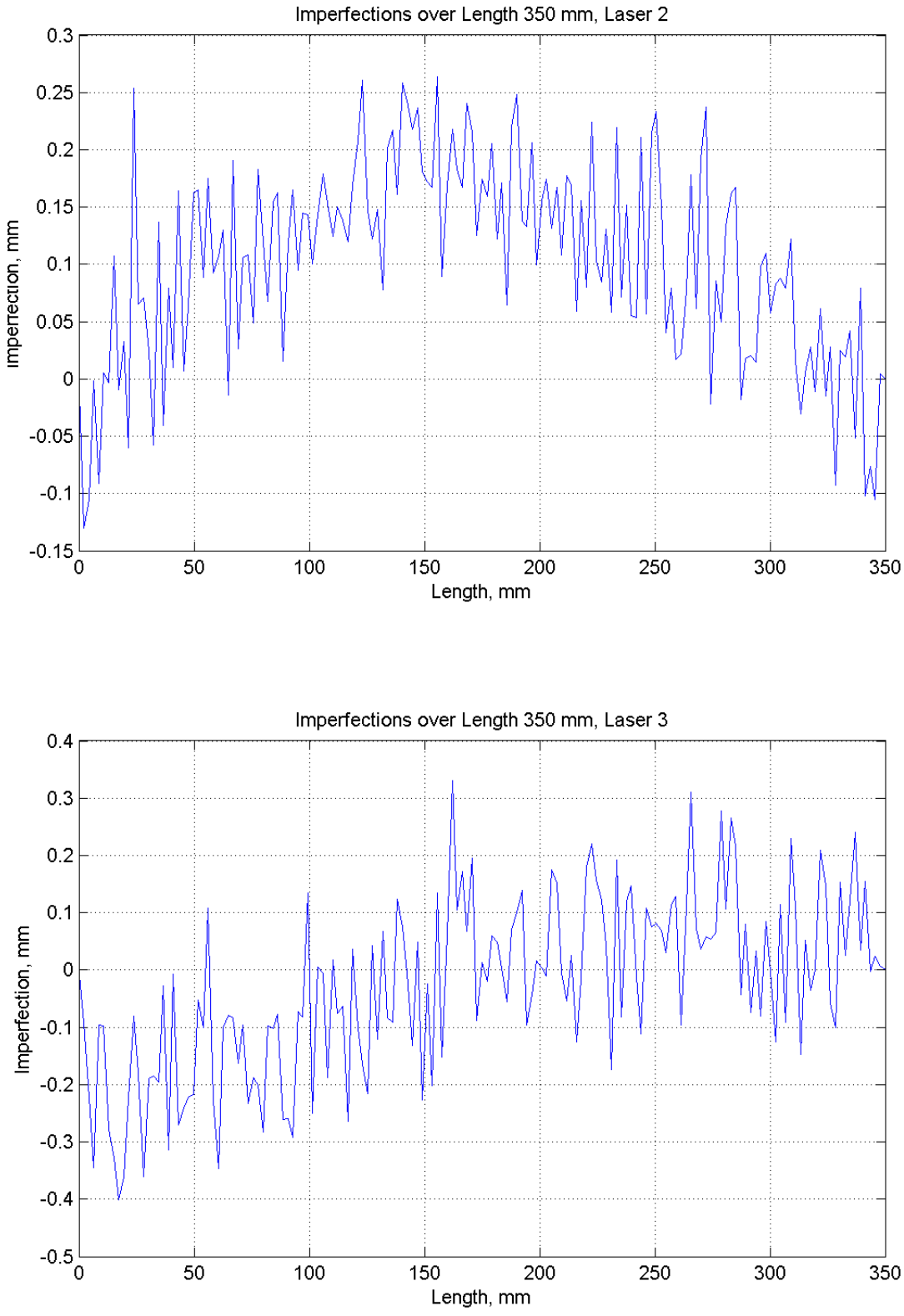

Figure A - 6 Imperfection measurement of SWC350_2 (Web)

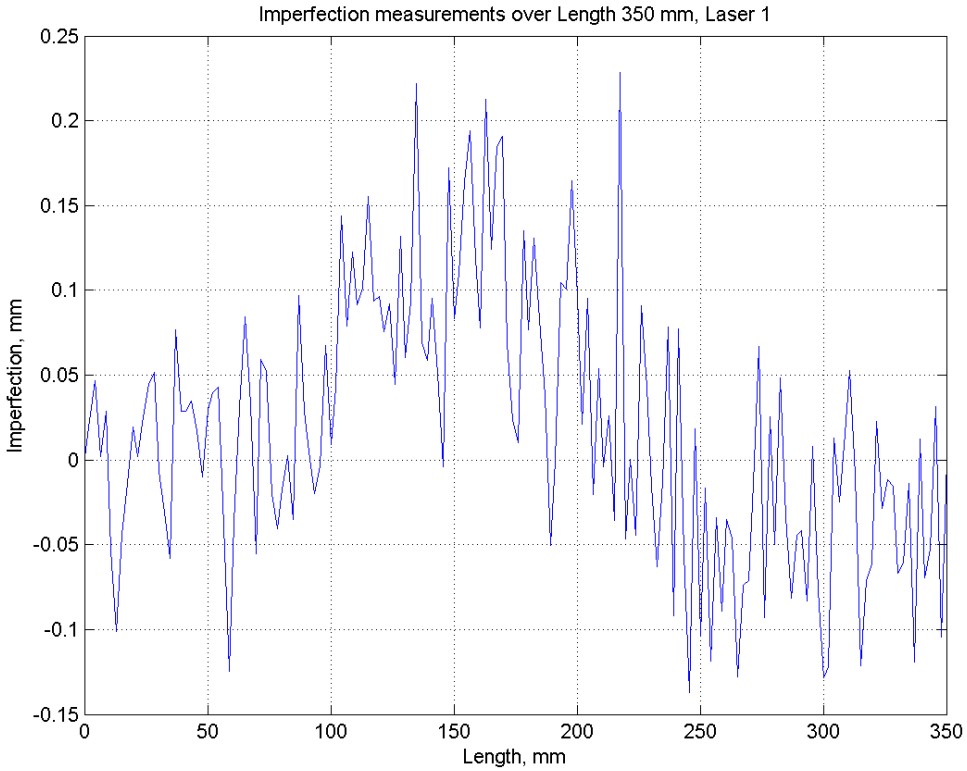

Figure A - 7 Imperfection measurement of SWC350_3 (Right flange)

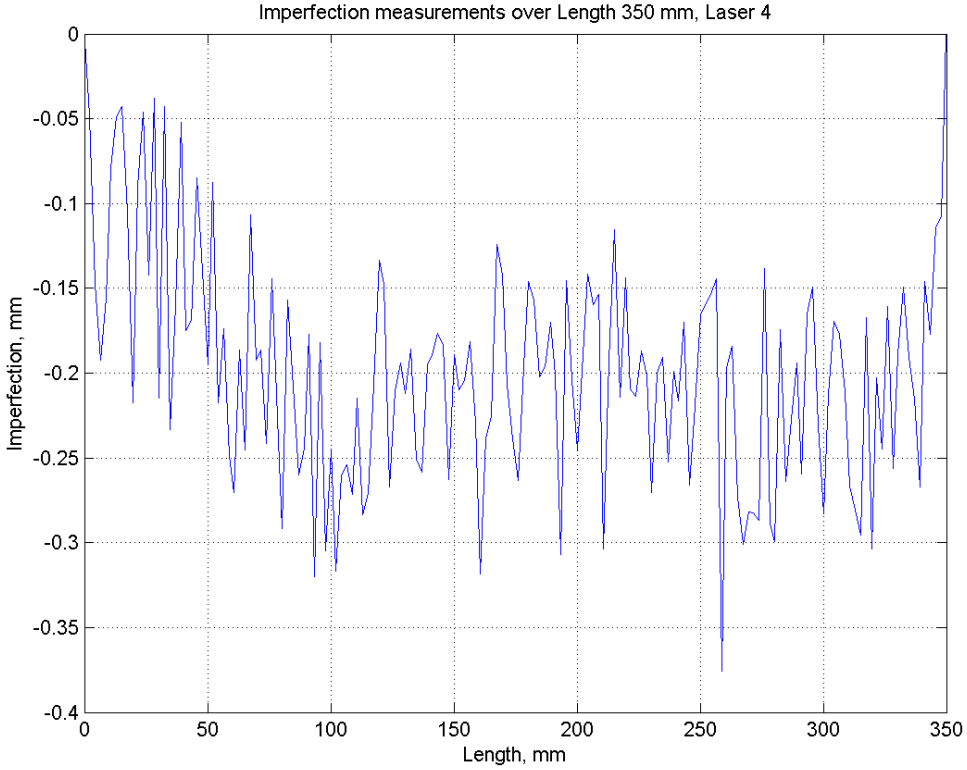

Figure A - 8 Imperfection measurement of SWC350_3 (Left flange)

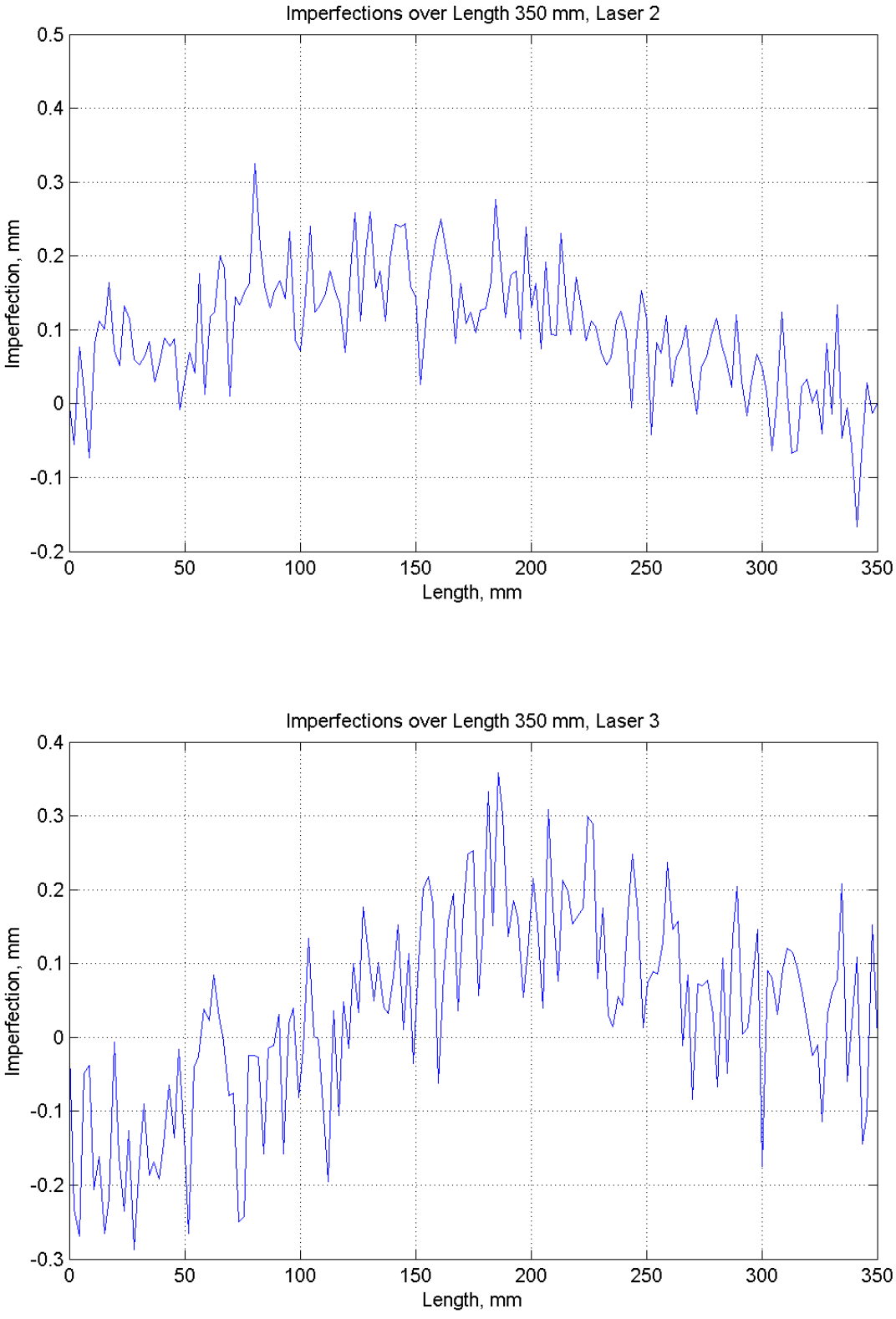

Figure A - 9 Imperfection measurement of SWC350_3 (Web)

A.2 Stiffened-web channel section with length 700 mm

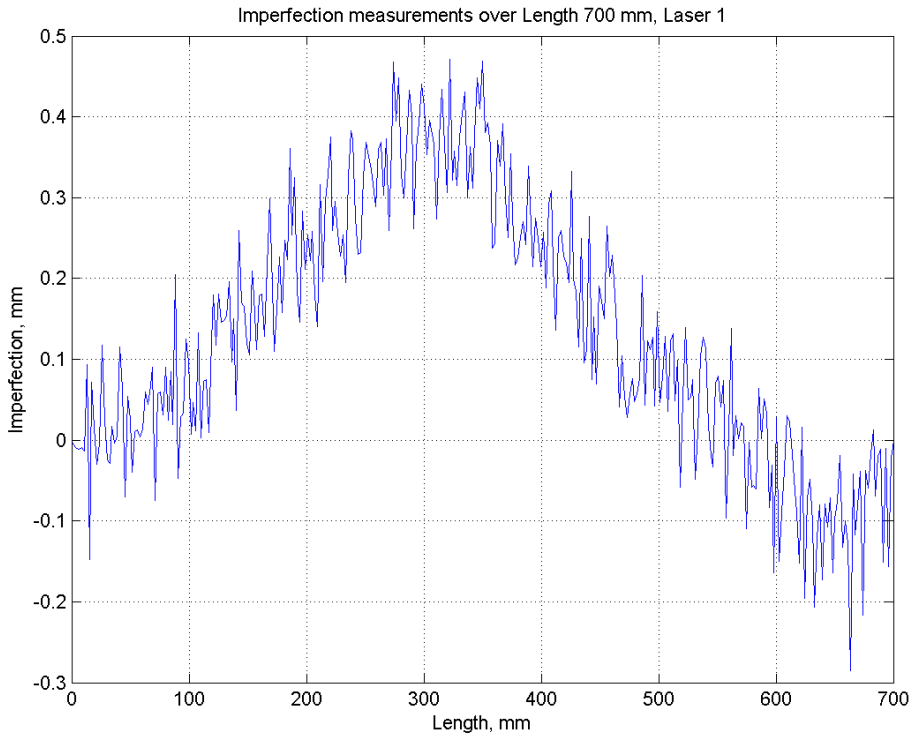

Figure A - 10 Imperfection measurement of SWC700_1 (Right flange)

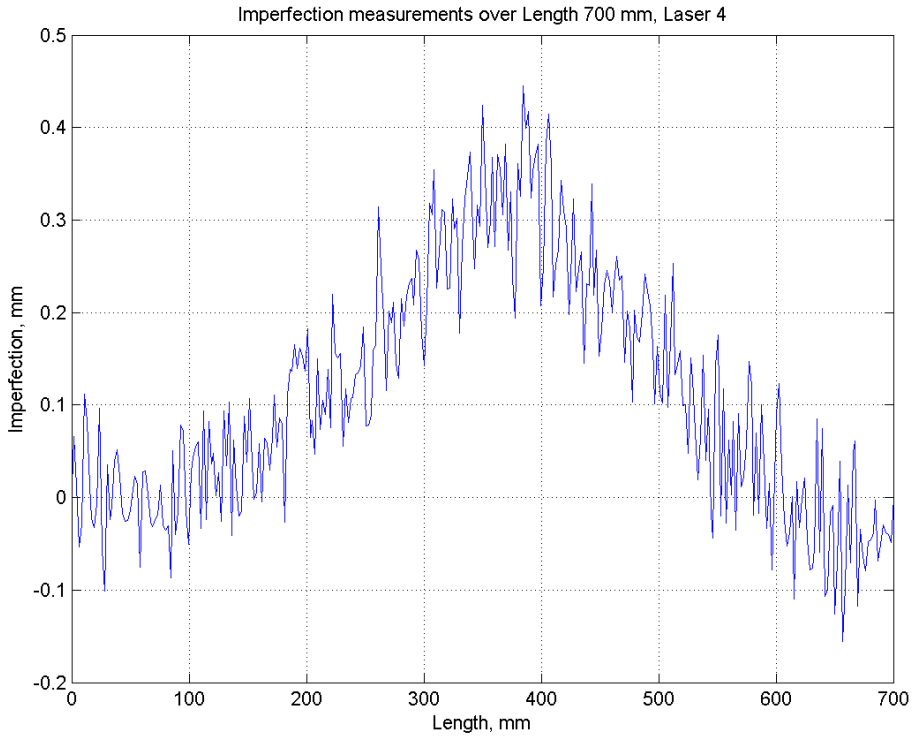

Figure A - 11 Imperfection measurement of SWC700_1 (Left flange)

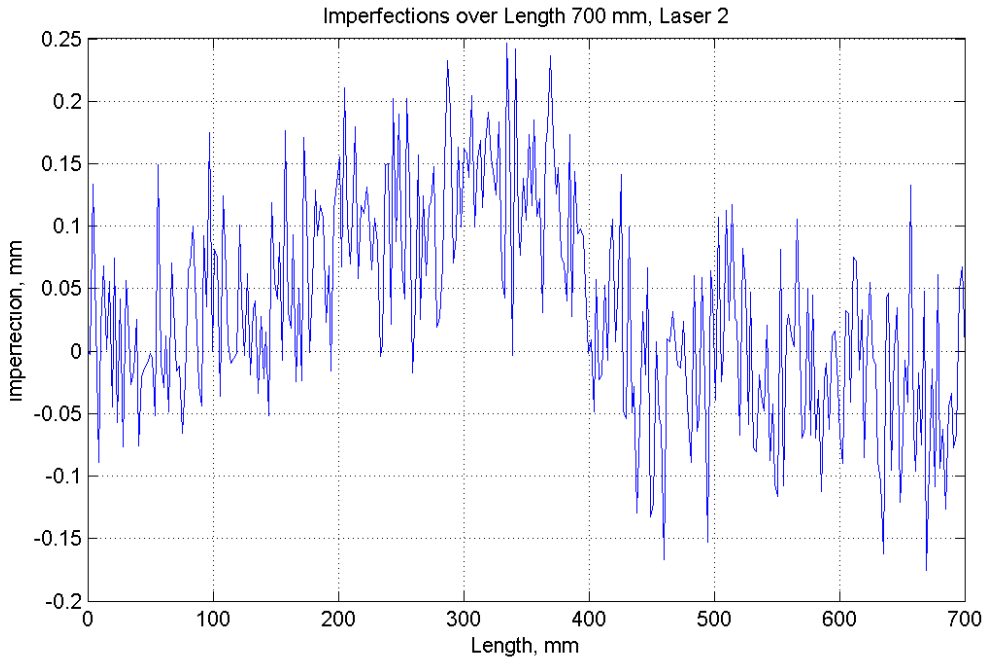

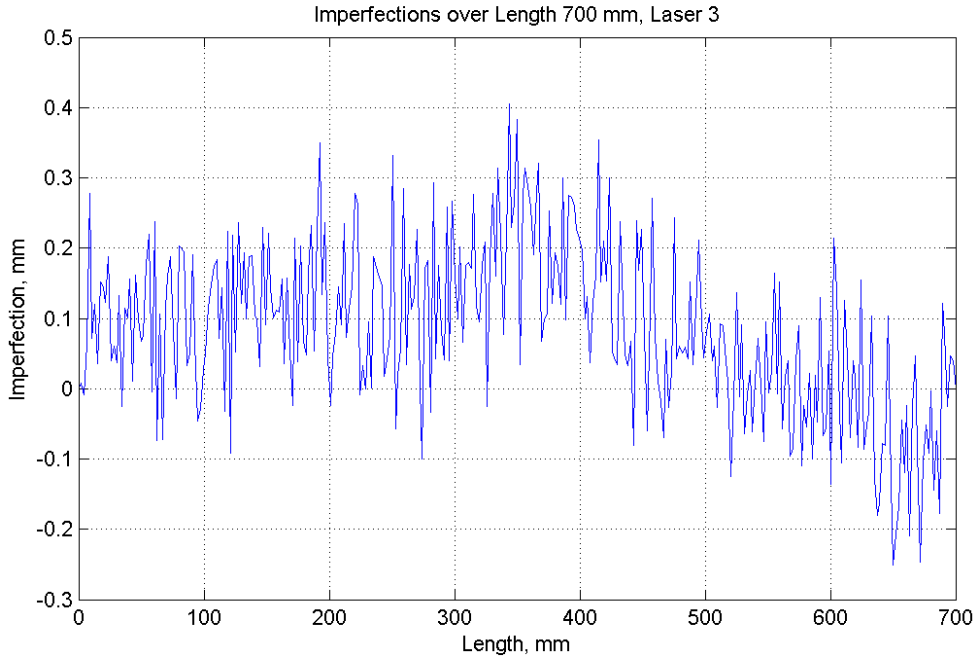

Figure A - 12 Imperfection measurement of SWC700_1 (Web)

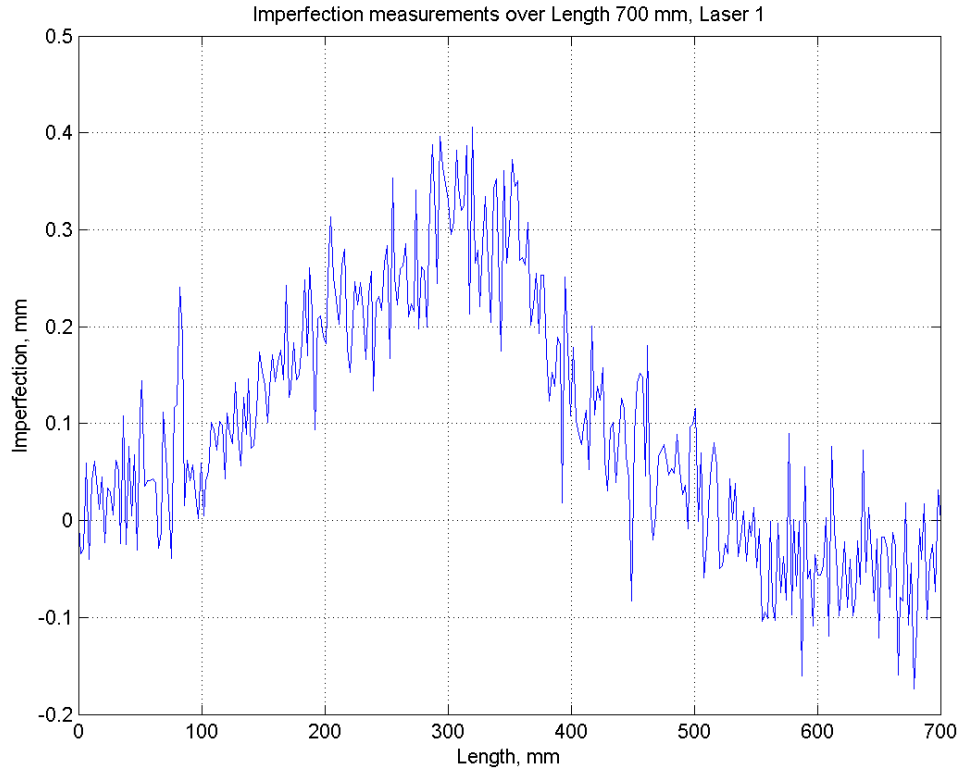

Figure A - 13 Imperfection measurement of SWC700_2 (Right flange)

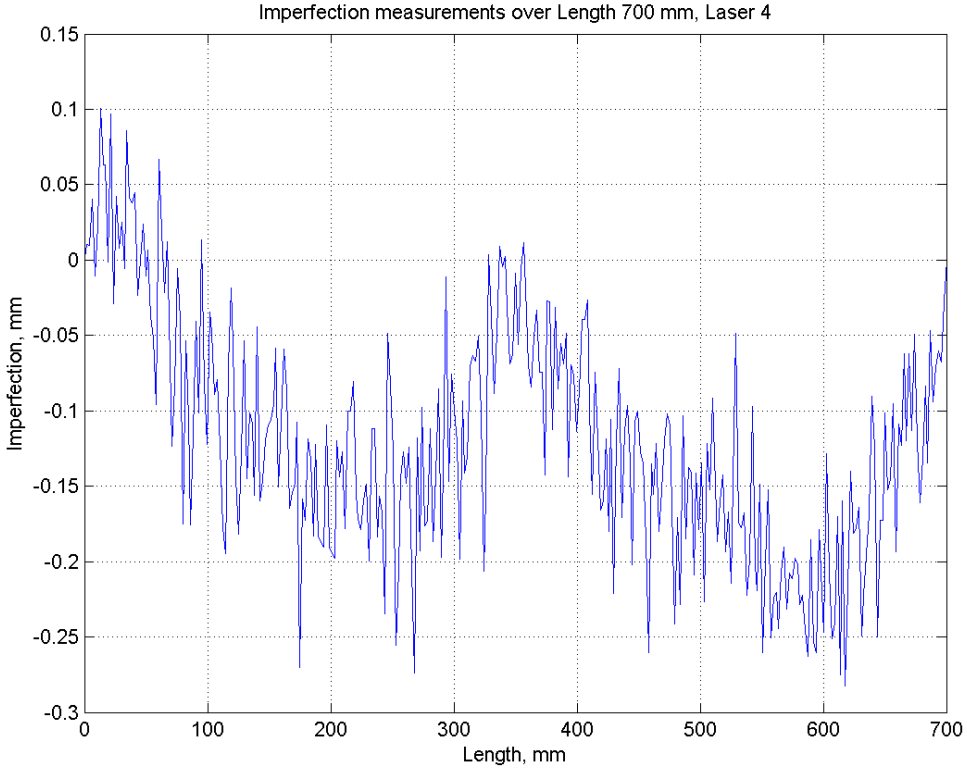

Figure A - 14 Imperfection measurement of SWC700_2 (Left flange)

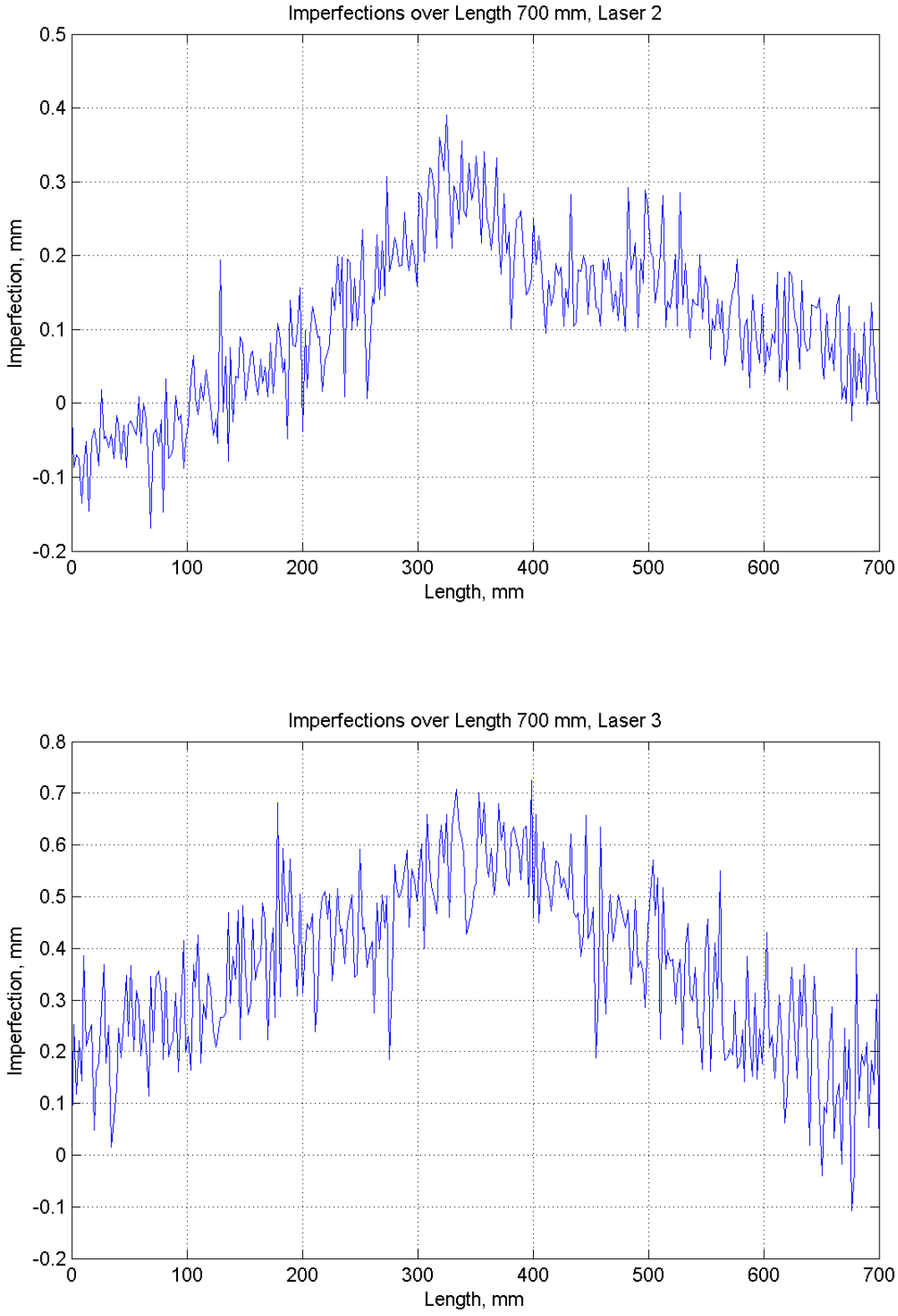

Figure A - 15 Imperfection measurement of SWC700_2 (Web)

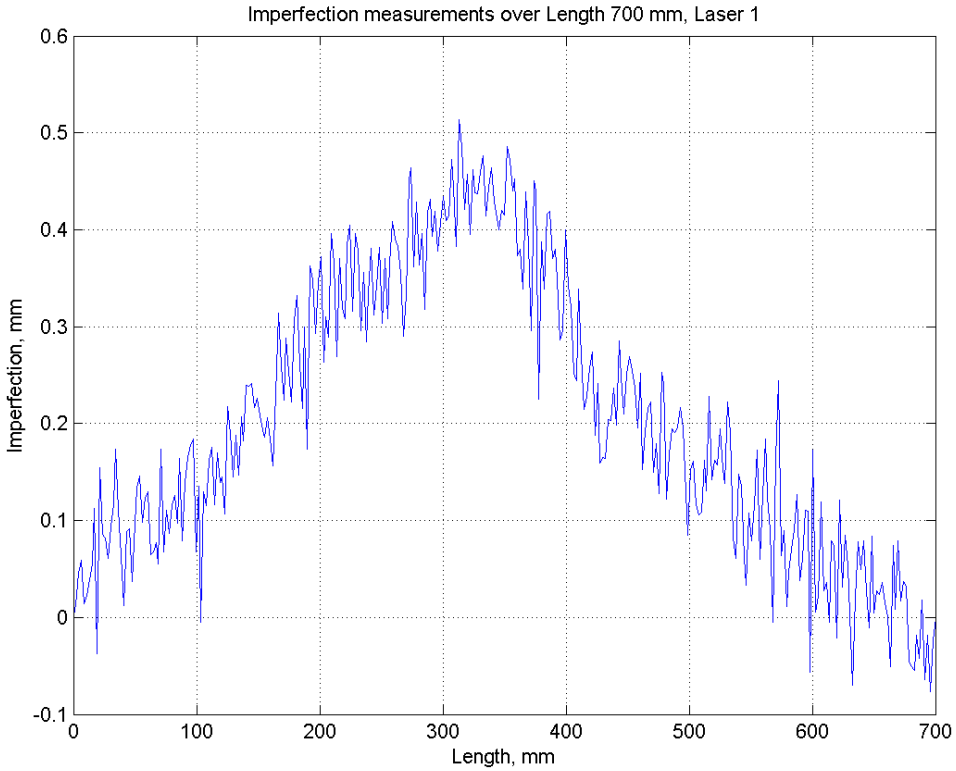

Figure A - 16 Imperfection measurement of SWC700_3 (Right flange)

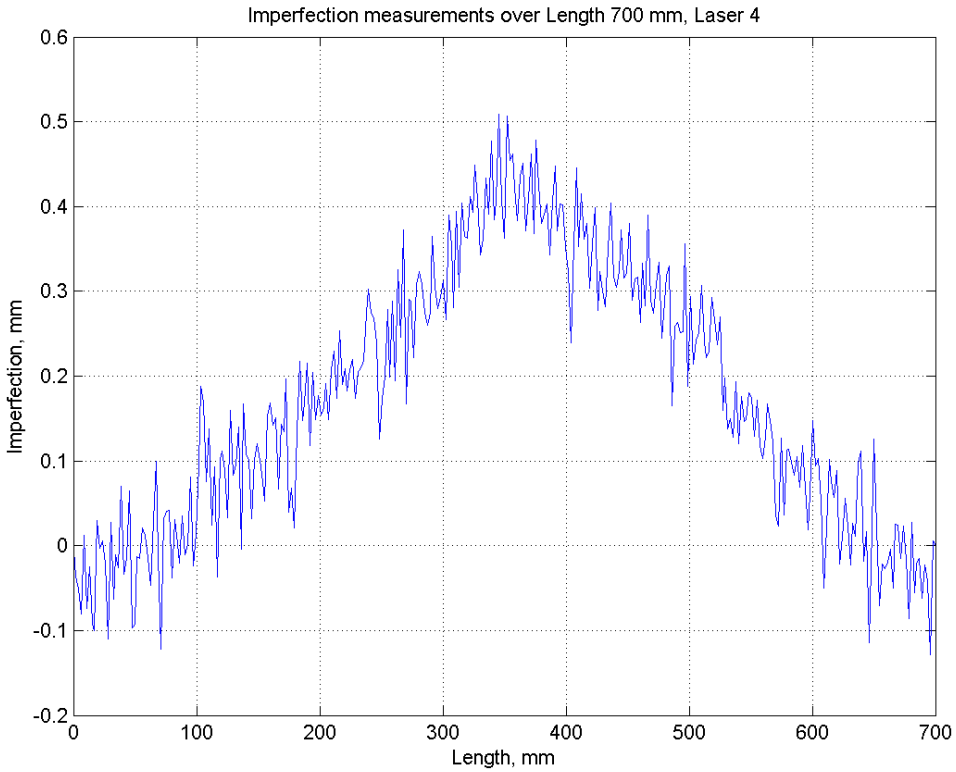

Figure A - 17 Imperfection measurement of SWC700_3 (Left flange)

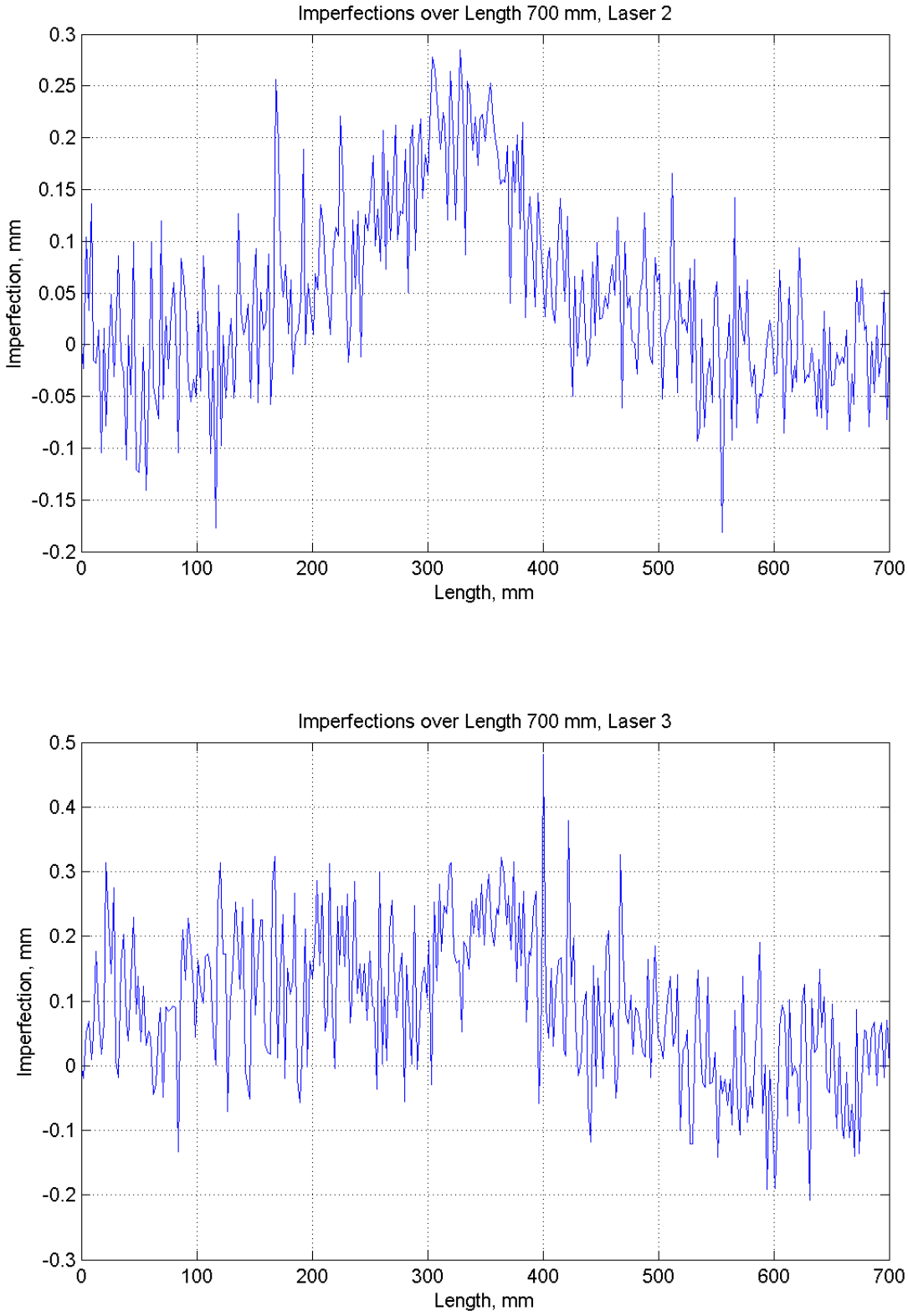

Figure A - 18 Imperfection measurement of SWC700_3 (Web)

A.3 Stiffened-web channel section with length 1000 mm

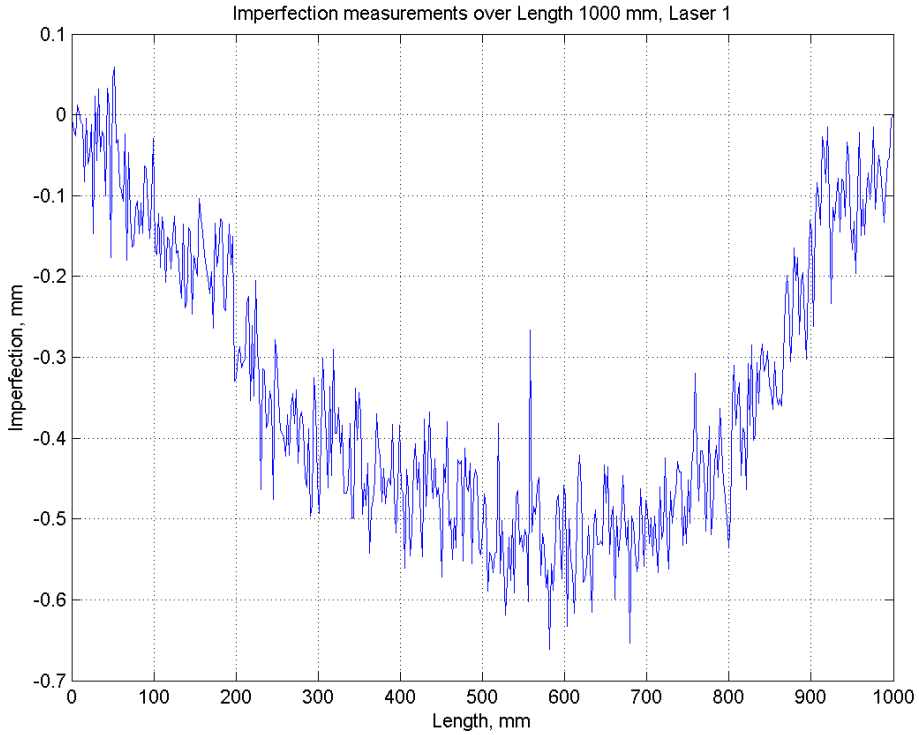

Figure A - 19 Imperfection measurement of SWC1000_1 (Right flange)

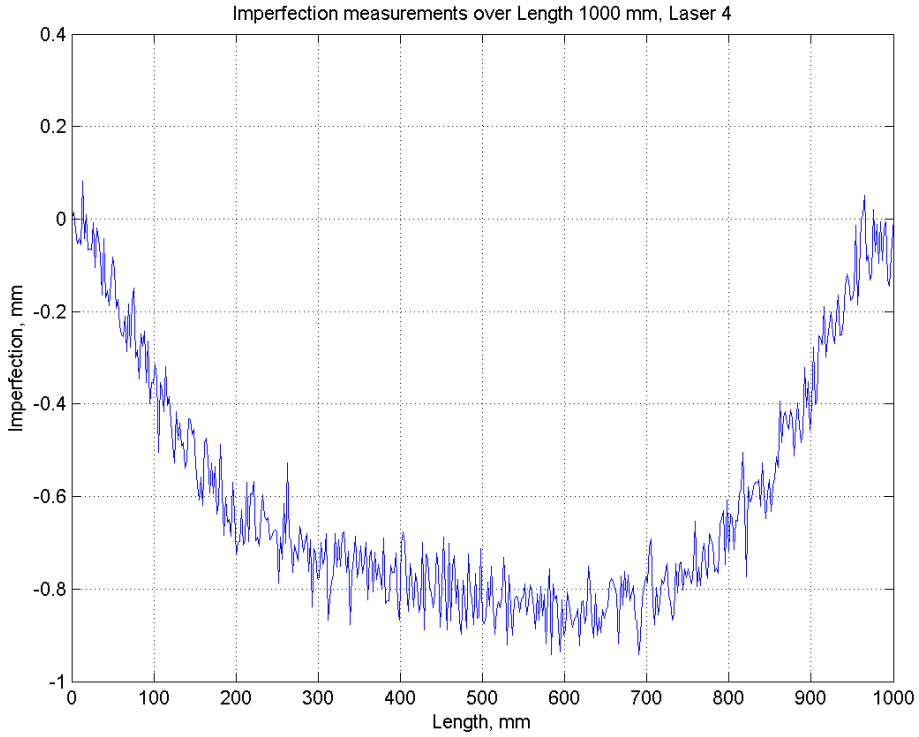

Figure A - 20 Imperfection measurement of SWC1000_1 (Left flange)

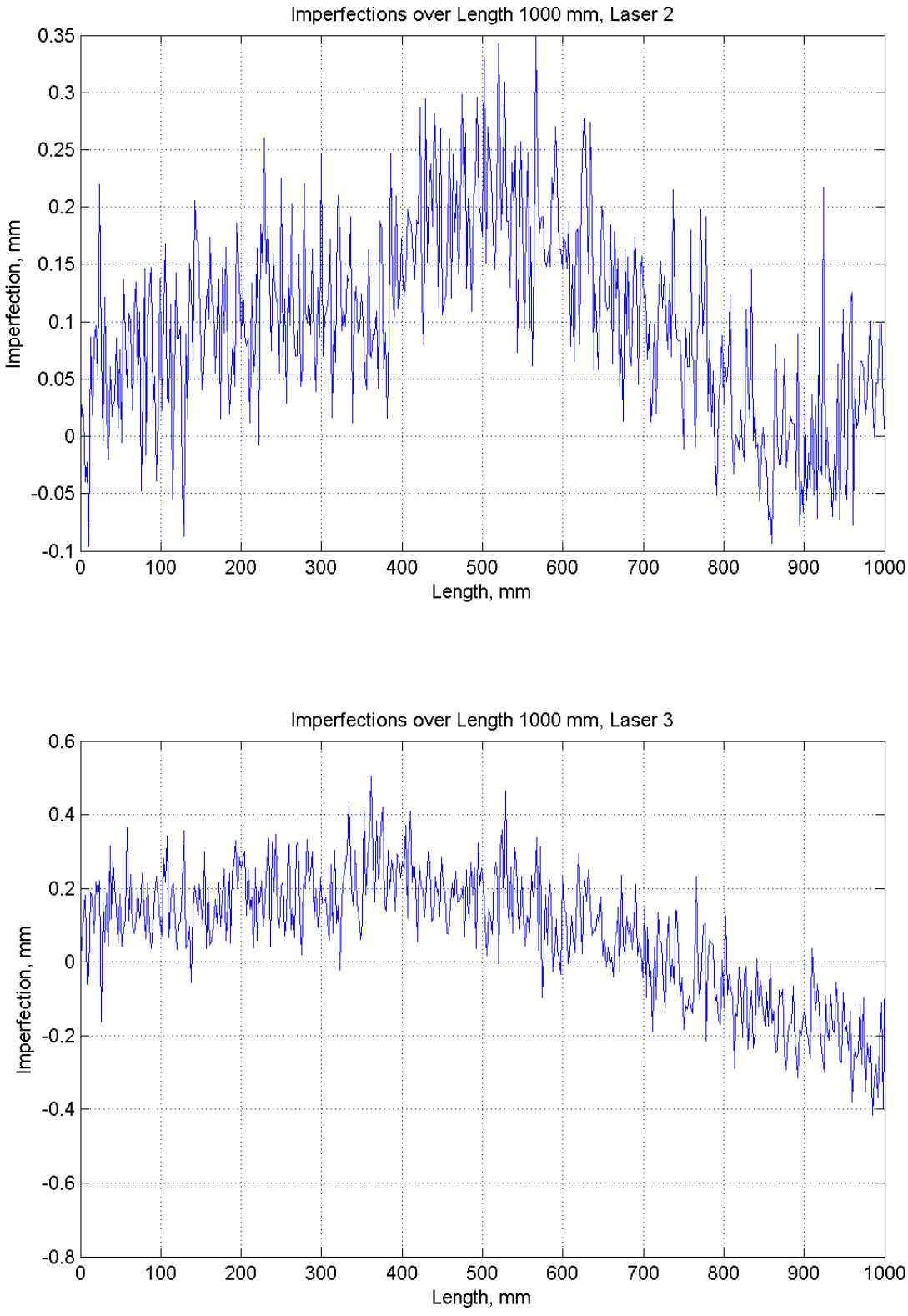

Figure A - 21 Imperfection measurement of SWC1000_1 (Web)

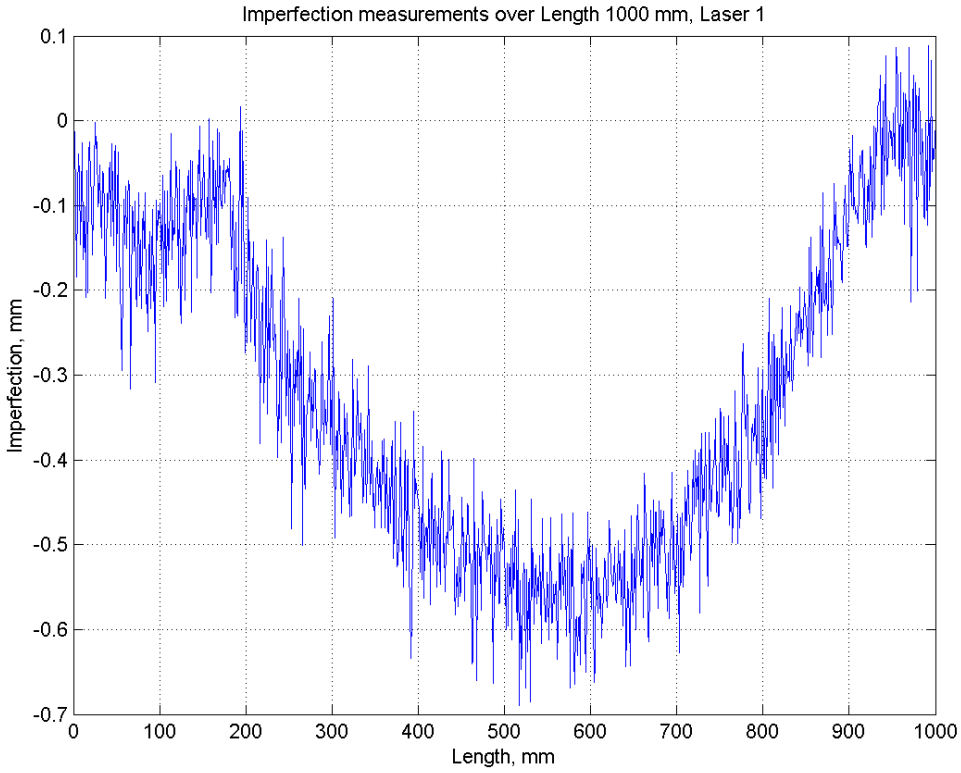

Figure A - 22 Imperfection measurement of SWC1000_2 (Right flange)

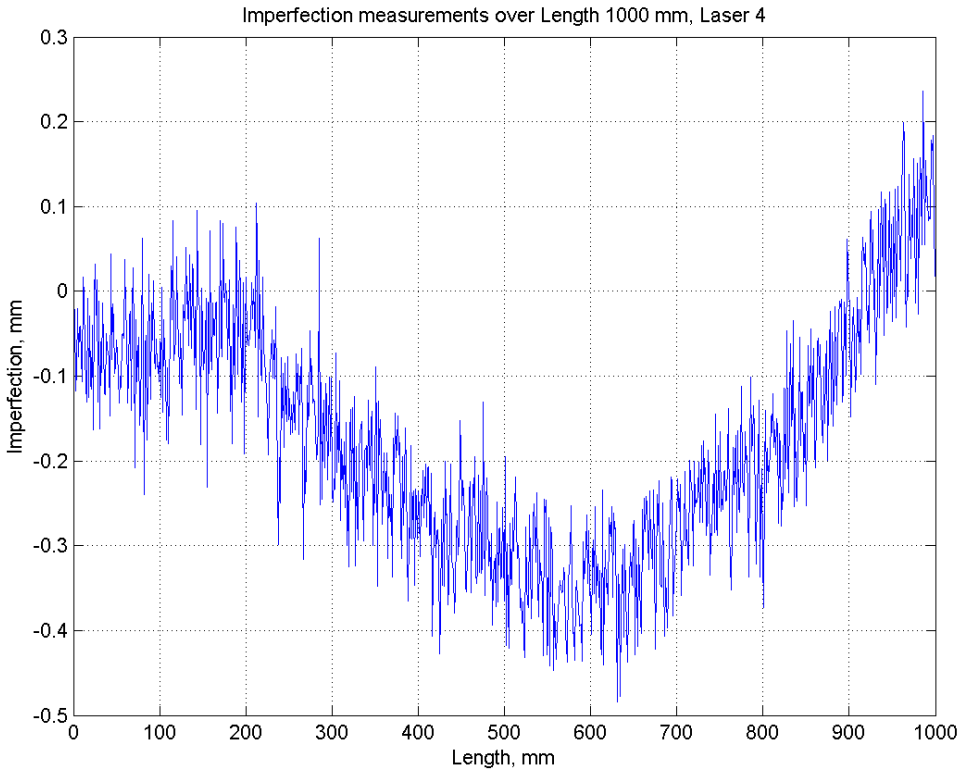

Figure A - 23 Imperfection measurement of SWC1000_2 (Left flange)

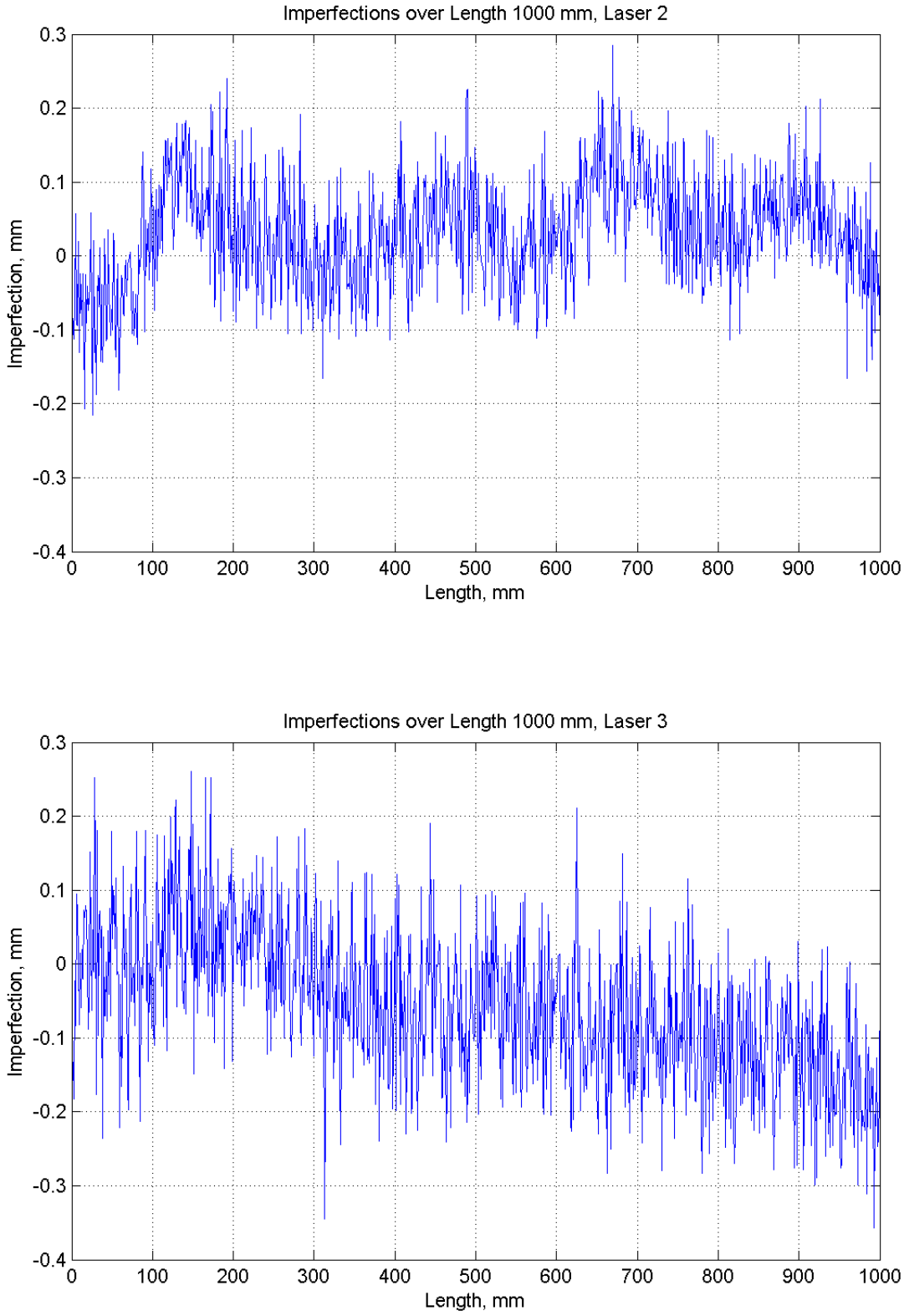

Figure A - 24 Imperfection measurement of SWC1000_2 (Web)

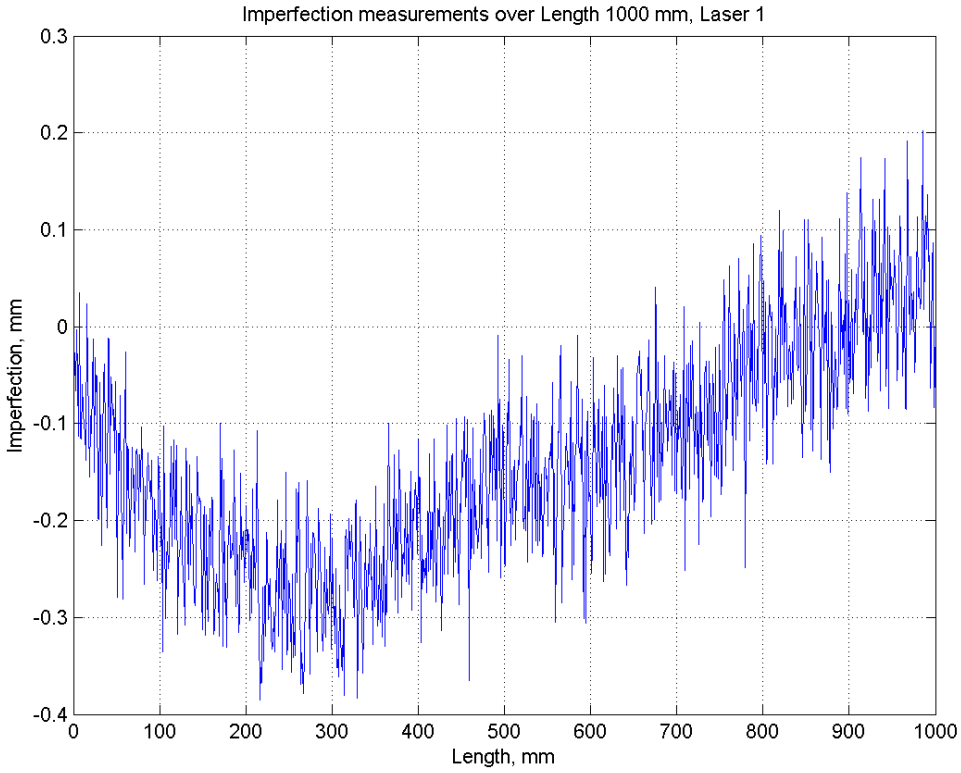

Figure A - 25 Imperfection measurement of SWC1000_3 (Right flange)

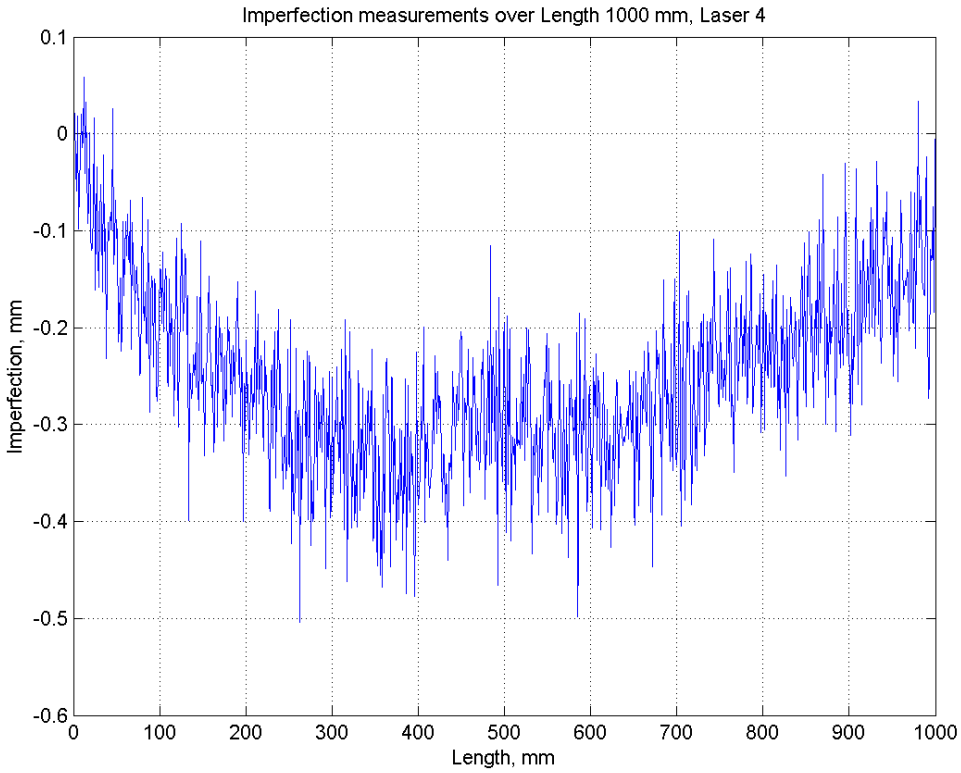

Figure A - 26 Imperfection measurement of SWC1000_3 (Left flange)

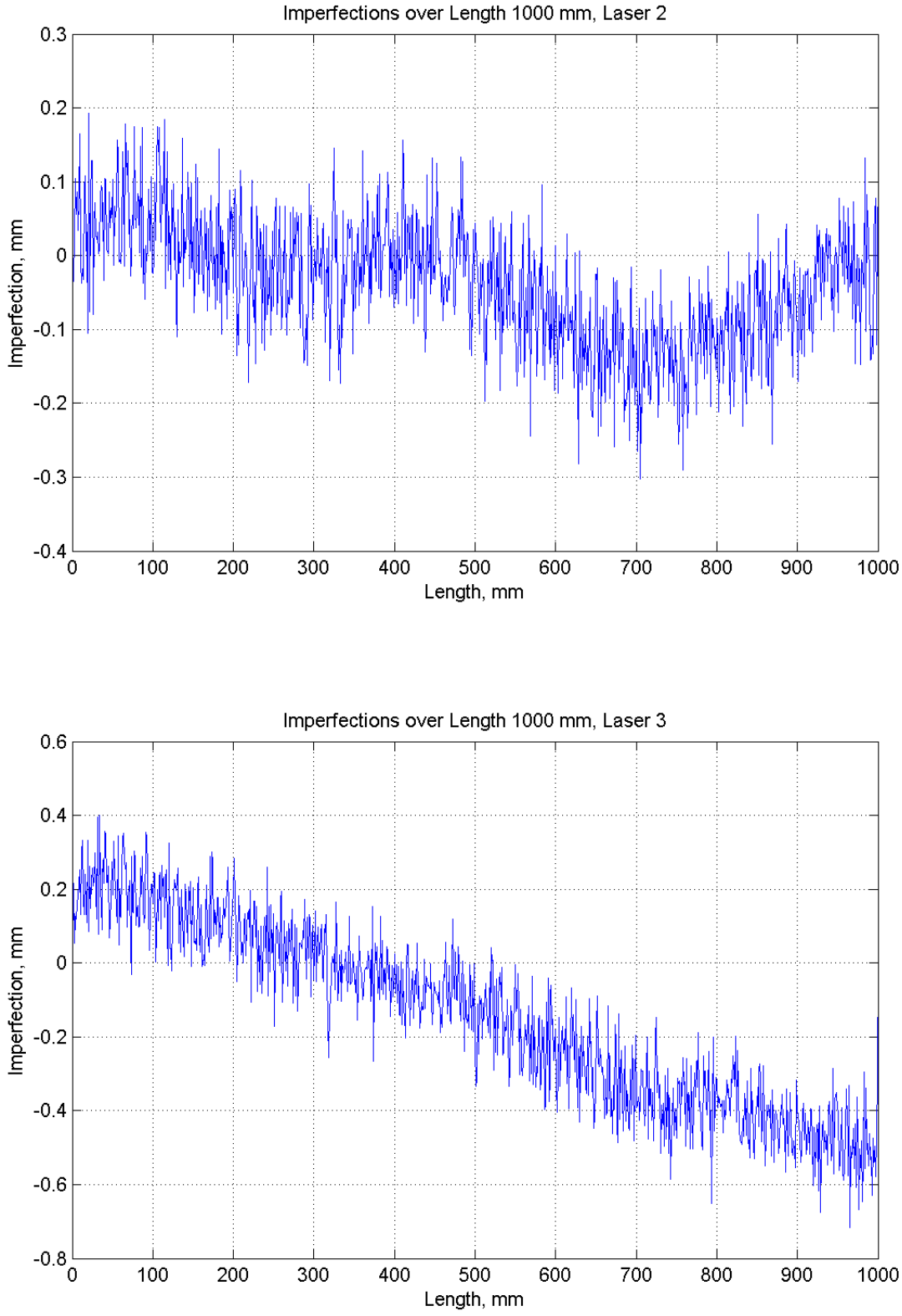

Figure A - 27 Imperfection measurement of SWC1000_3 (Web)

A.4 Stiffened-web channel section with length 1300 mm

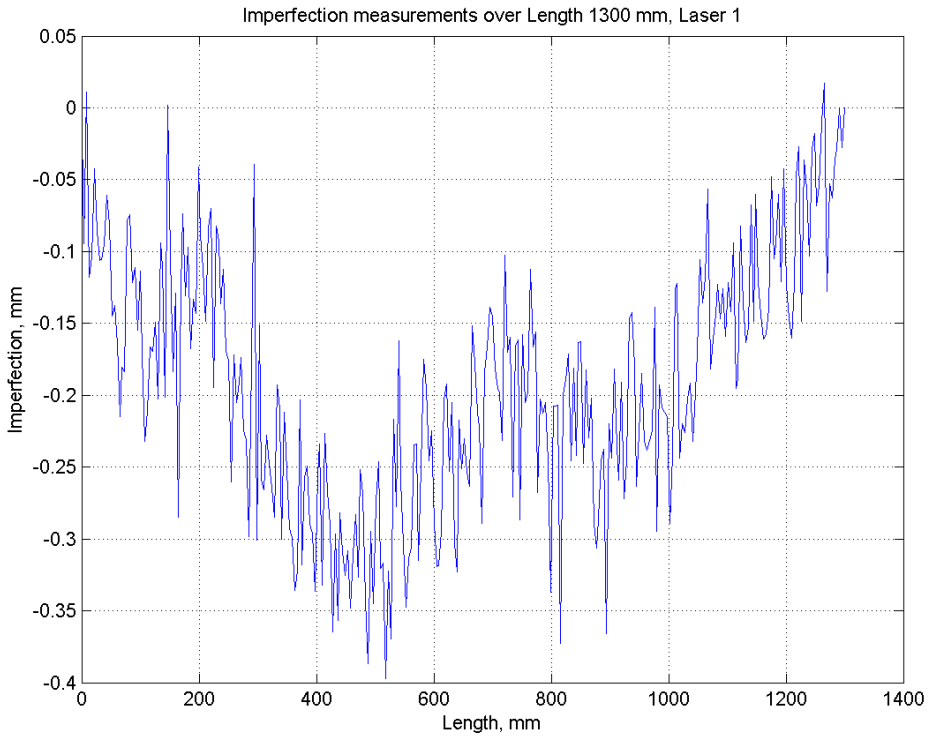

Figure A - 28 Imperfection measurement of SWC1300_1 (Right flange)

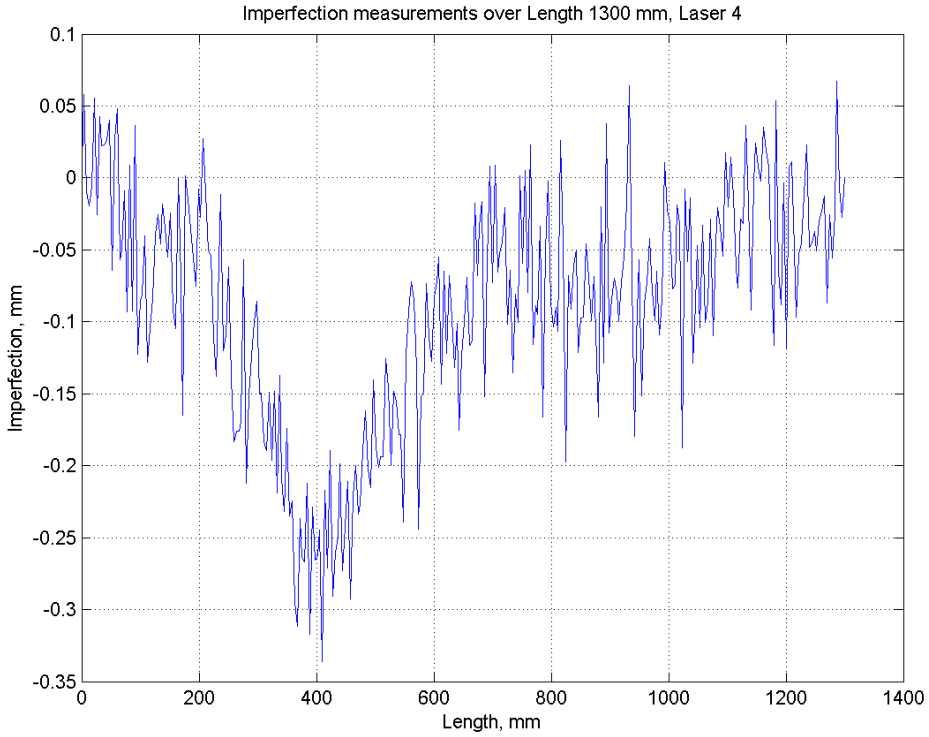

Figure A - 29 Imperfection measurement of SWC1300_1 (Left flange)

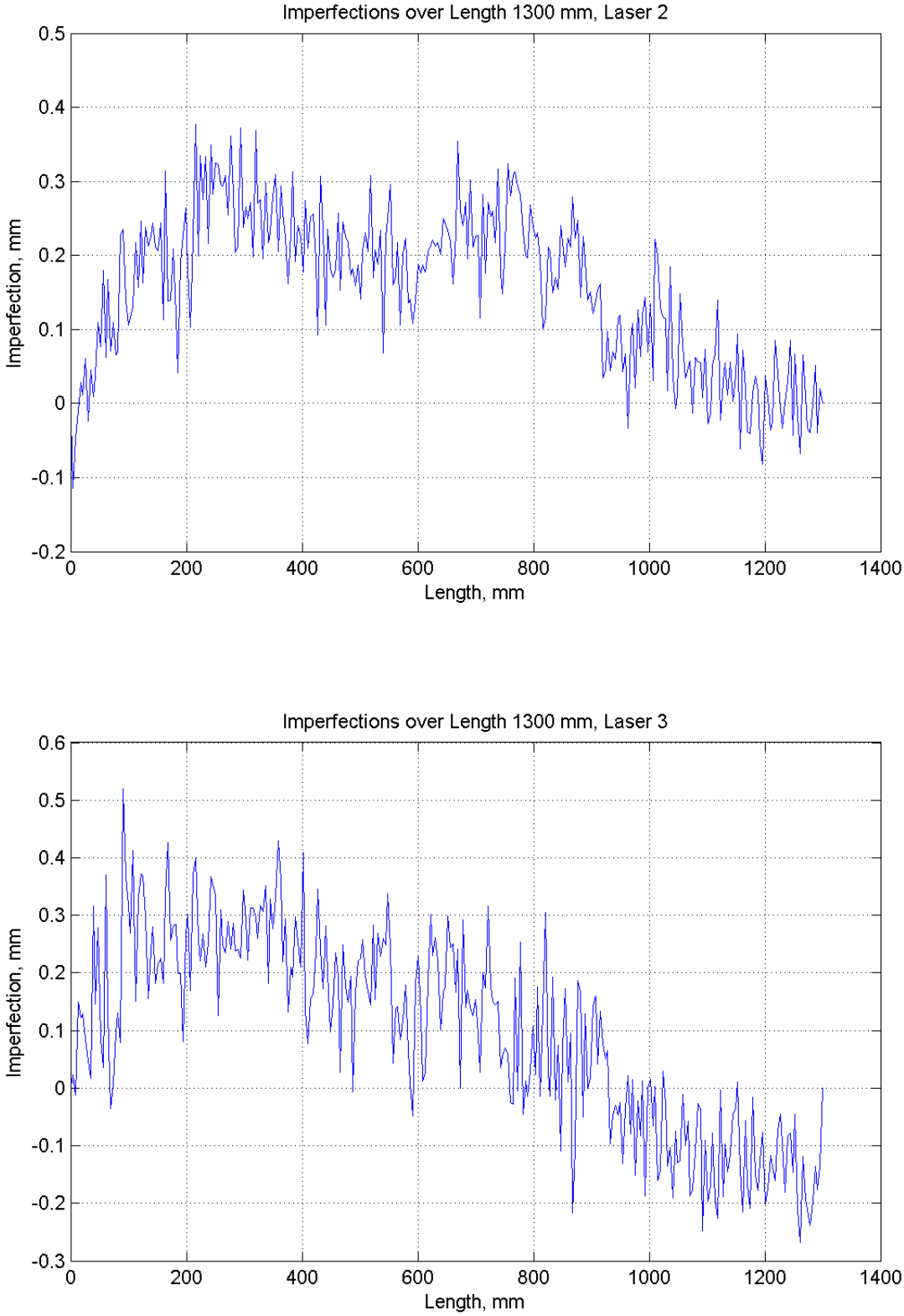

Figure A - 30 Imperfection measurement of SWC1300_1 (Web)

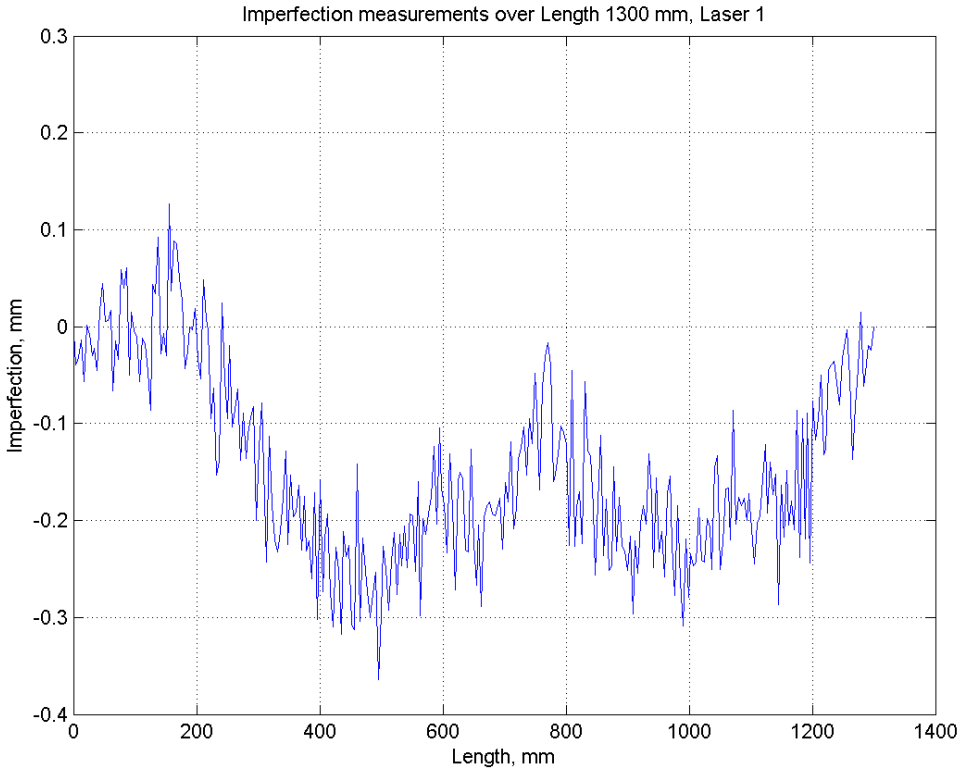

Figure A - 31 Imperfection measurement of SWC1300_2 (Right flange)

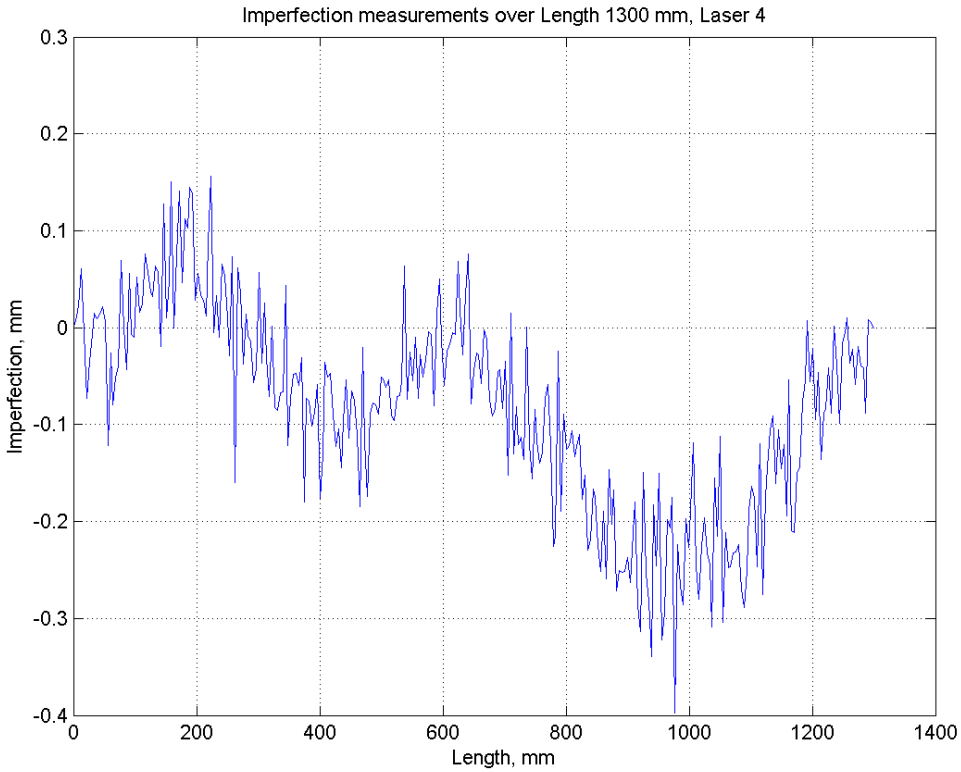

Figure A - 32 Imperfection measurement of SWC1300_2 (Left flange)

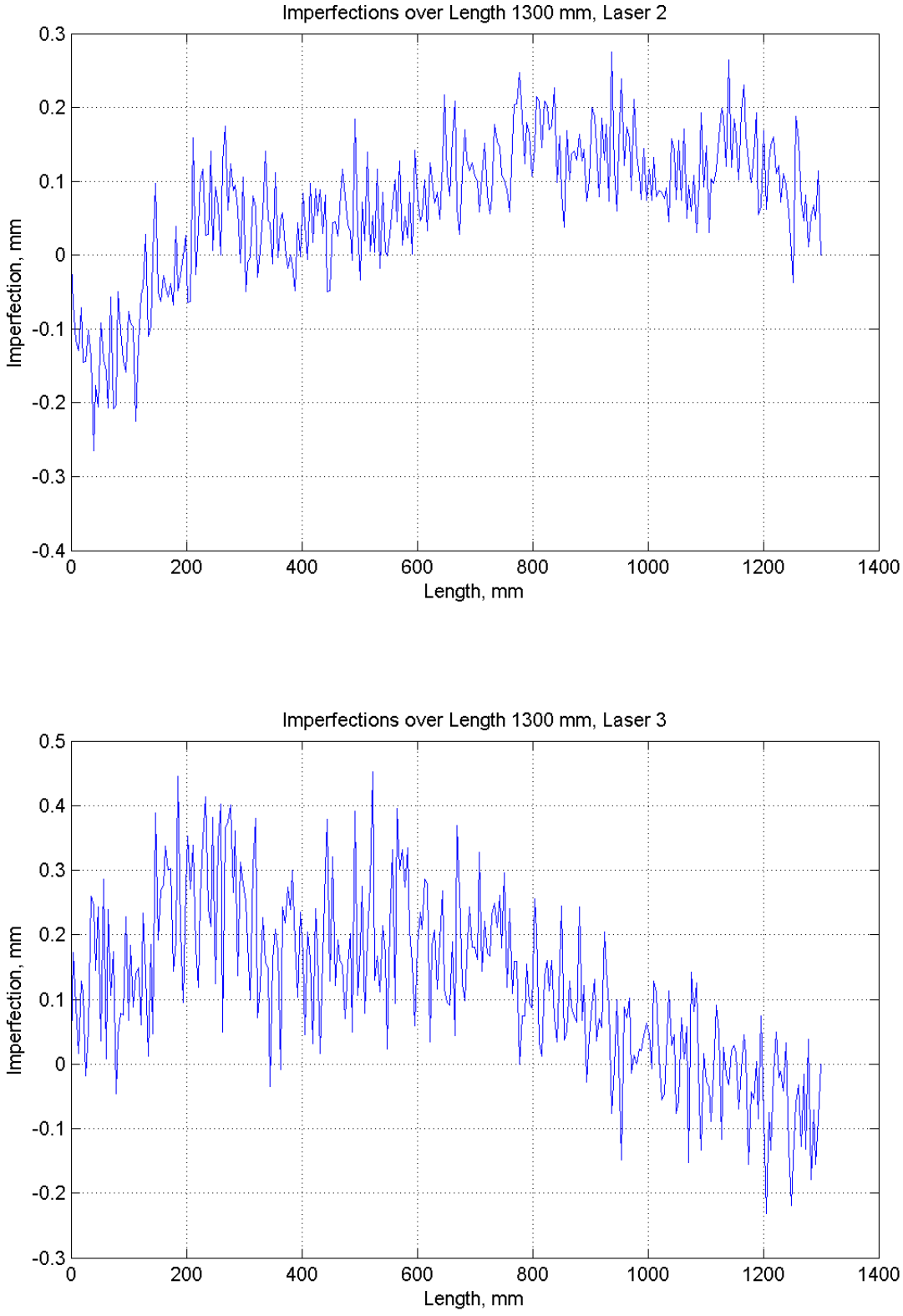

Figure A - 33 Imperfection measurement of SWC1300_2 (Web)

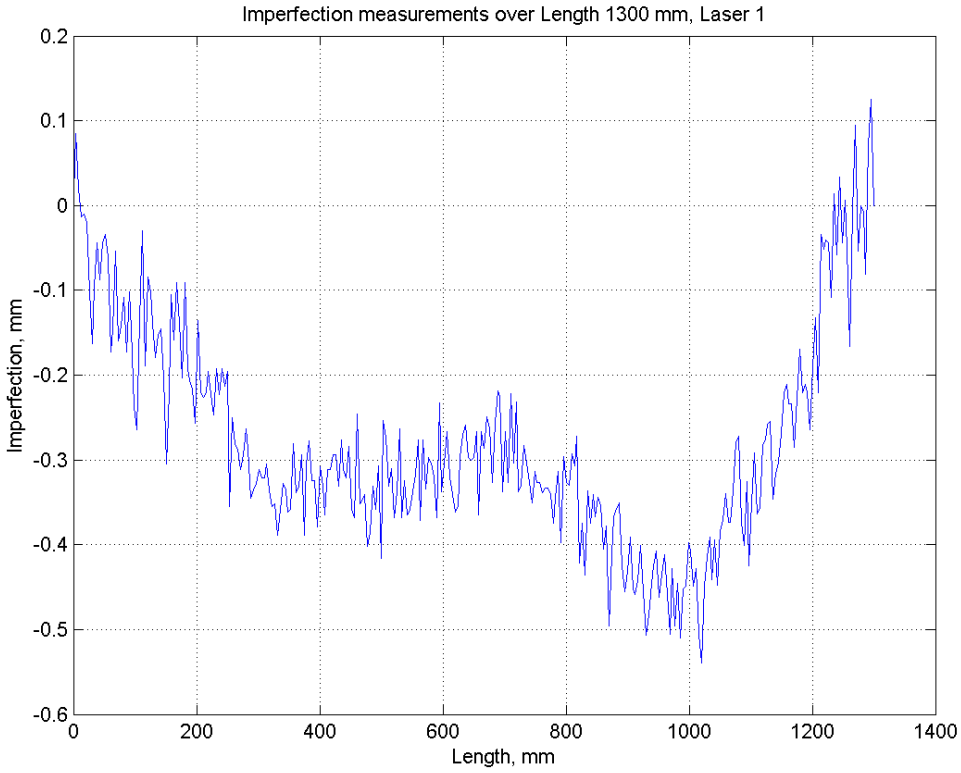

Figure A - 34 Imperfection measurement of SWC1300_3 (Right flange)

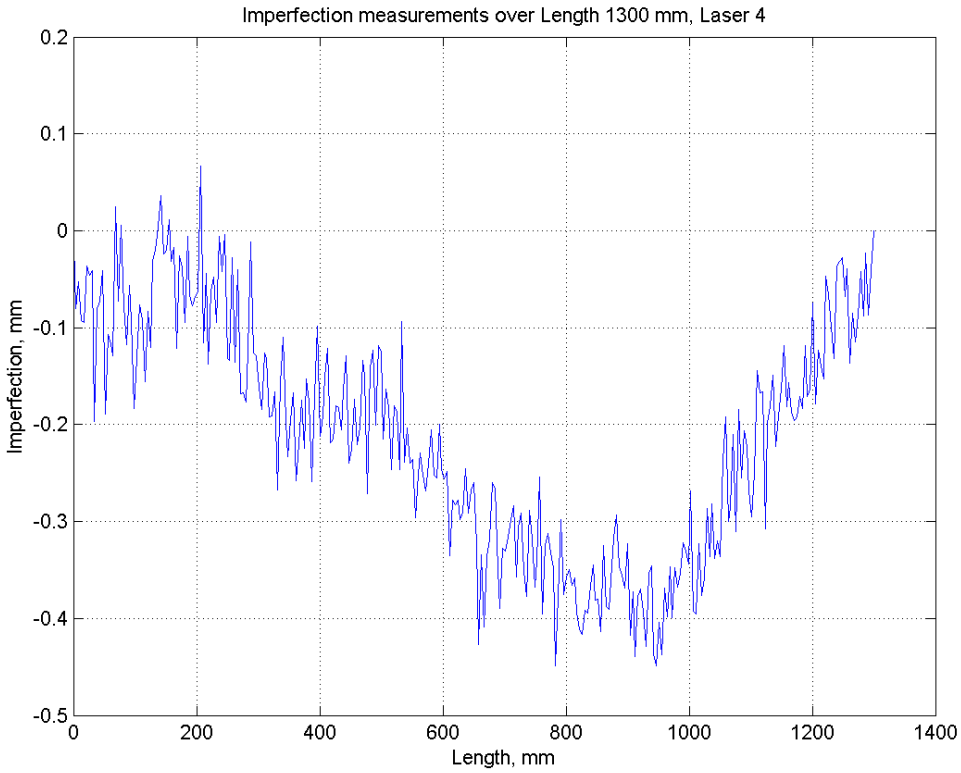

Figure A - 35 Imperfection measurement of SWC1300_3 (Left flange)

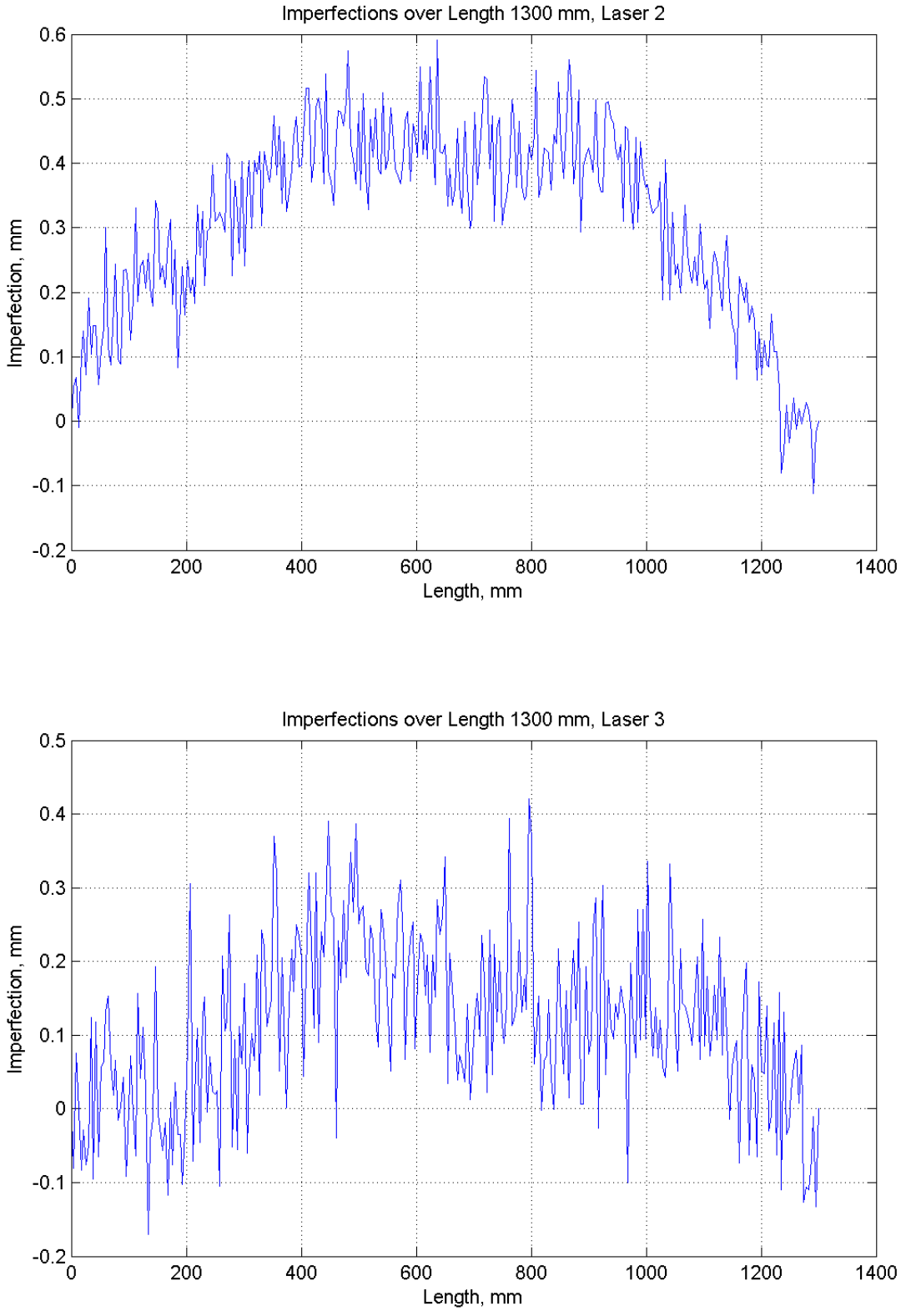

Figure A - 36 Imperfection measurement of SWC1300_3 (Web)

A.5 Stiffened-web channel section with length 2000 mm

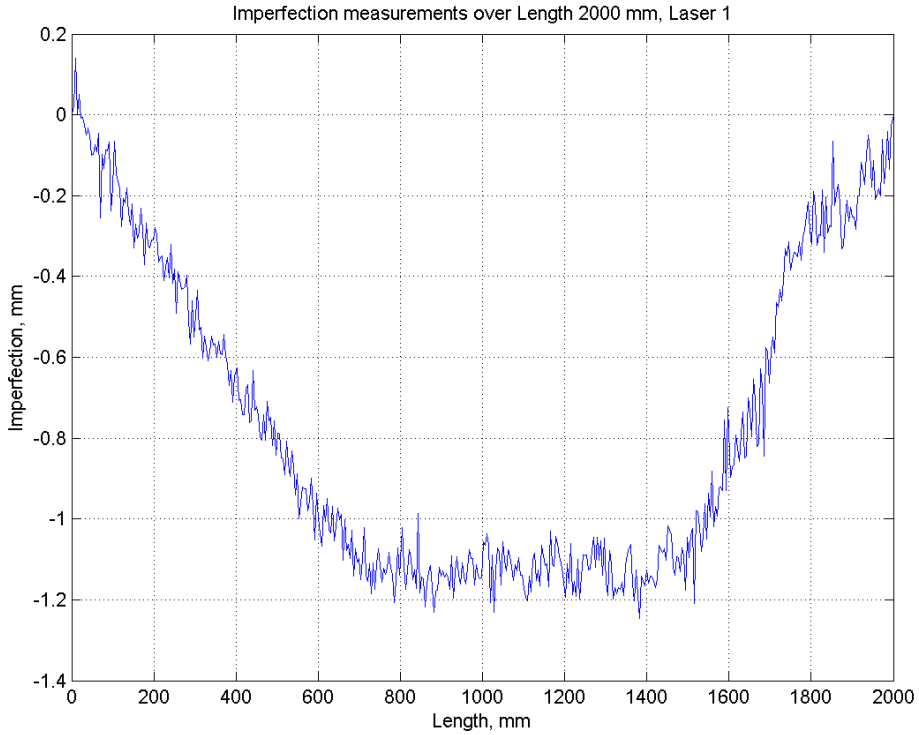

Figure A - 37 Imperfection measurement of SWC2000_1 (Right flange)

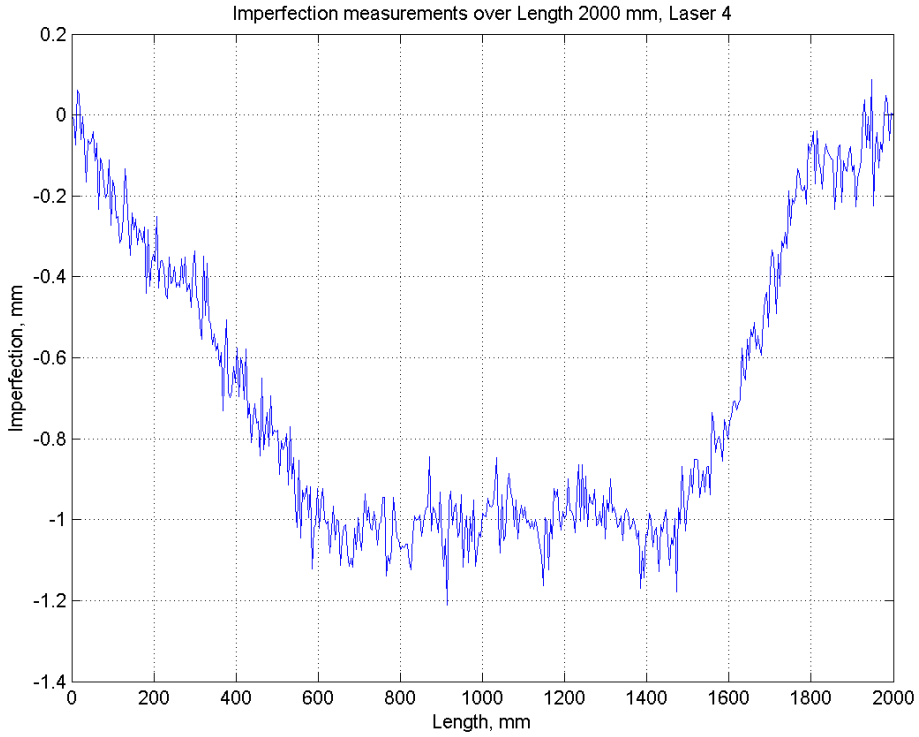

Figure A - 38 Imperfection measurement of SWC2000_1 (Left flange)

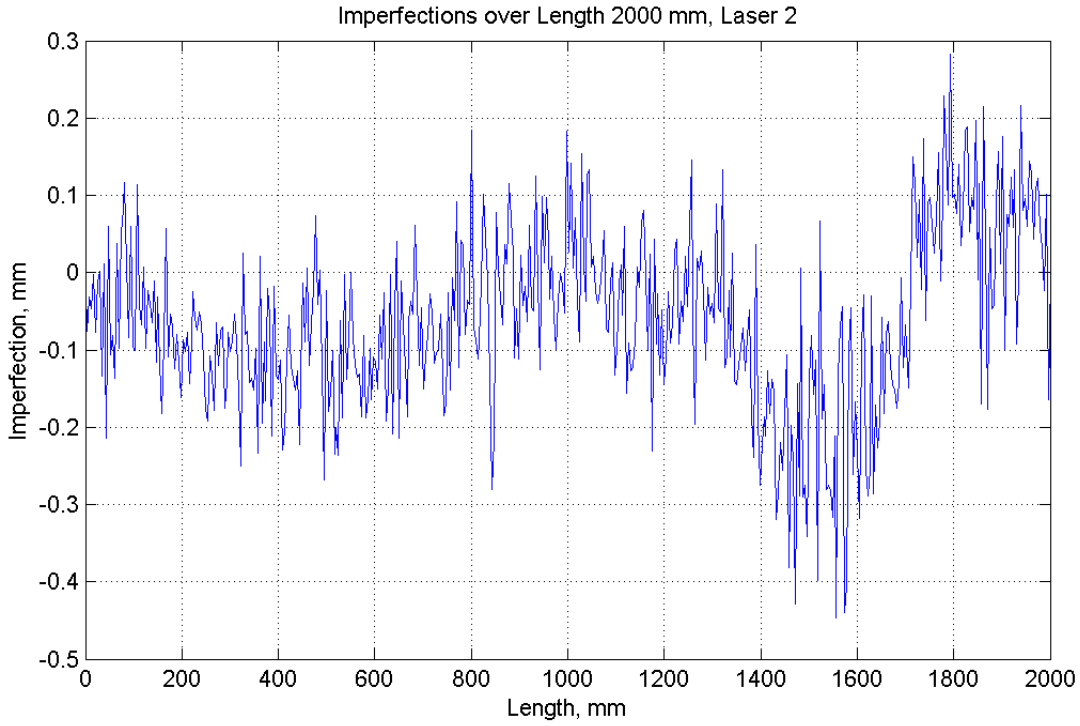

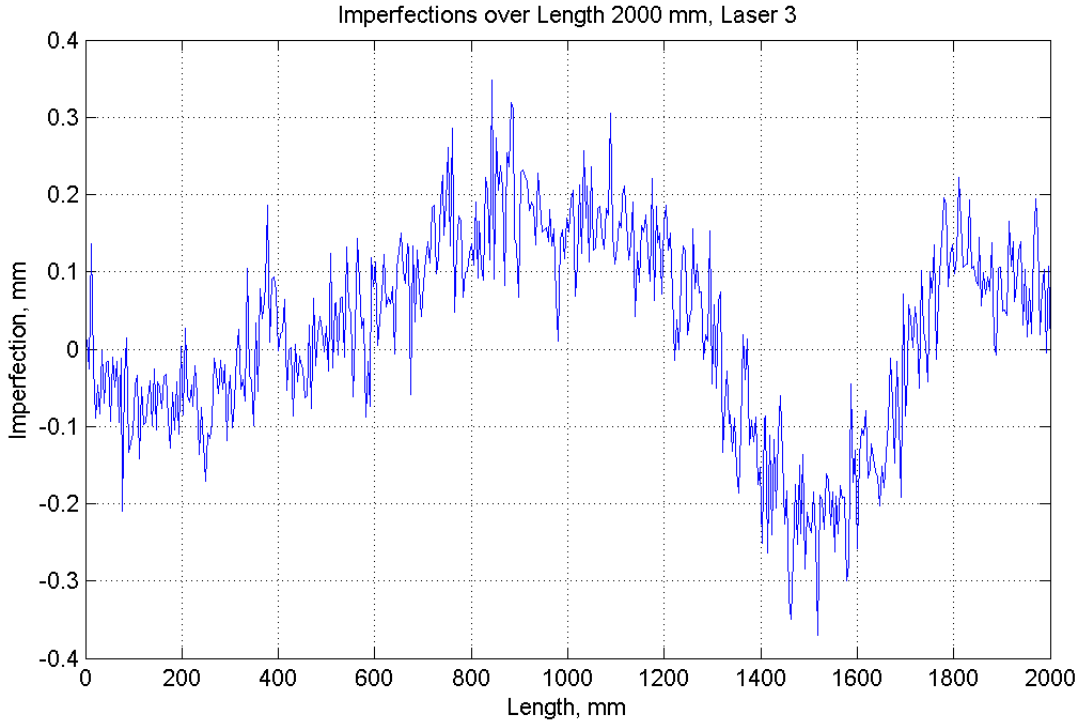

Figure A - 39 Imperfection measurement of SWC2000_1 (Web)

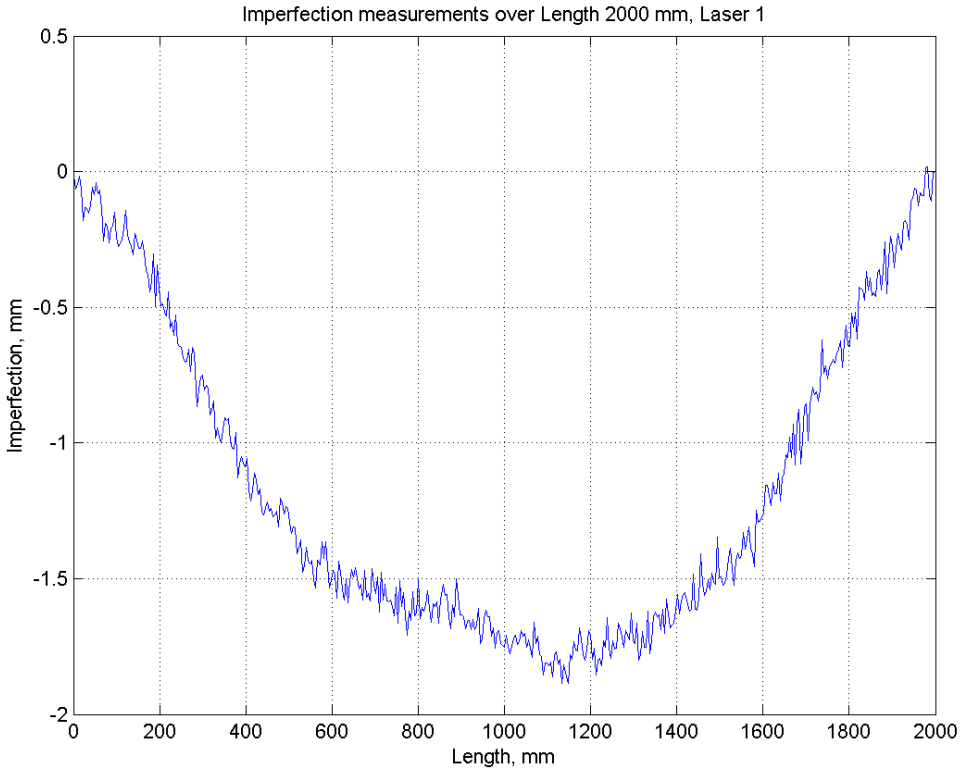

Figure A - 40 Imperfection measurement of SWC2000_2 (Right flange)

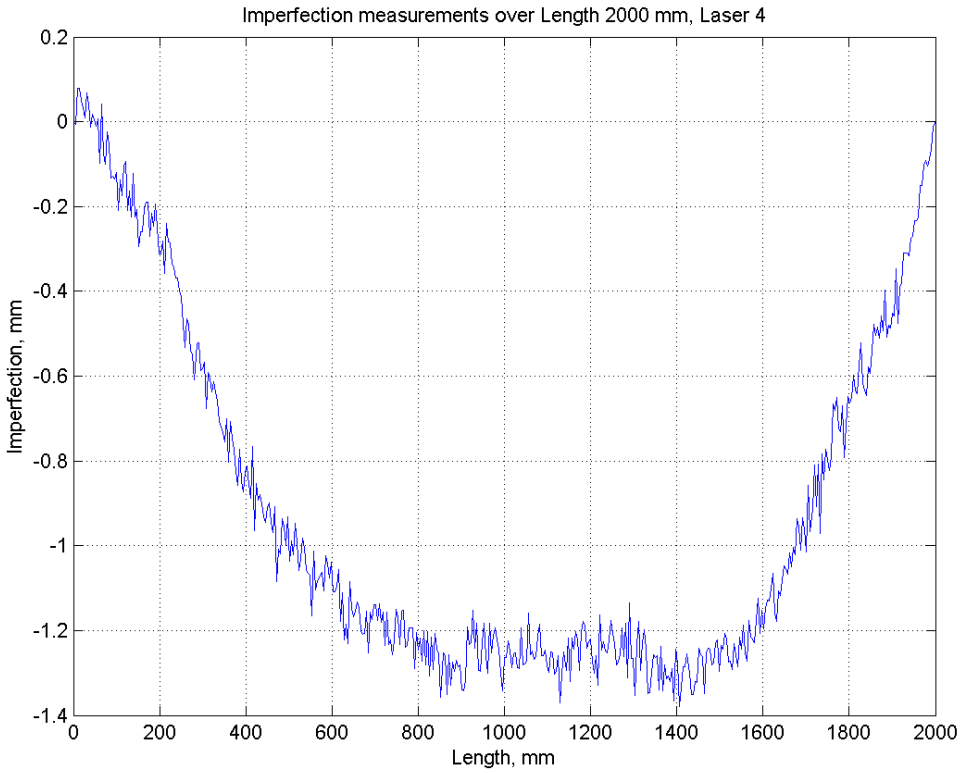

Figure A - 41 Imperfection measurement of SWC2000_2 (Left flange)

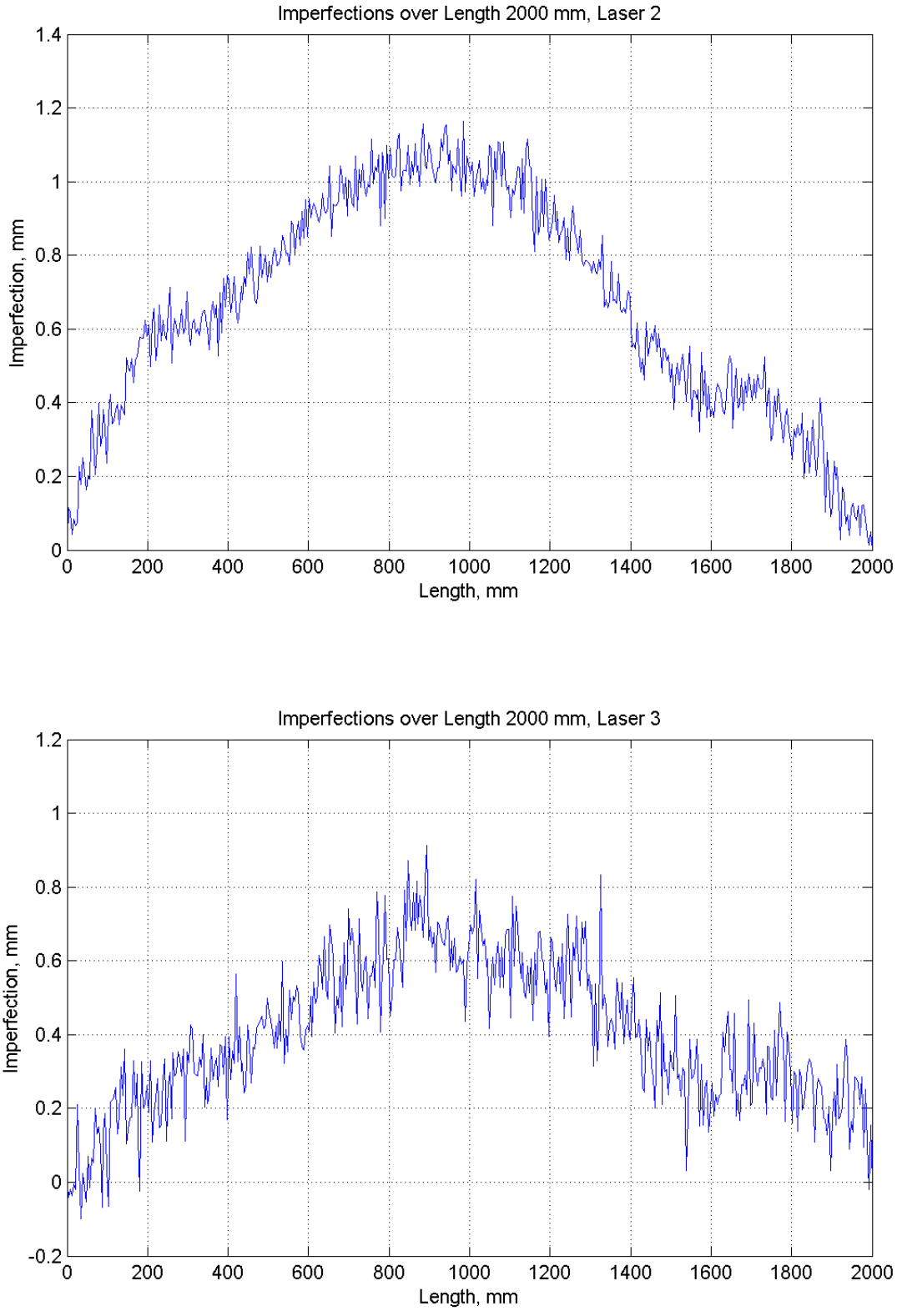

Figure A - 42 Imperfection measurement of SWC2000_2 (Web)

APPENDIX B

Experimental graphs

Appendix B shows the graphs that detail the LVDT measurements taken during the compression tests. There are generally four graphs per specimen. The first graph shows the load versus axis shortening and is followed by the load versus lateral displacements of the right and left flanges and web. The positions of the transducers are on both edge-stiffened flanges as well as on the stiffened web. The transducers are generally positioned at the quarter, mid and three-quarter height of the specimen.

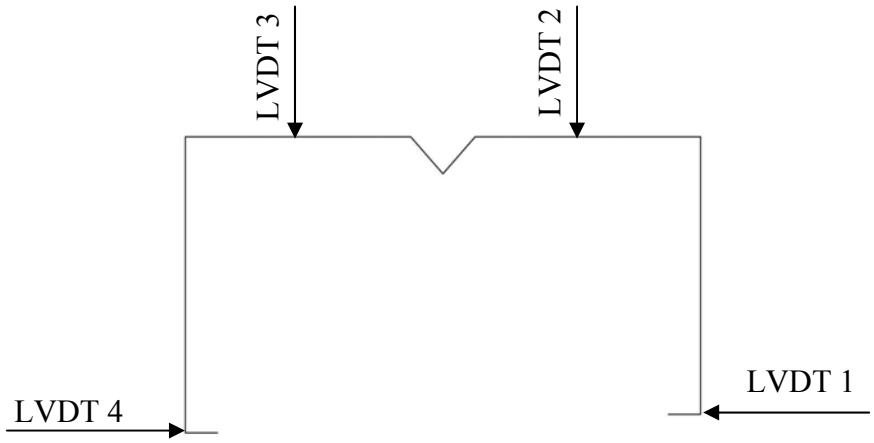

B.1 Stiffened-web channel section with length 350 mm

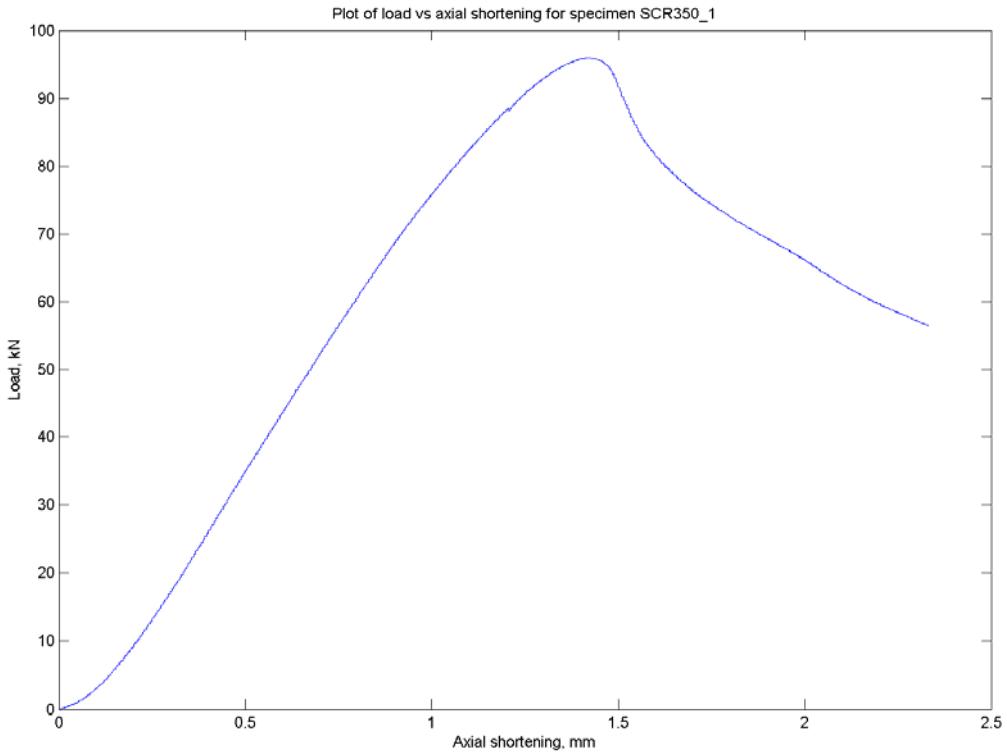

Figure B - 1 Plot of load vs. axial shortening for specimen SWC350_1

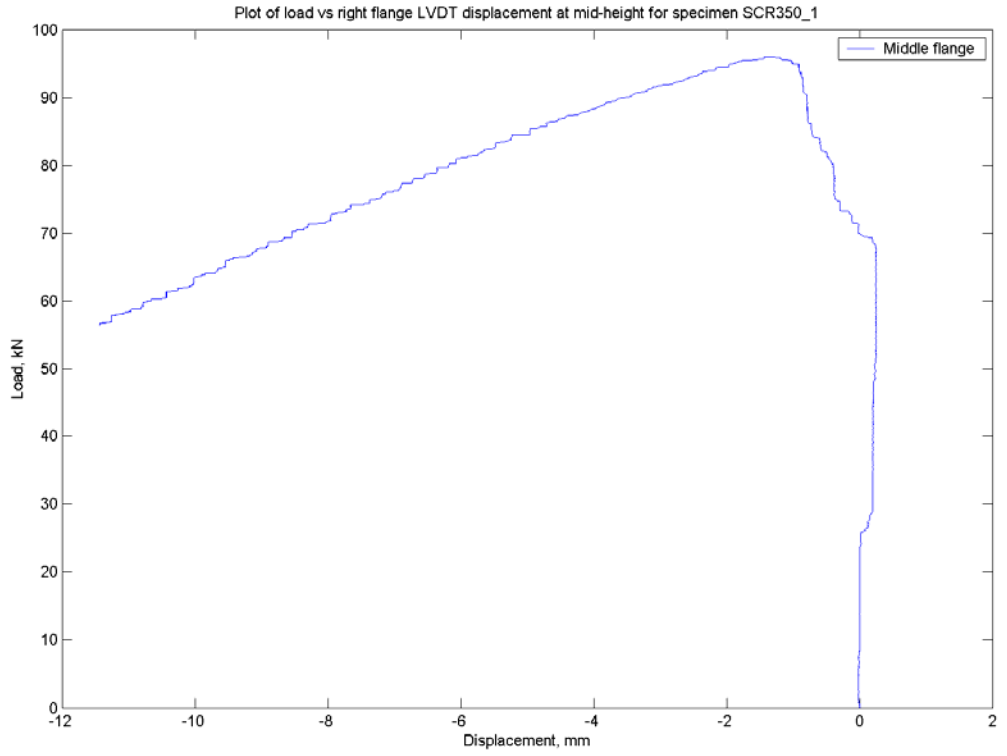

Figure B - 2 Plot of load vs. right flange LVDT displacement for specimen SWC350_1

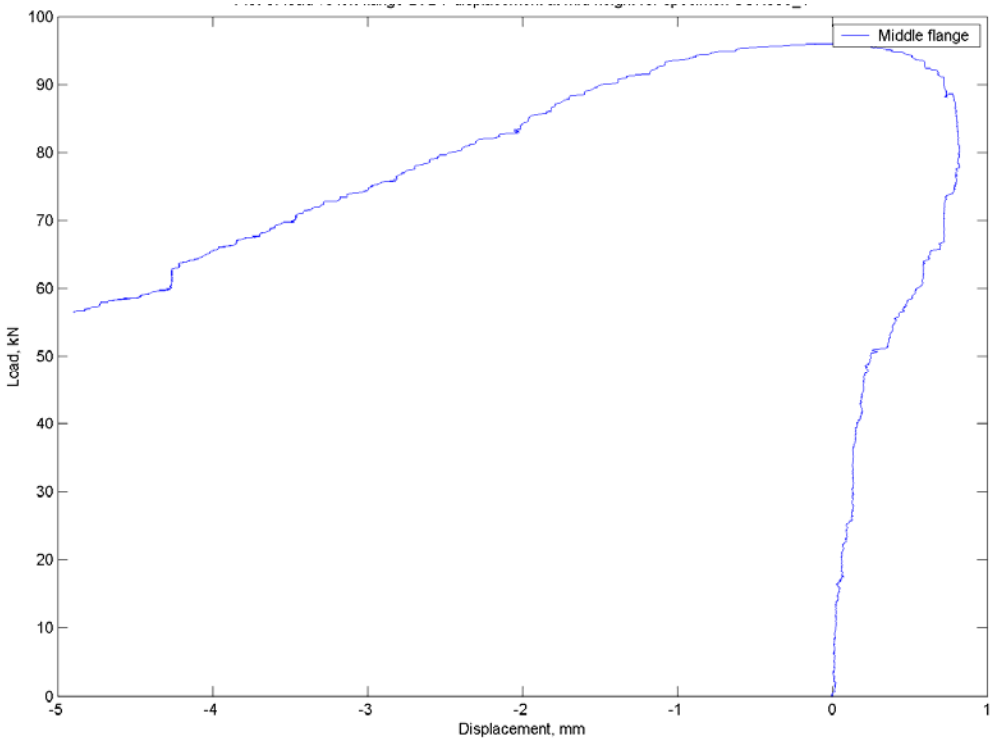

Figure B - 3 Plot of load vs. left flange LVDT displacement for specimen SWC350_1

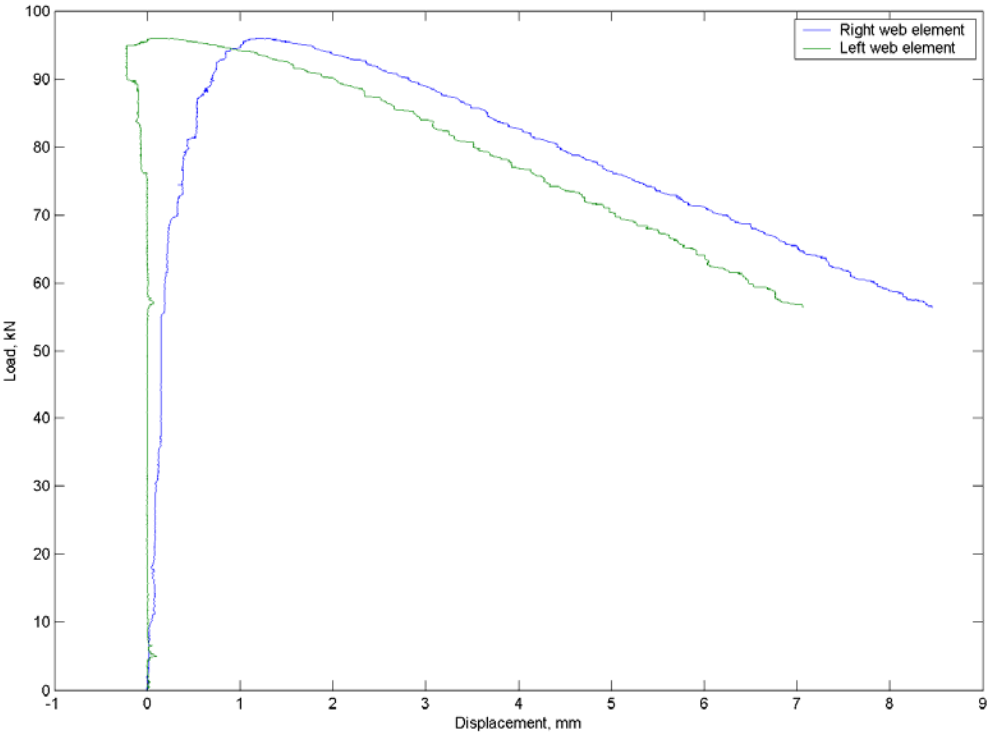

Figure B - 4 Plot of load vs. web LVDT displacements for specimen SWC350_1

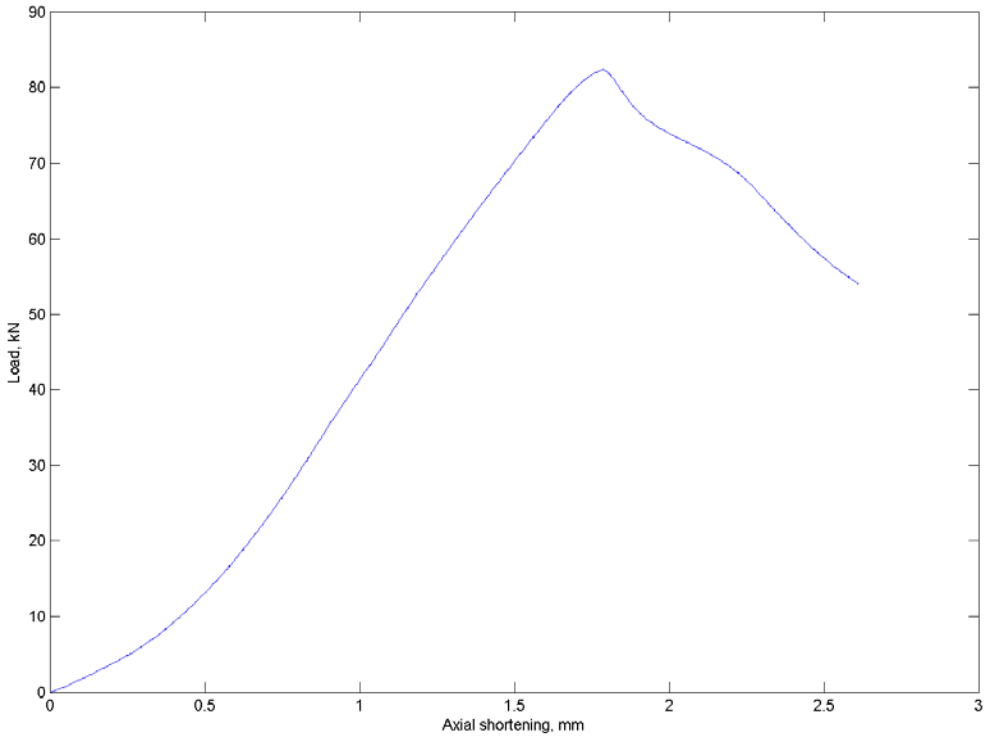

Figure B - 5 Plot of load vs. axial shortening for specimen SWC350_2

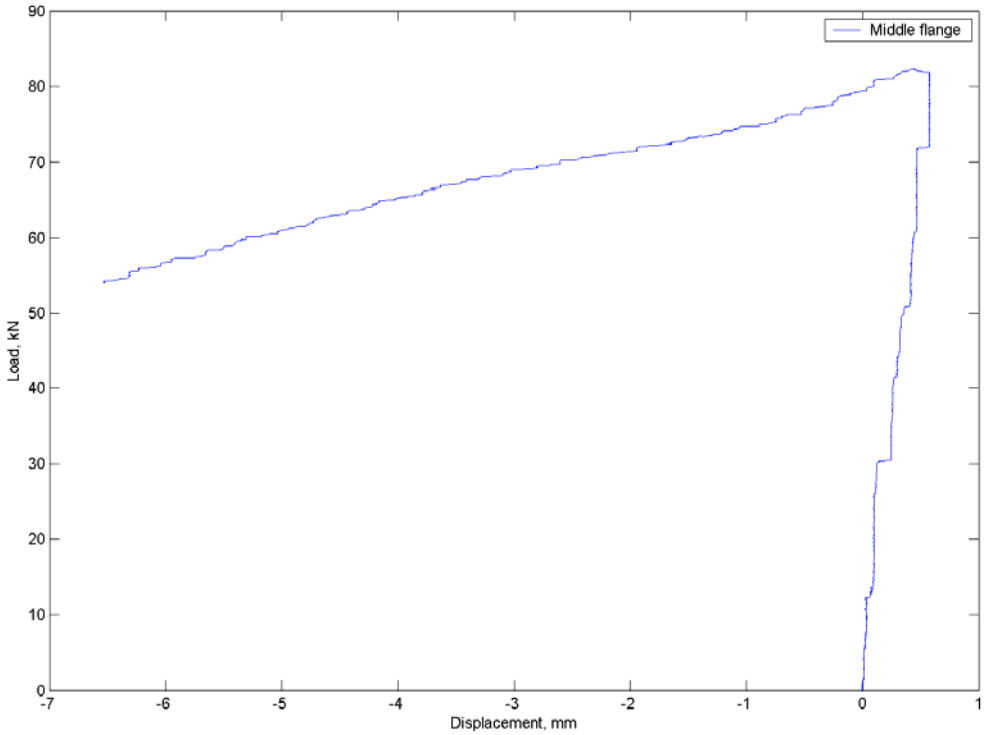

Figure B - 6Plot of load vs. right flange LVDT displacement for specimen SWC350_2

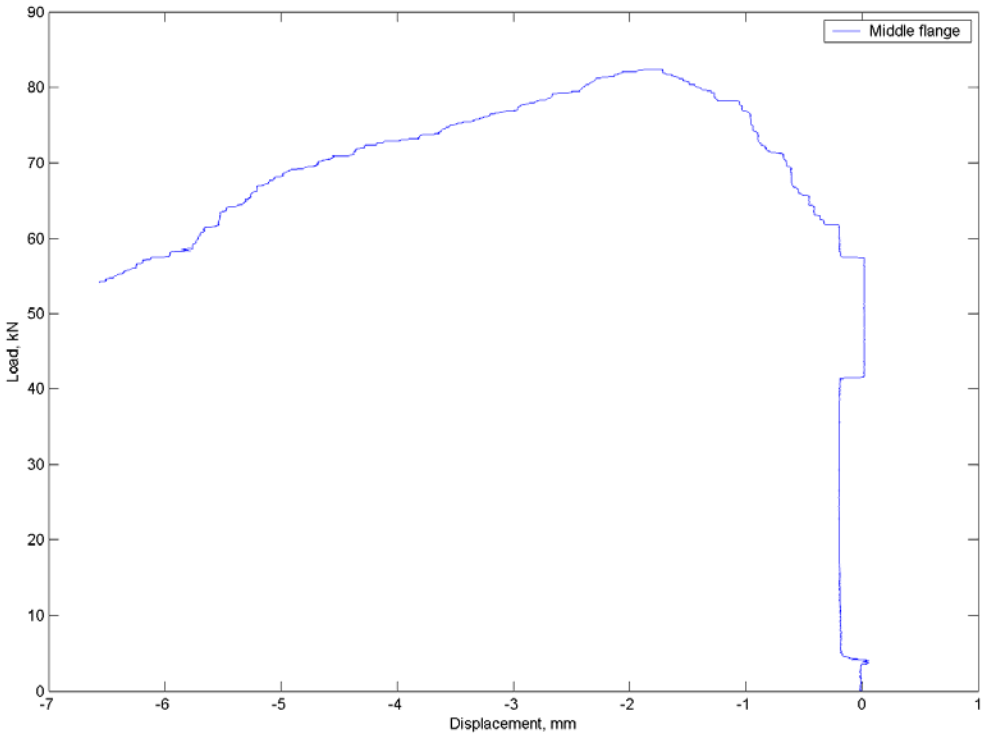

Figure B - 7 Plot of load vs. left flange LVDT displacement for specimen SWC350_2

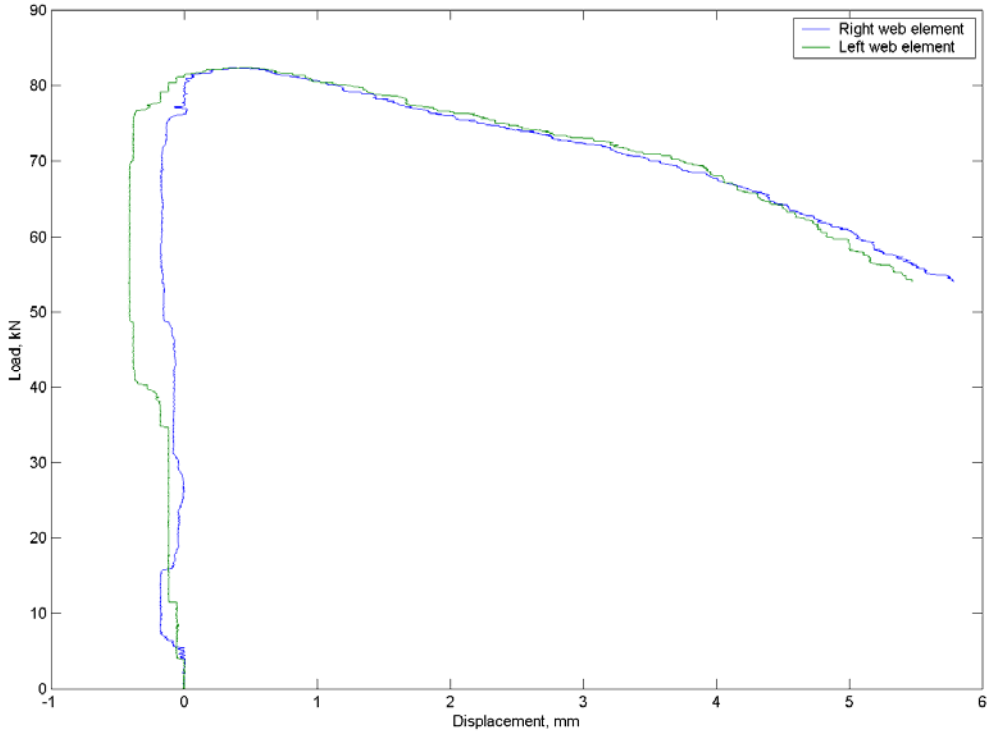

Figure B - 8 Plot of load vs. web LVDT displacements for specimen SWC350_2

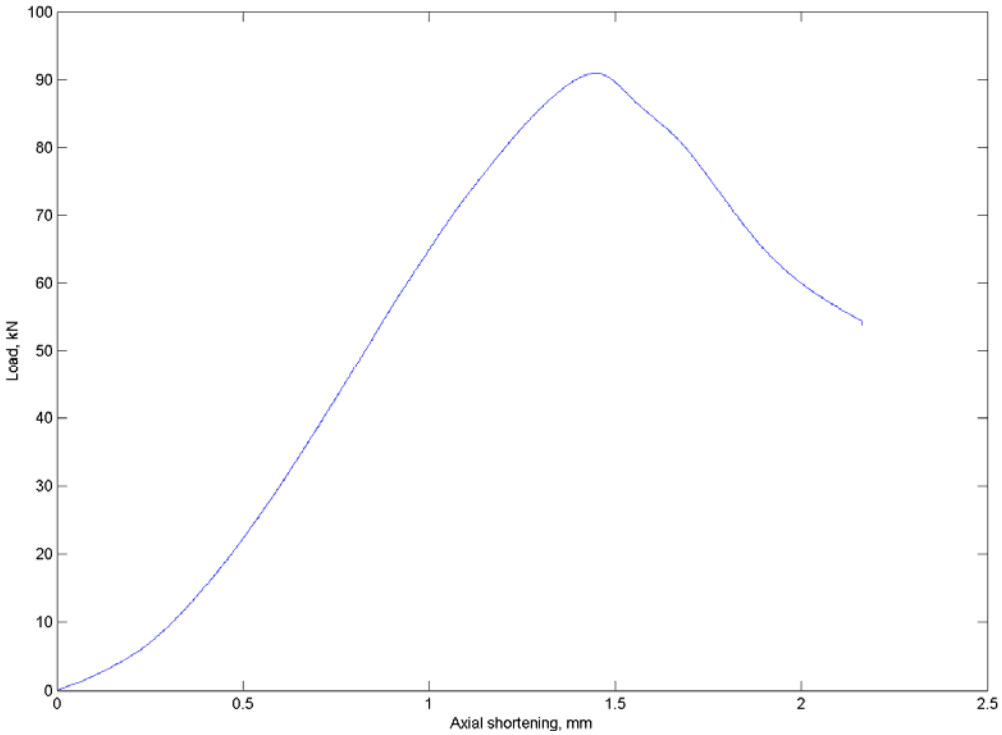

Figure B - 9 Plot of load vs. axial shortening for specimen SWC350_3

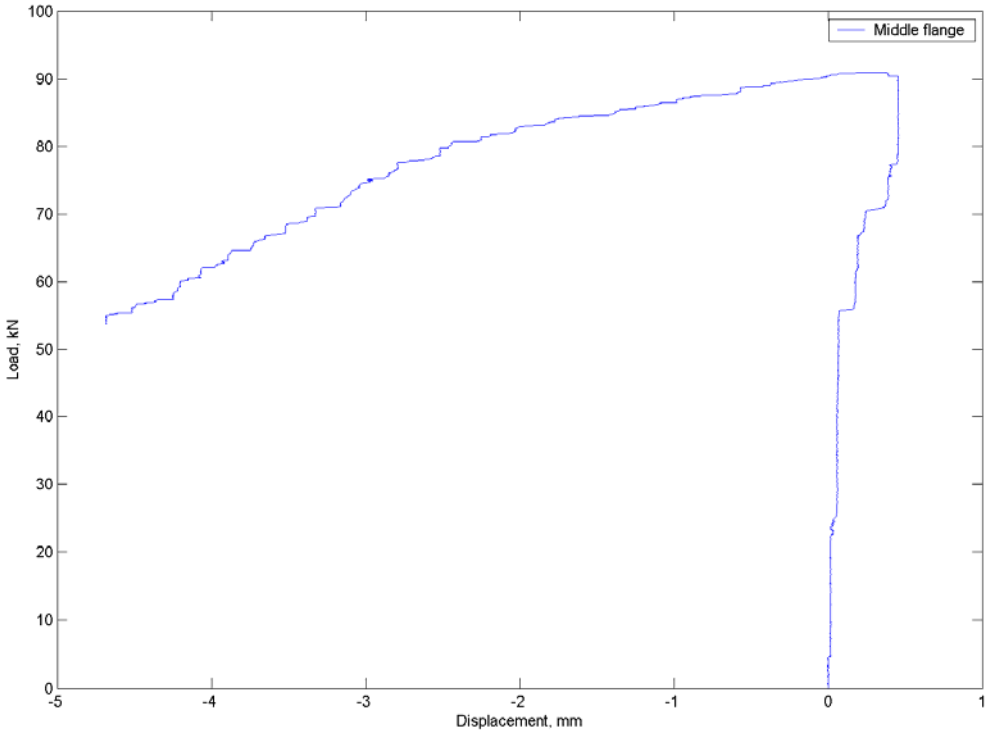

Figure B - 10 Plot of load vs. right flange LVDT displacement for specimen SWC350_3

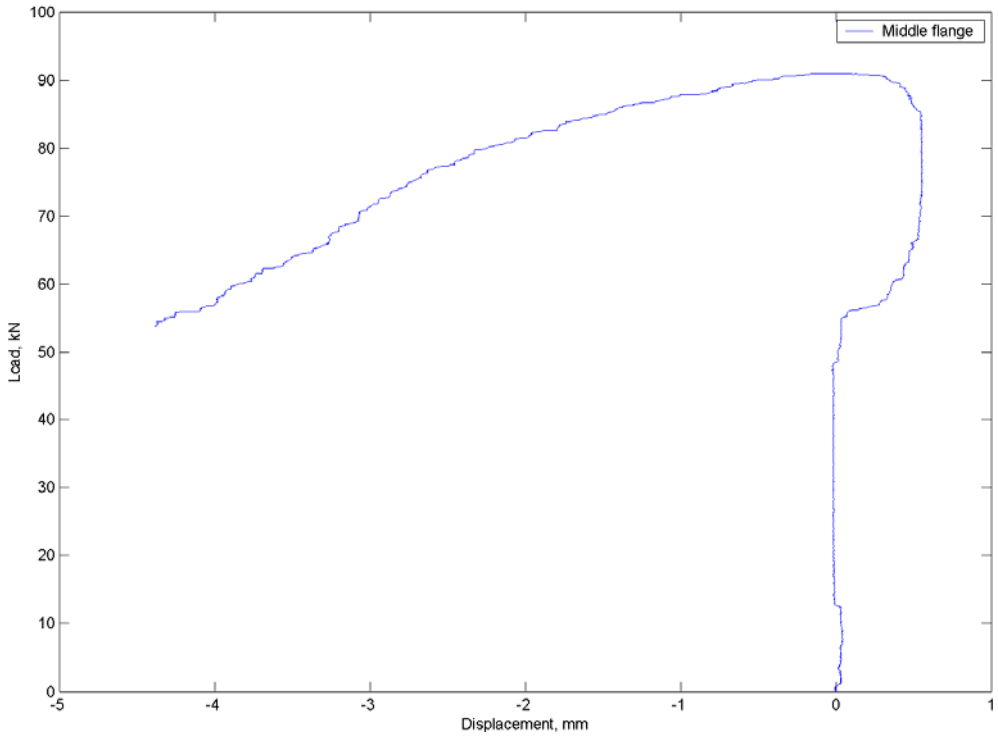

Figure B - 11 Plot of load vs. left flange LVDT displacement for specimen SWC350_3

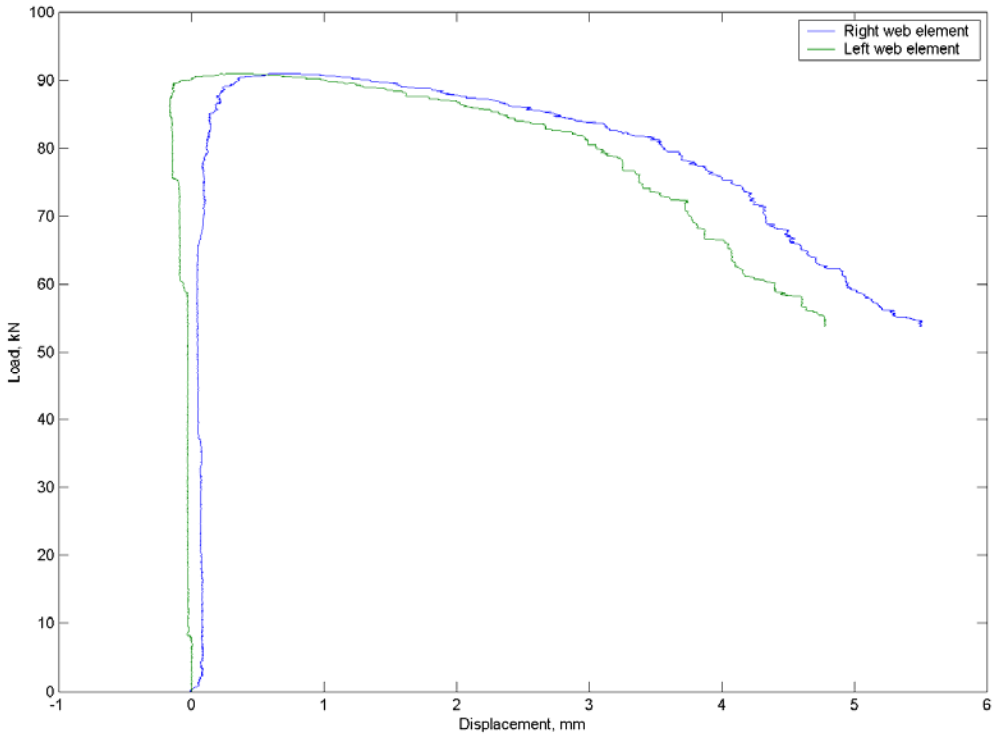

Figure B - 12 Plot of load web LVDT displacements for specimen SWC350_3

B.2 Stiffened-web channel section with length 700 mm

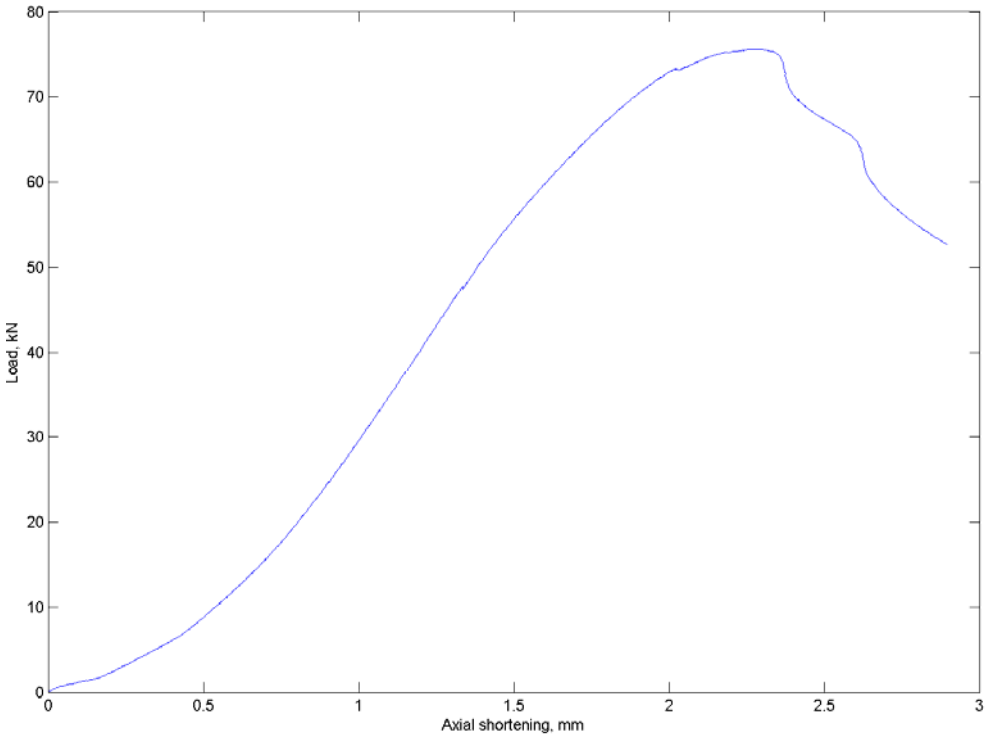

Figure B - 13 Plot of load vs. axial shortening for specimen SWC700_1

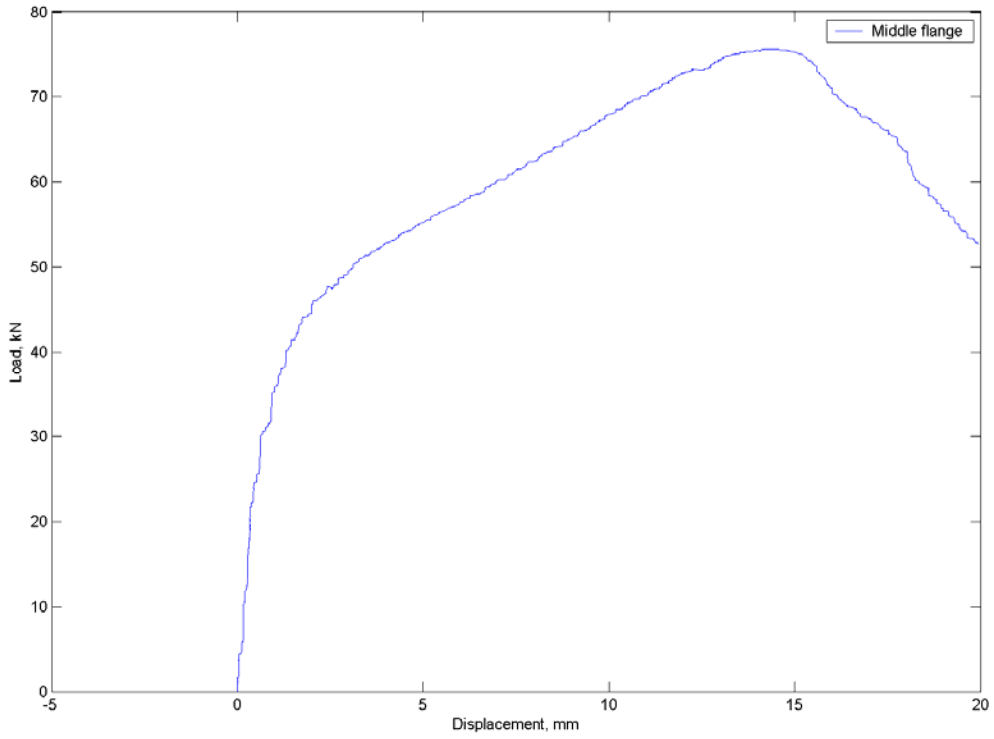

Figure B – 14 Plot of load vs. right flange LVDT displacement for specimen SWC700_1

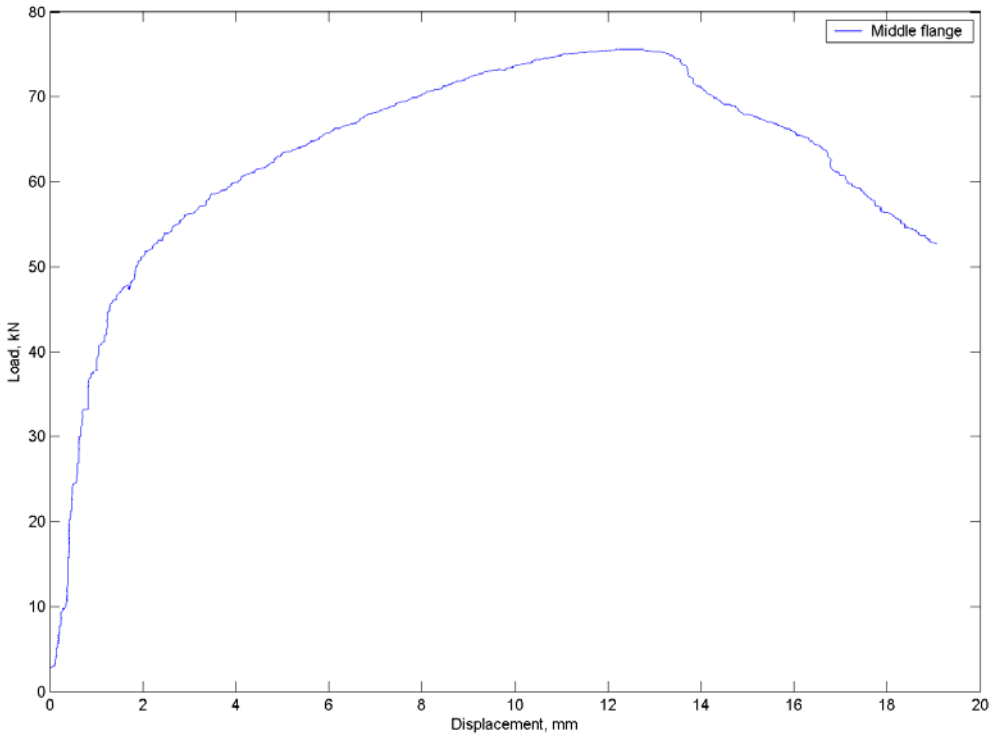

Figure B - 15 Plot of load vs. left flange LVDT displacement for specimen SWC700_1

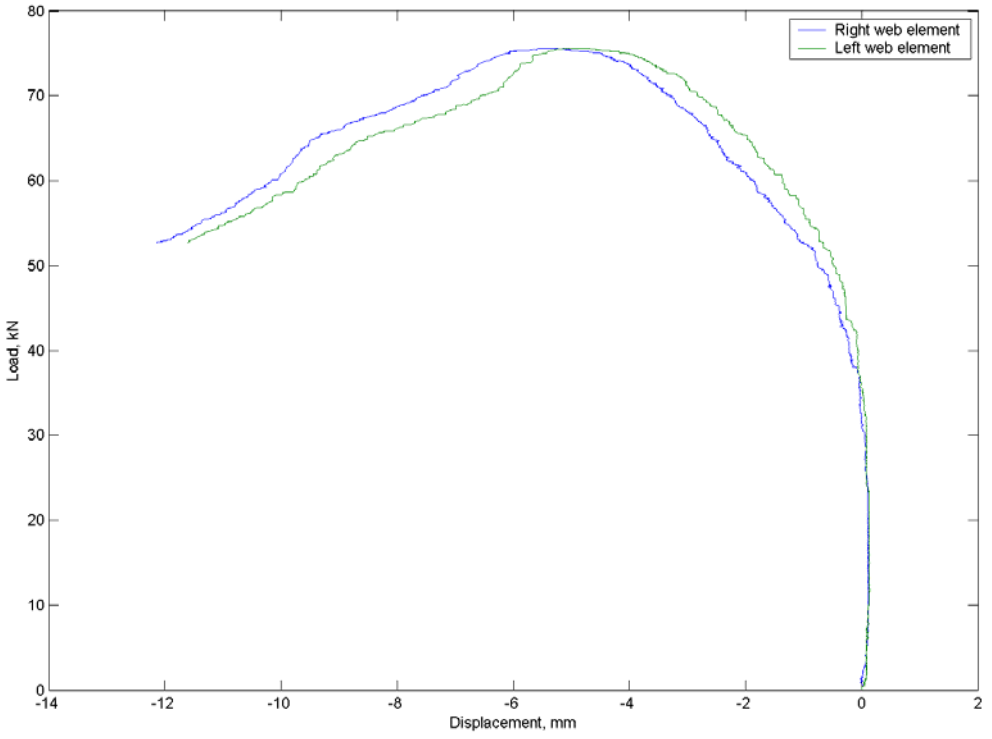

Figure B - 43 Plot of load vs. web LVDT displacements for specimen SWC700_1

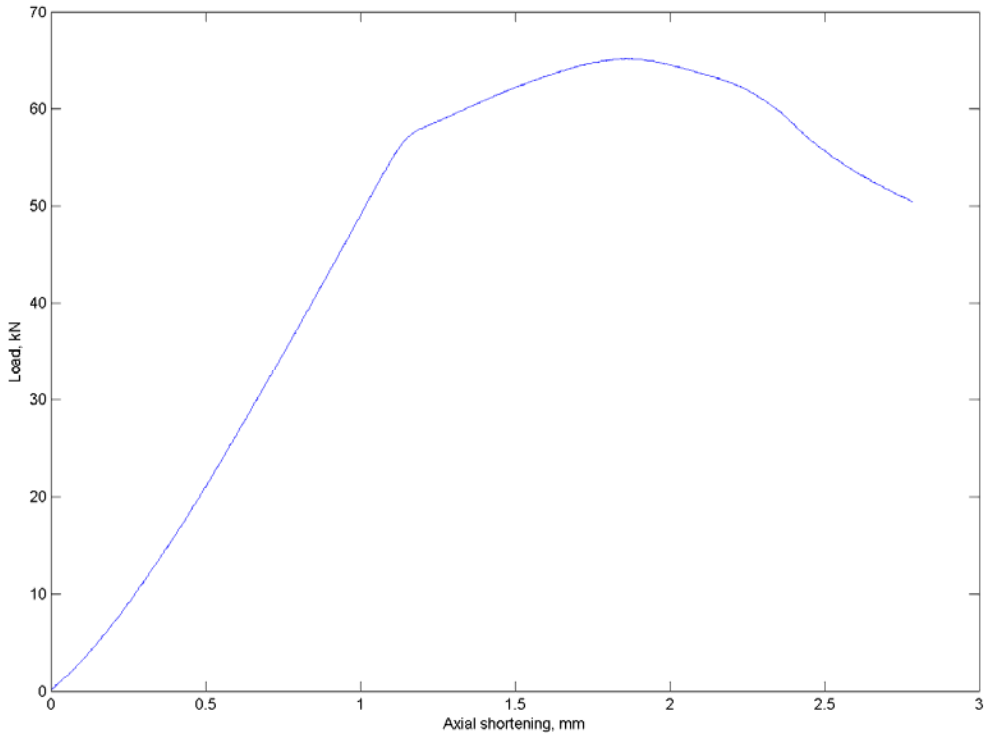

Figure B - 17 Plot of load vs. axial shortening for specimen SWC700_2

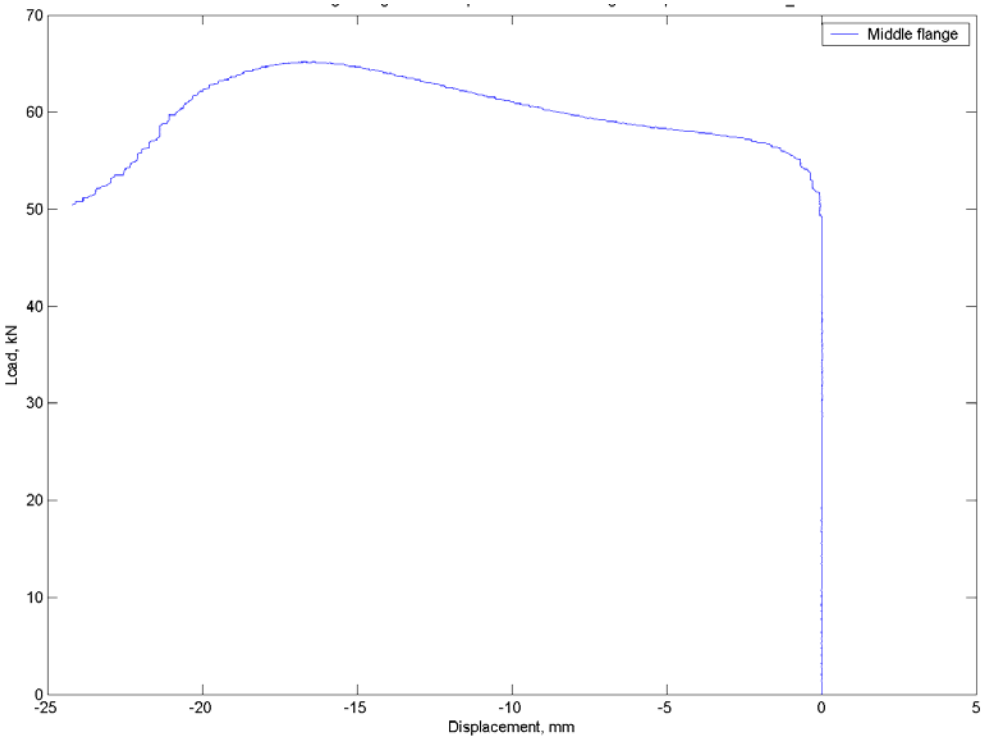

Figure B - 18 Plot of load vs. right flange LVDT displacement for specimen SWC700_2

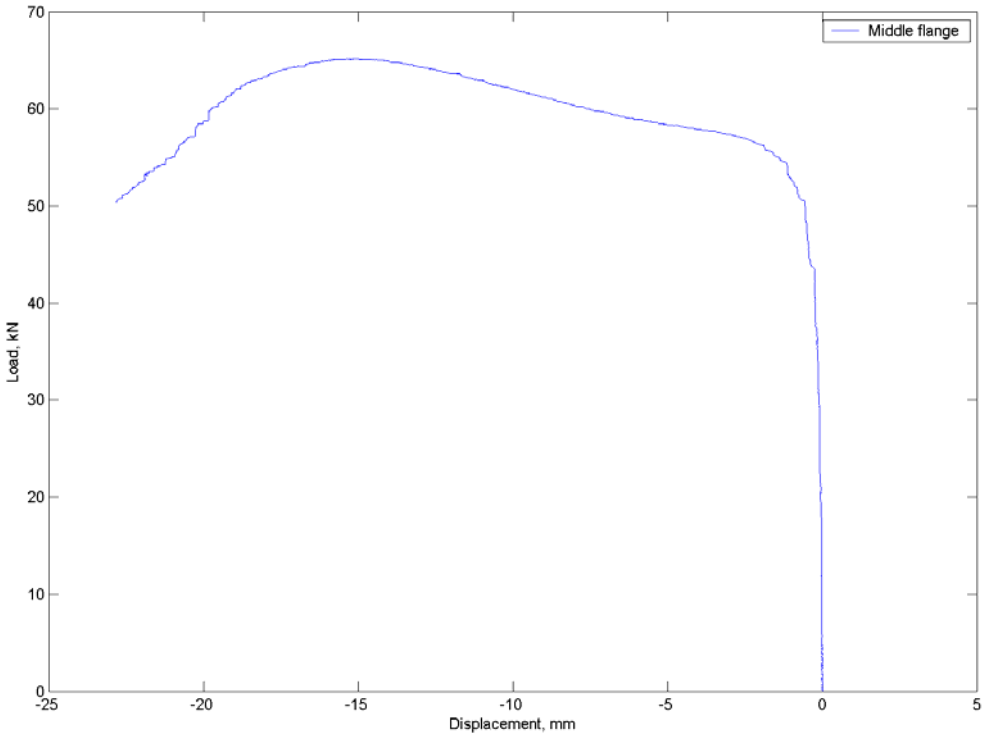

Figure B - 19 Plot of load vs. left flange LVDT displacement for specimen SWC700_2

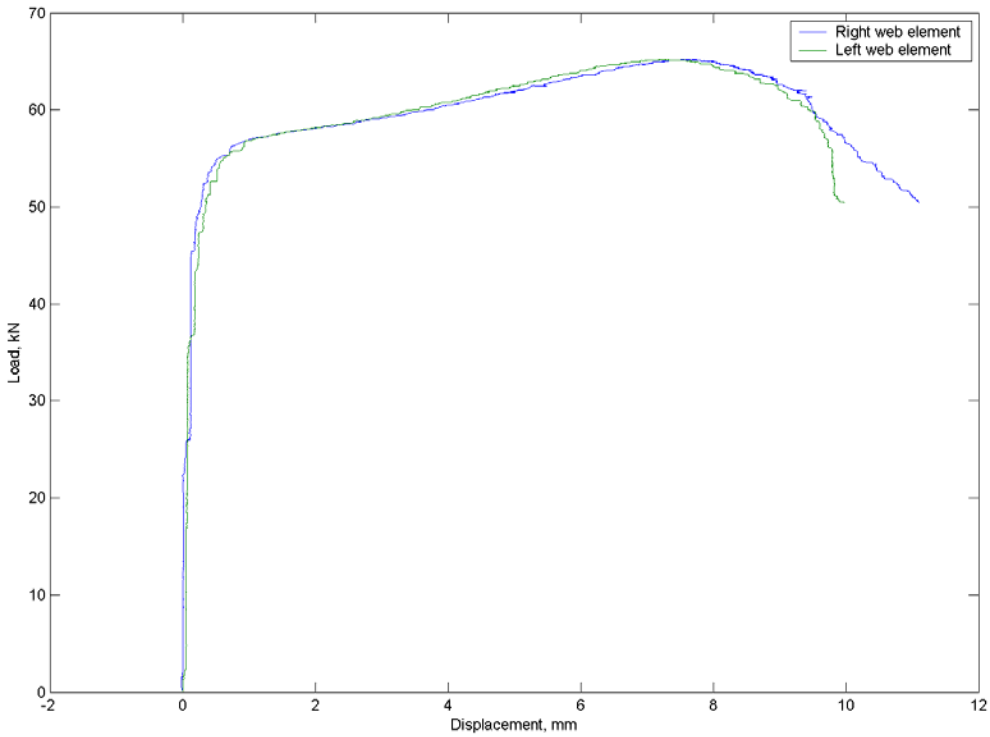

Figure B - 20 Plot of load vs. web LVDT displacements for specimen SWC700_2

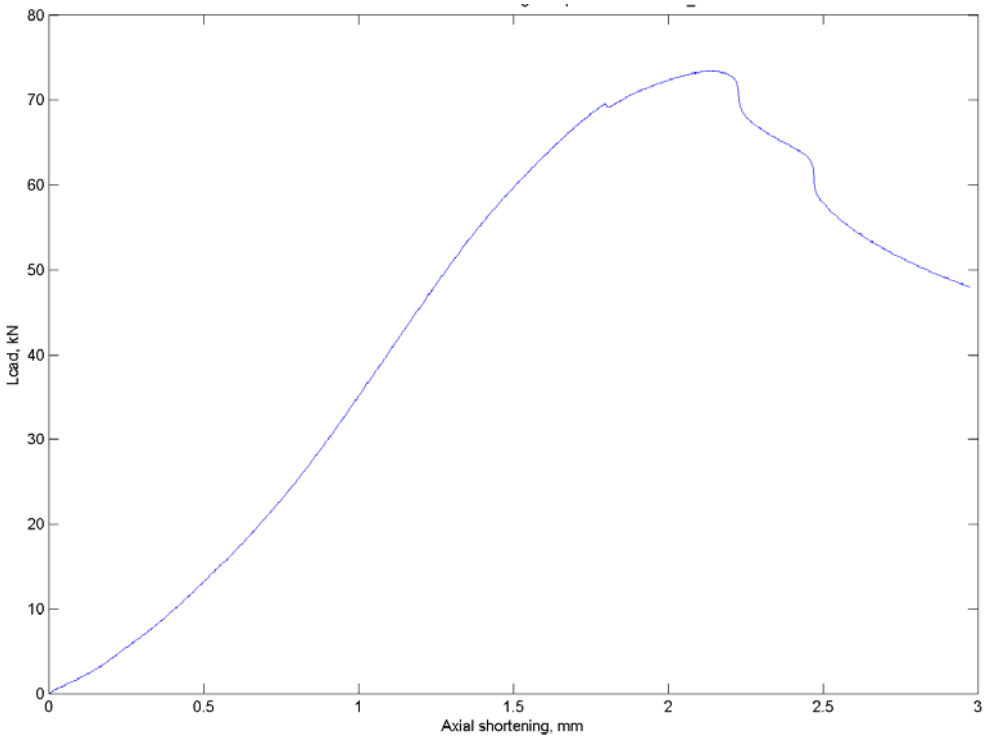

Figure B - 21 Plot of load vs. axial shortening for specimen SWC700_3

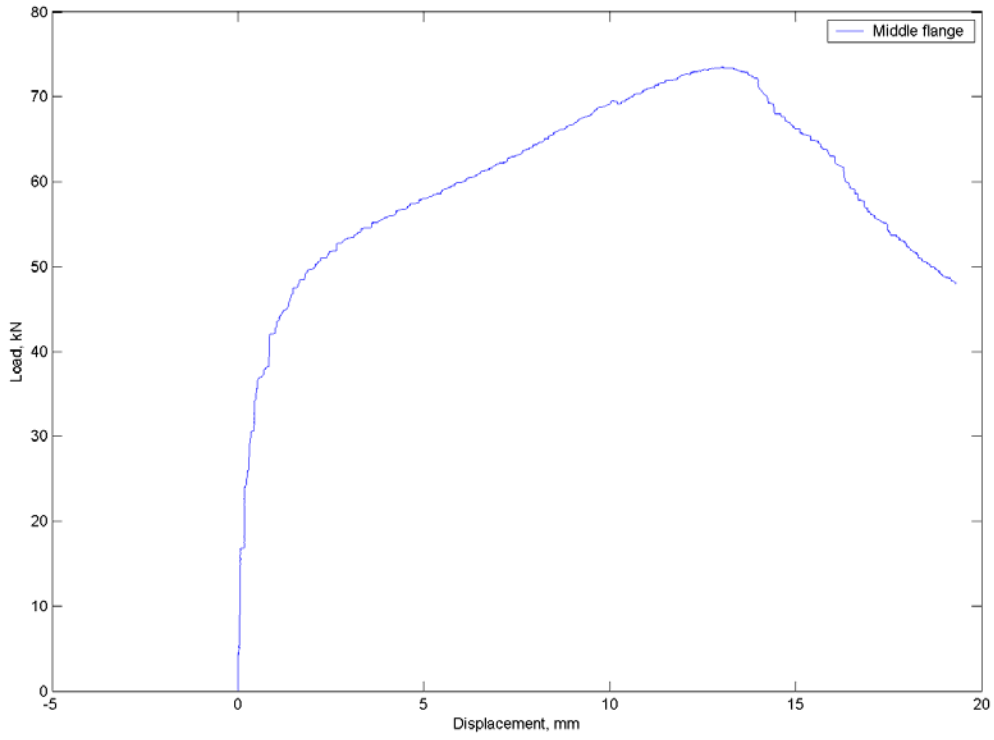

Figure B - 22 Plot of load vs. right flange LVDT displacement for specimen SWC700_3

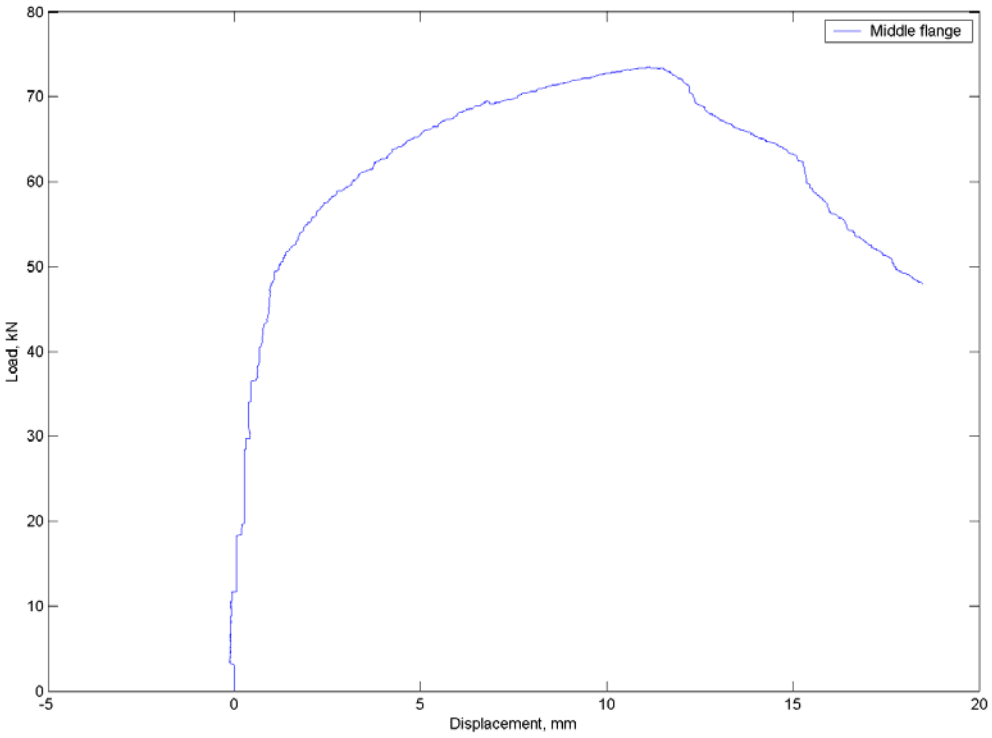

Figure B – 23 Plot of load vs. left flange LVDT displacement for specimen SWC700_3

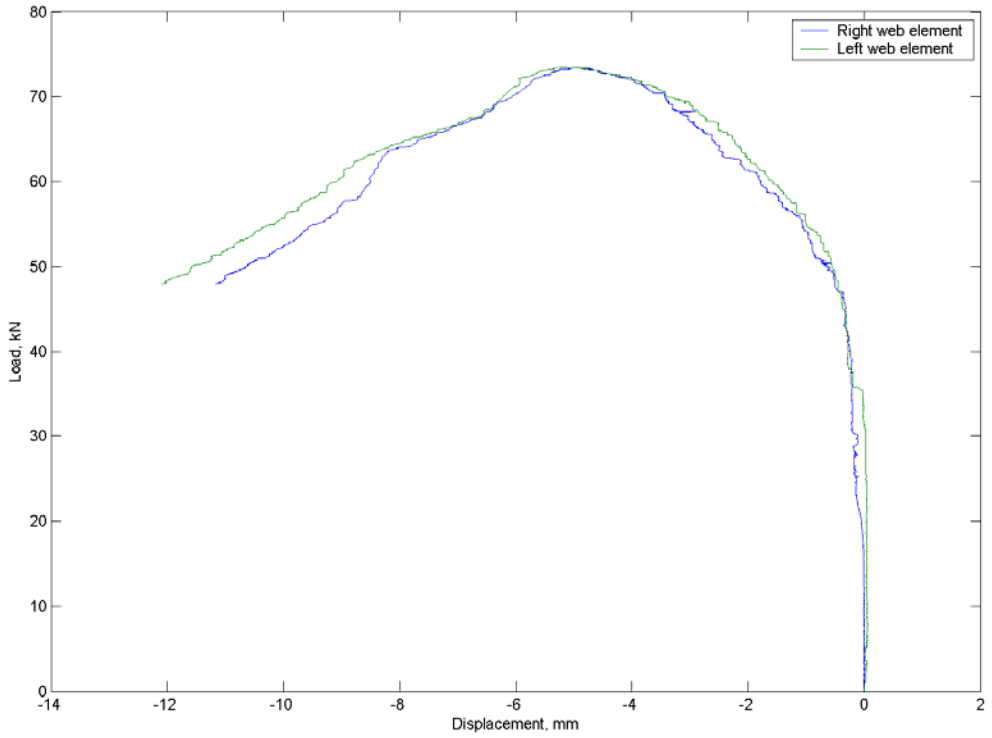

Figure B - 24 Plot of load vs. web LVDT displacements for specimen SWC700_3

B.3 Stiffened-web channel section with length 1000 mm

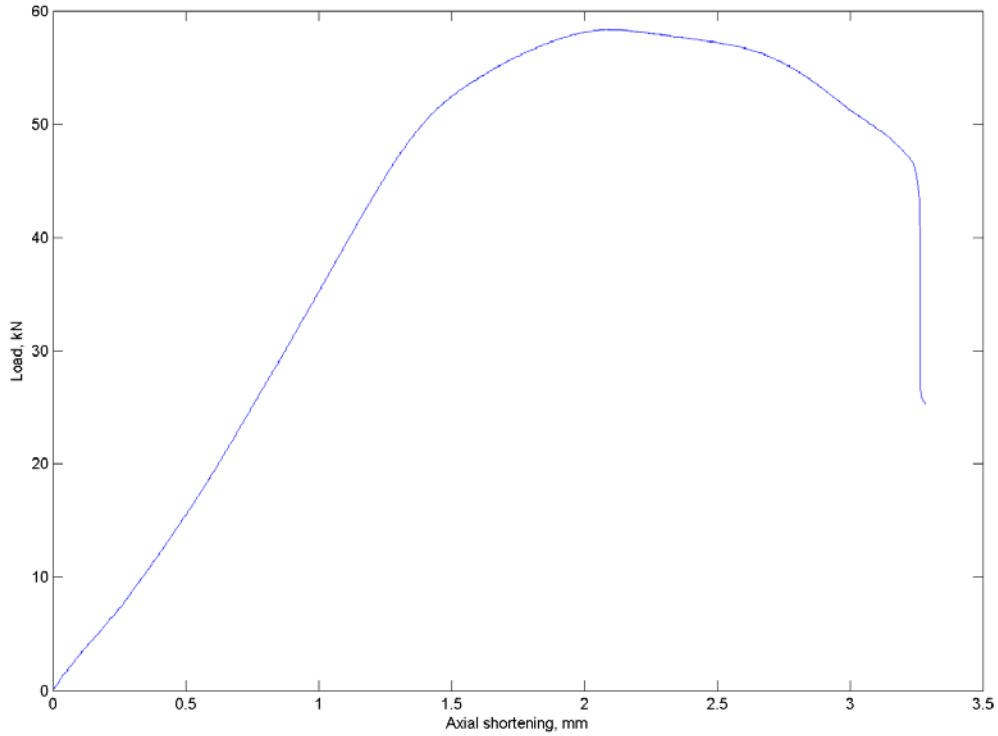

Figure B - 25 Plot of load vs. axial shortening for specimen SWC1000_1

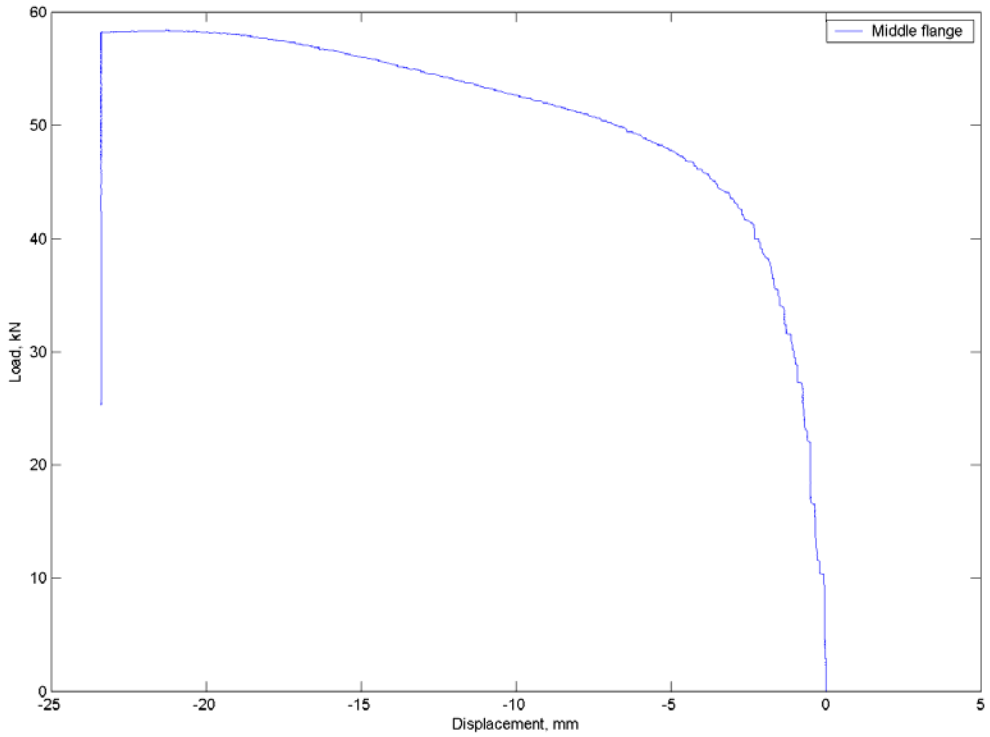

Figure B - 26 Plot of load vs. right flange LVDT displacement for specimen SWC1000_1

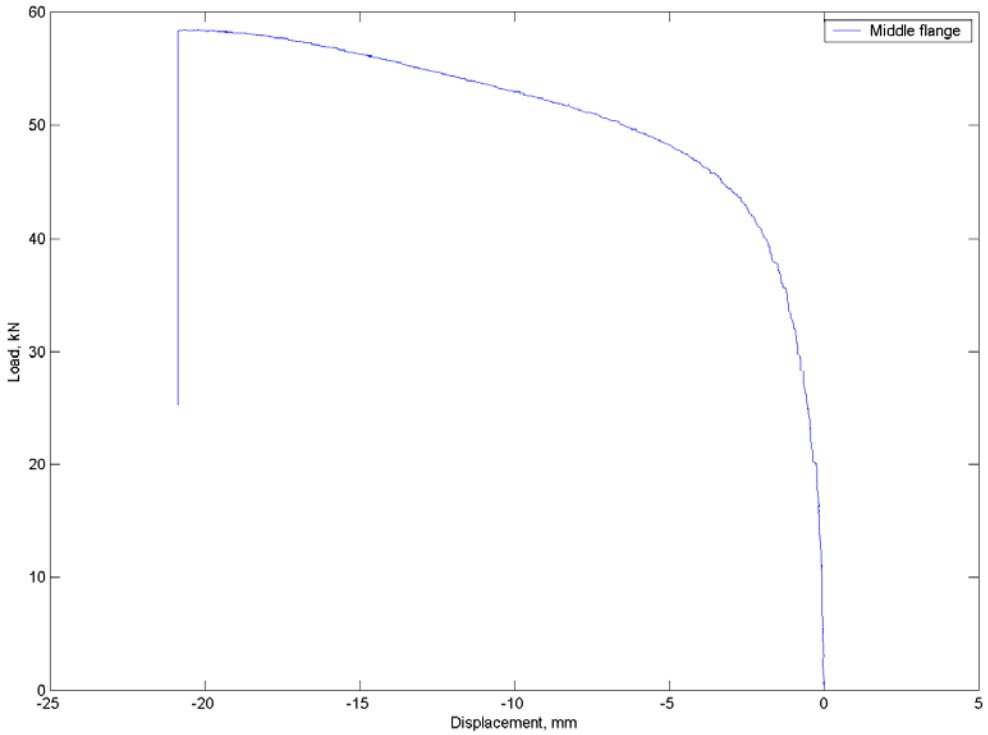

Figure B - 27 Plot of load vs. left flange LVDT displacement for specimen SWC1000_1

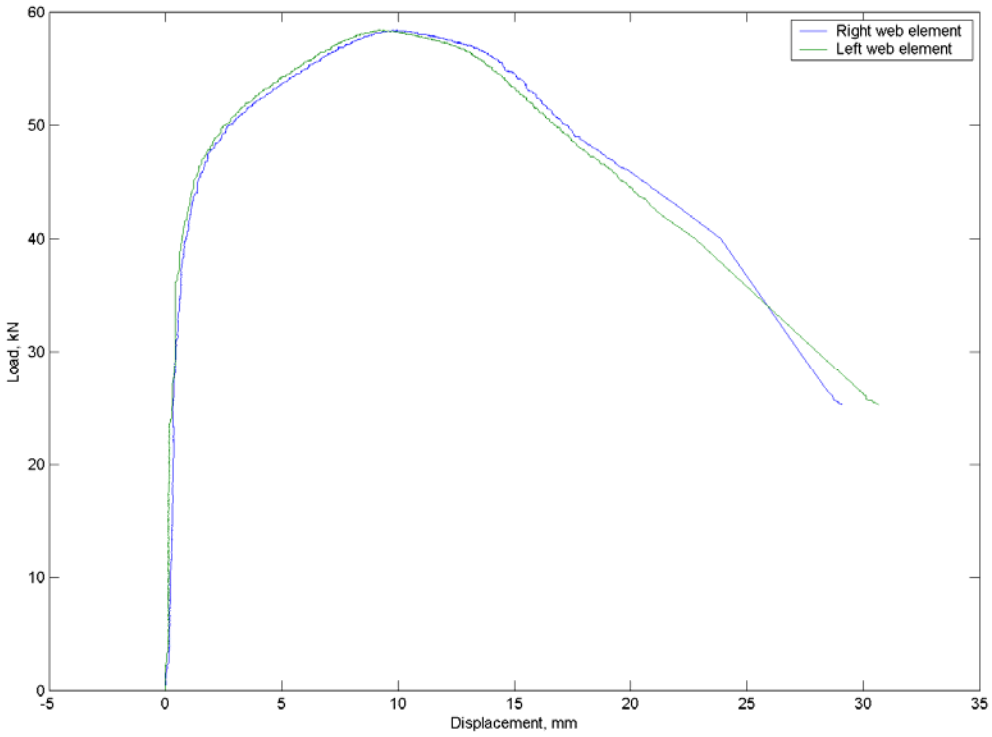

Figure B - 28 Plot of load vs. web LVDT displacements for specimen SWC1000_1

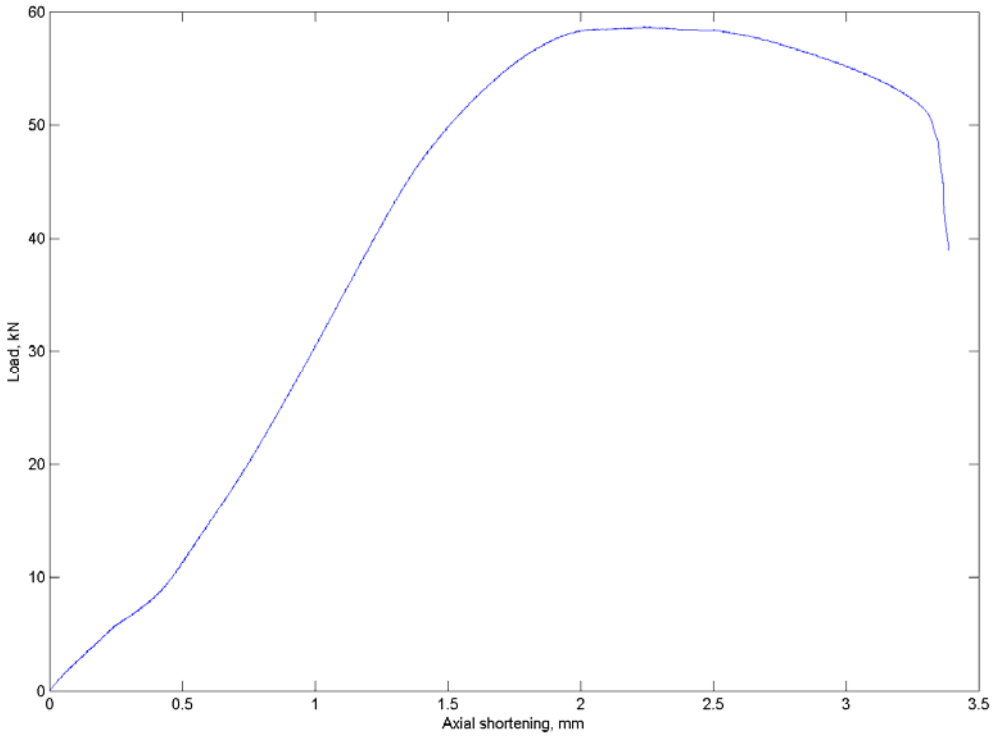

Figure B - 29 Plot of load vs. axial shortening for specimen SWC1000_2

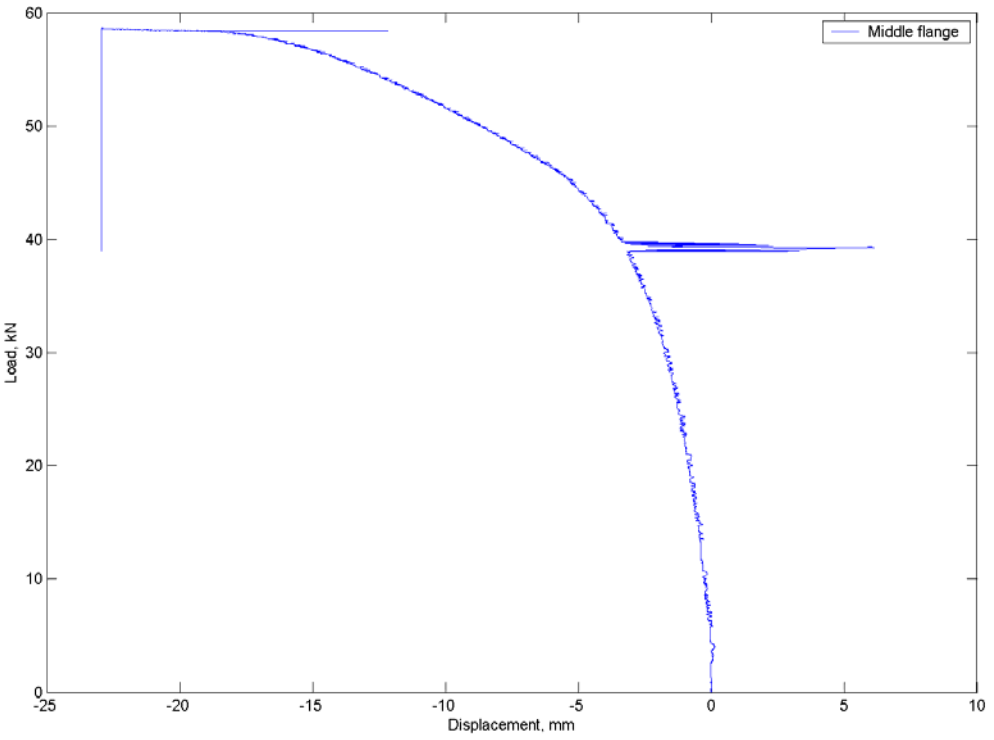

Figure B - 30 Plot of load vs. right flange LVDT displacement for specimen SWC1000_2

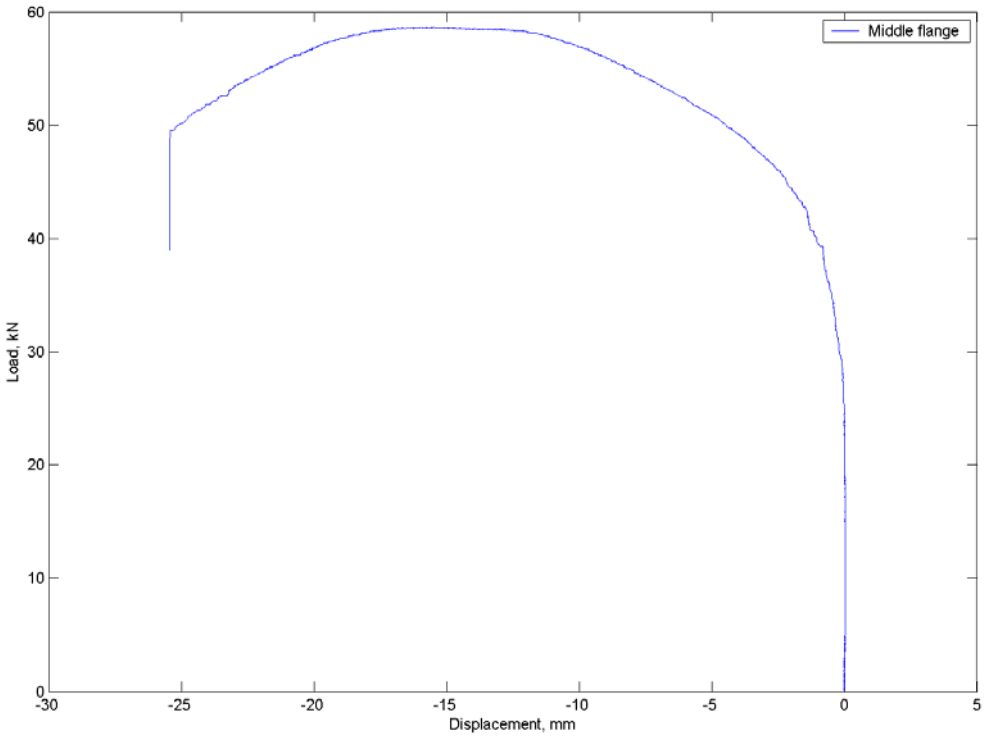

Figure B - 31 Plot of load vs. left flange LVDT displacement for specimen SWC1000_2

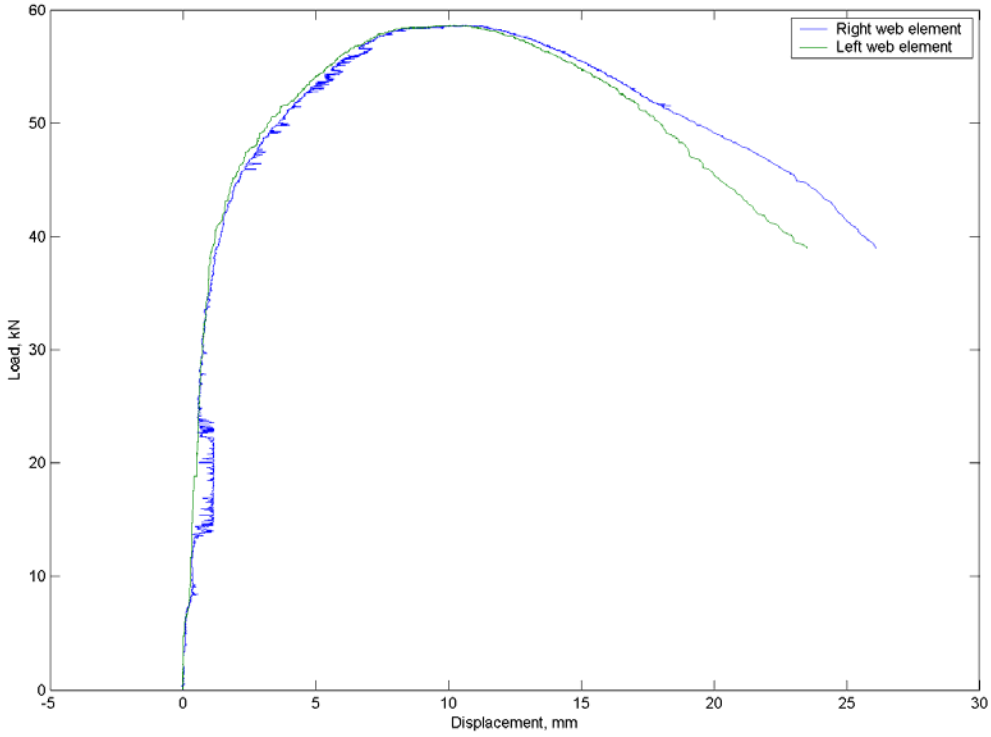

Figure B - 32 Plot of load vs. web LVDT displacements for specimen SWC1000_2

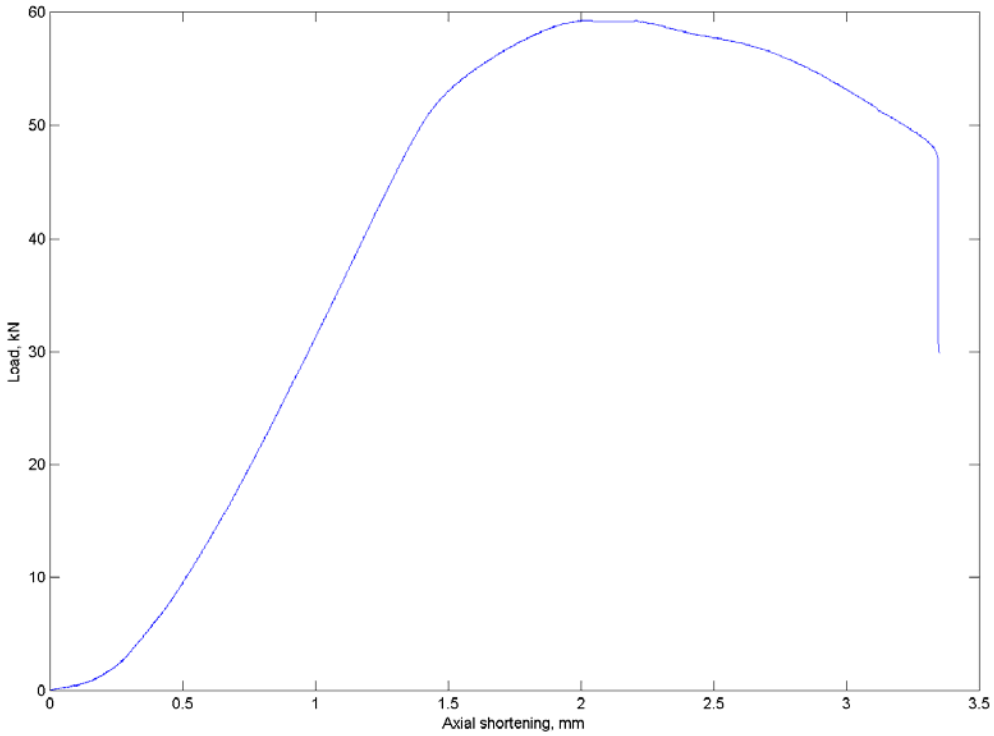

Figure B - 33 Plot of load vs. axial shortening for specimen SWC1000_3

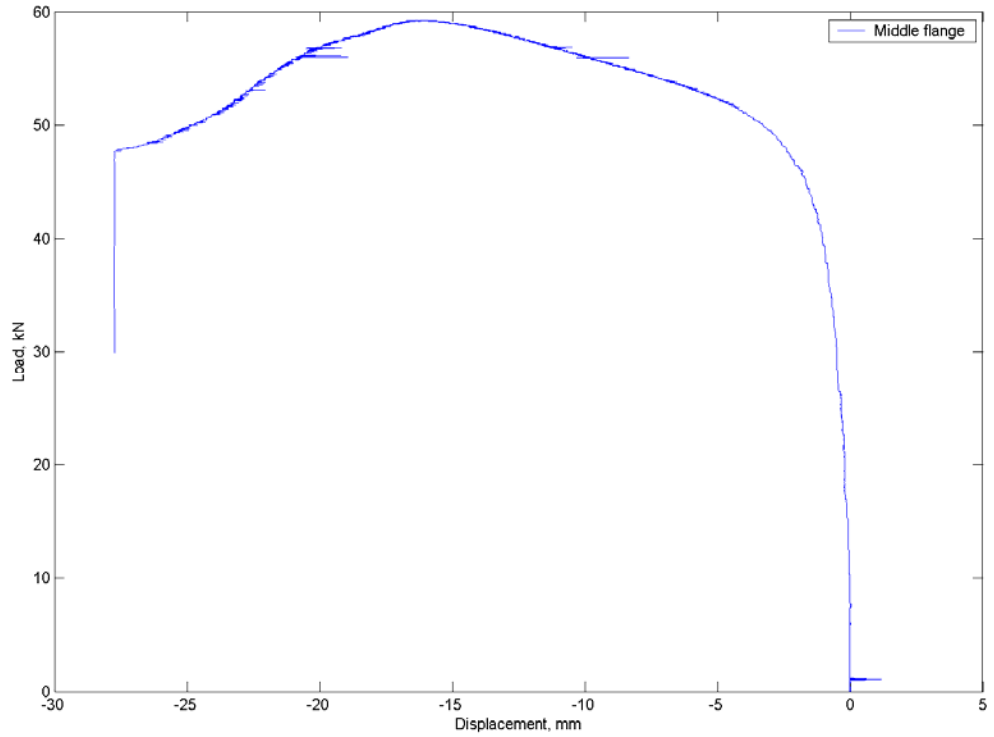

Figure B - 34 Plot of load vs. right flange LVDT displacement for specimen SWC1000_3

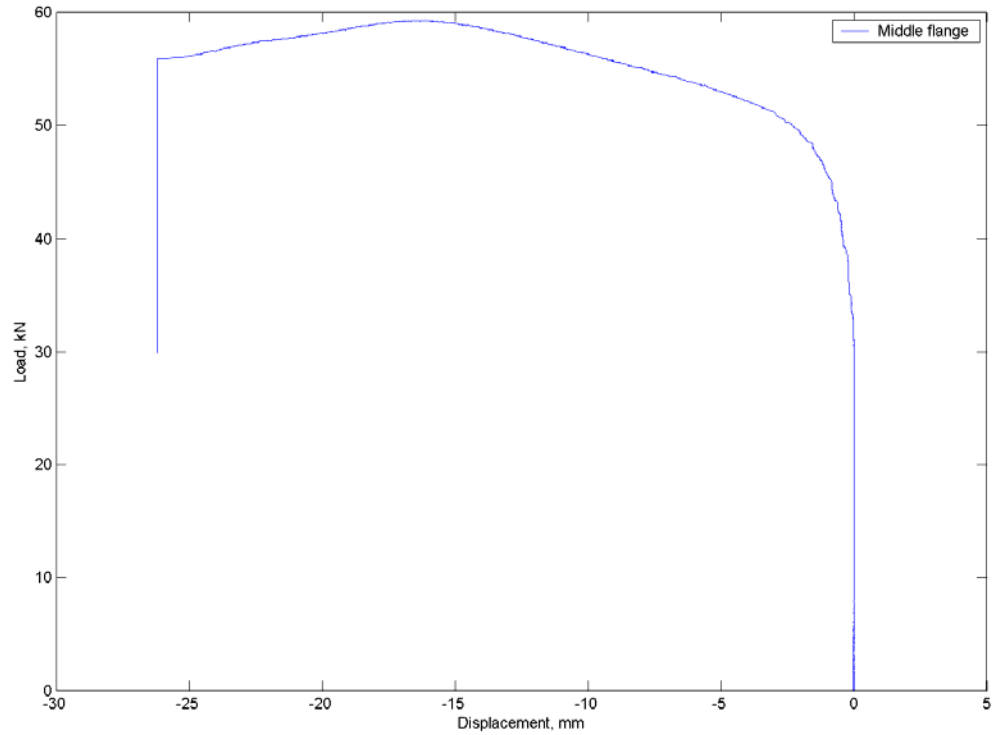

Figure B - 35 Plot of load vs. left flange LVDT displacement for specimen SWC1000_3

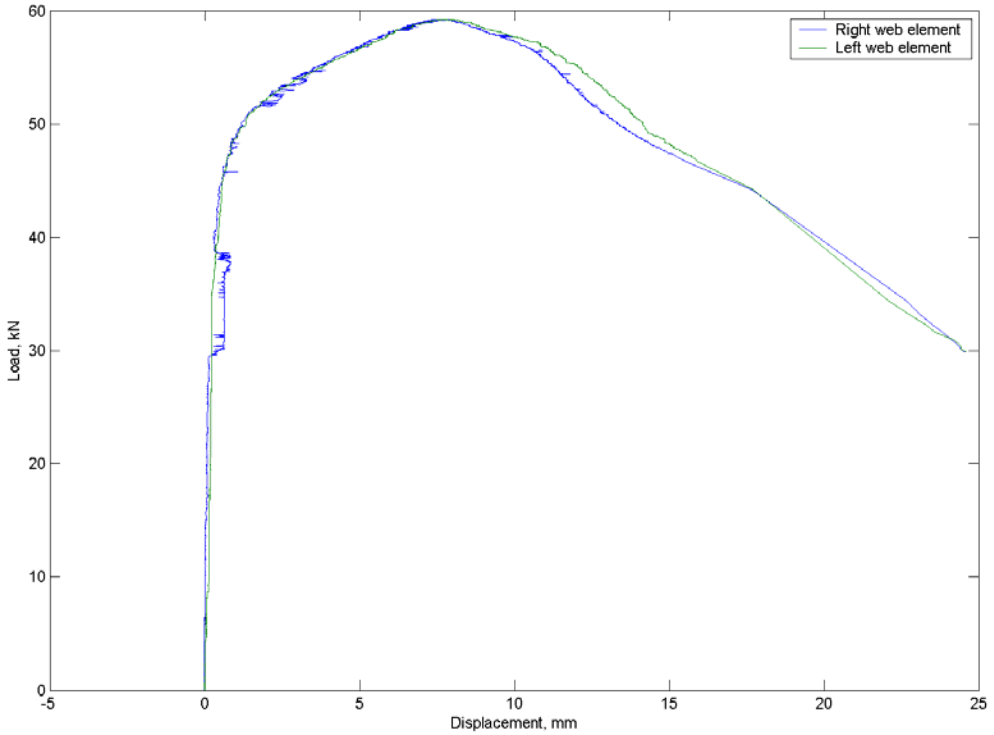

Figure B - 36 Plot of load vs. web LVDT displacements for specimen SWC1000_3

B.4 Stiffened-web channel section with length 1300 mm

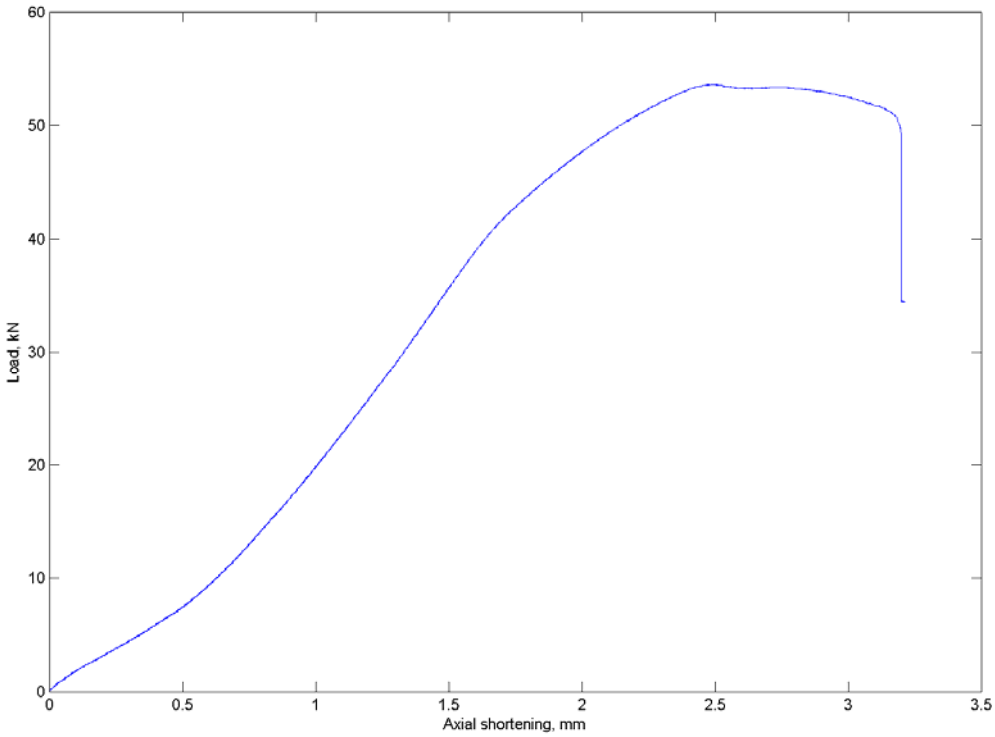

Figure B - 37 Plot of load vs. axial shortening for specimen SWC1300_1

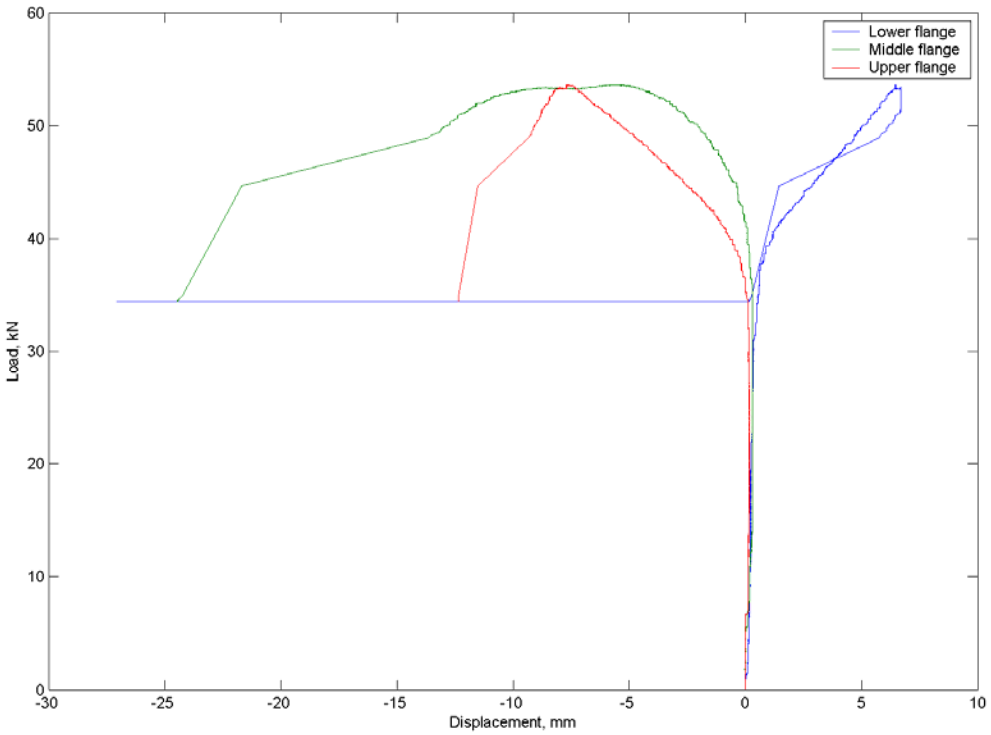

Figure B - 38 Plot of load vs. right flange LVDT displacements for specimen SWC1300_1

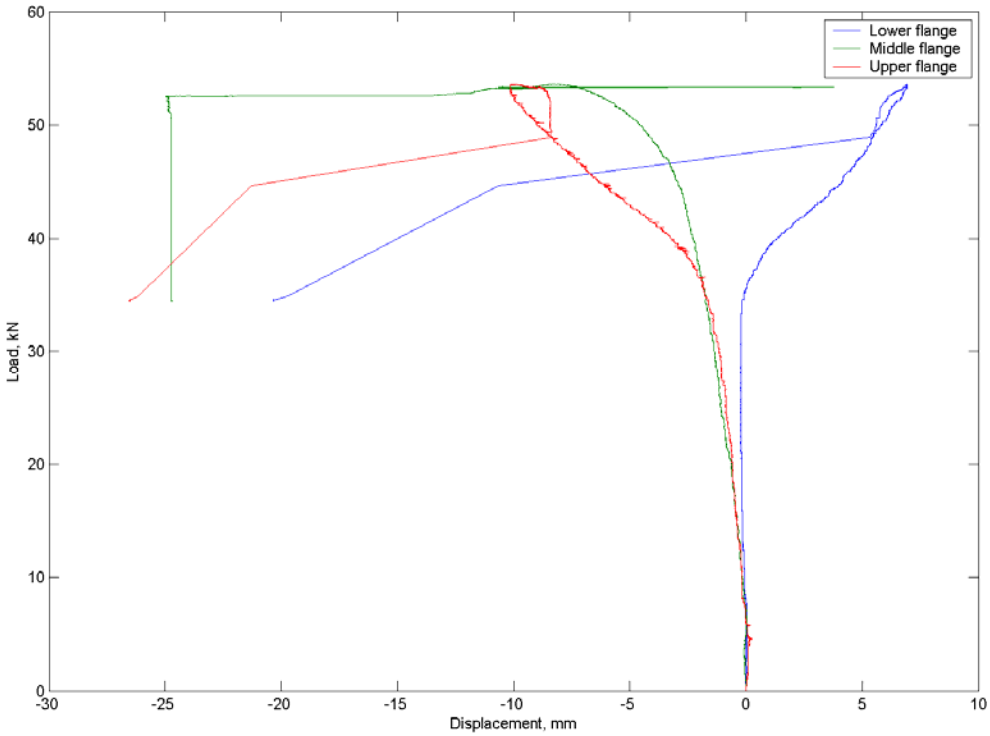

Figure B - 39 Plot of load vs. left flange LVDT displacements for specimen SWC1300_1

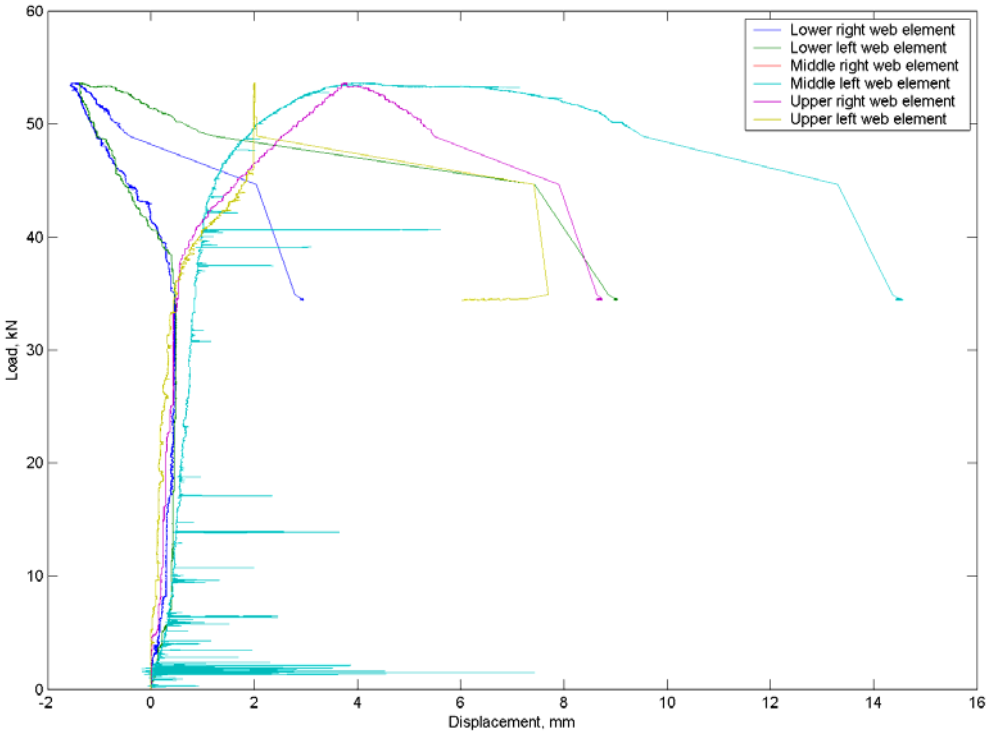

Figure B - 40 Plot of load vs. web LVDT displacements for specimen SWC1300_1

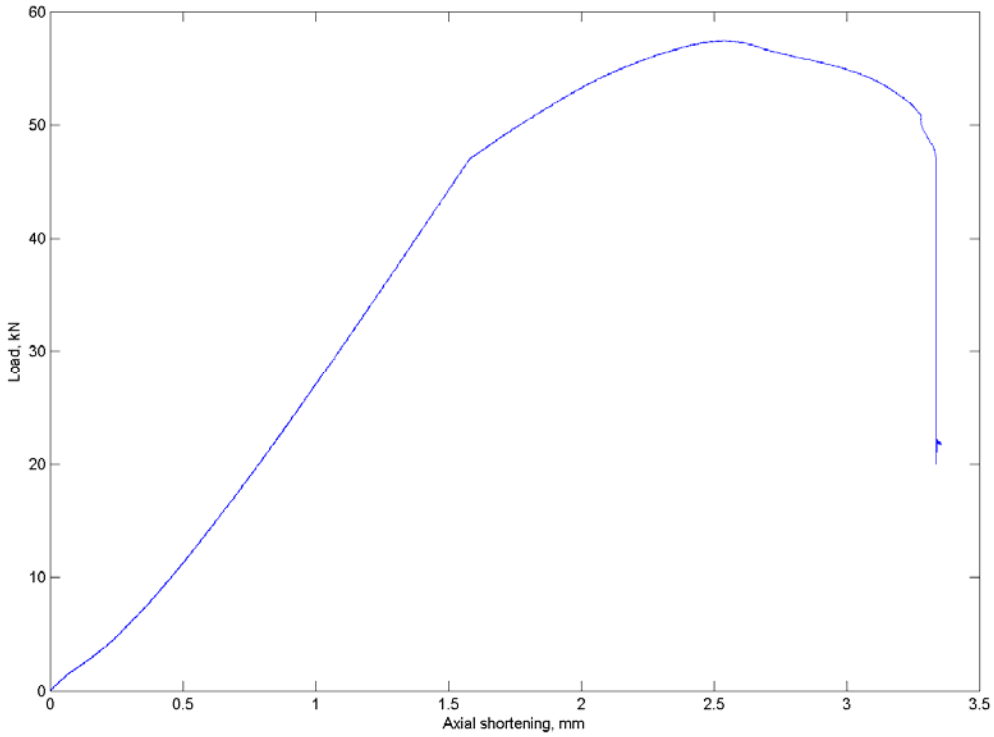

Figure B - 41 Plot of load vs. axial shortening for specimen SWC1300_2

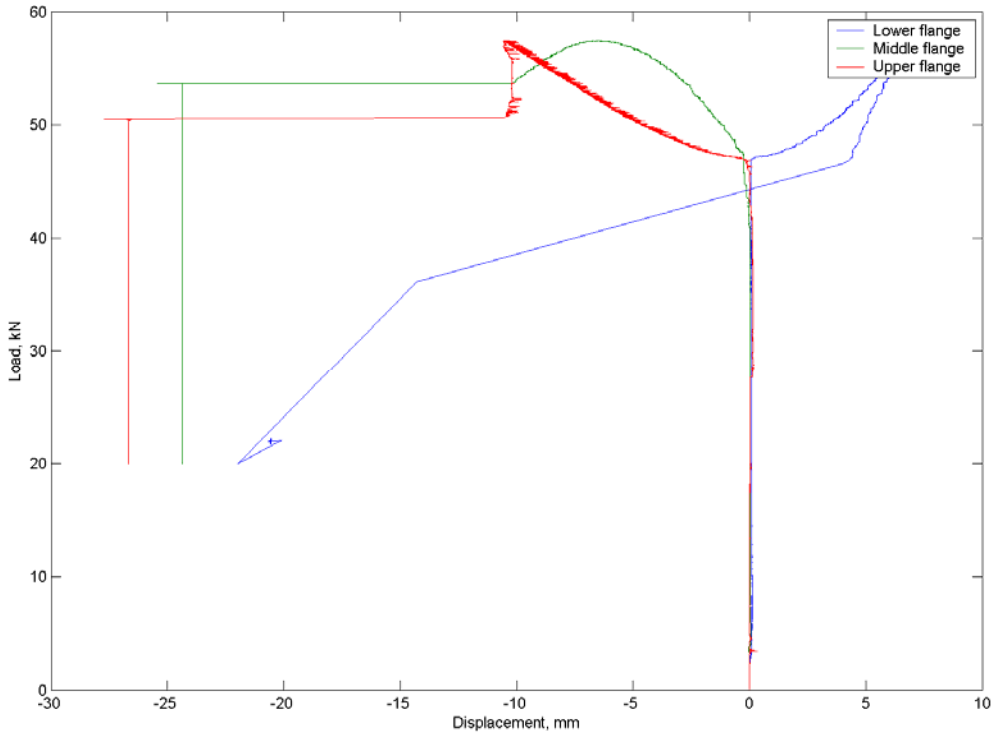

Figure B - 42 Plot of load vs. right flange LVDT displacements for specimen SWC1300_2

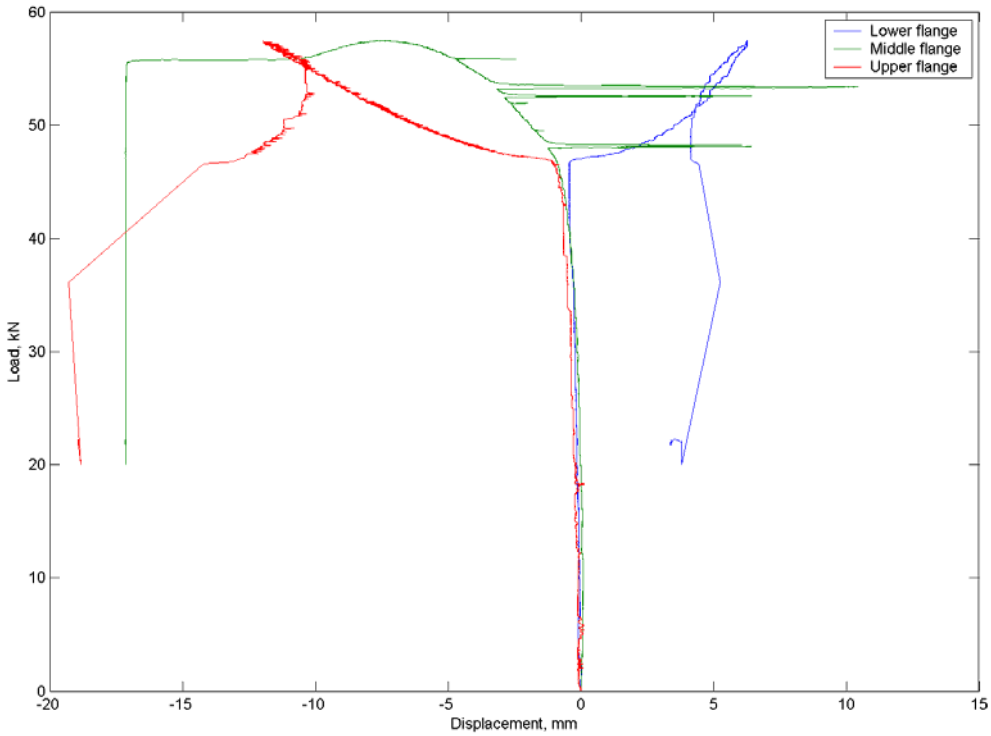

Figure B - 43 Plot of load vs. left flange LVDT displacements for specimen SWC1300_2

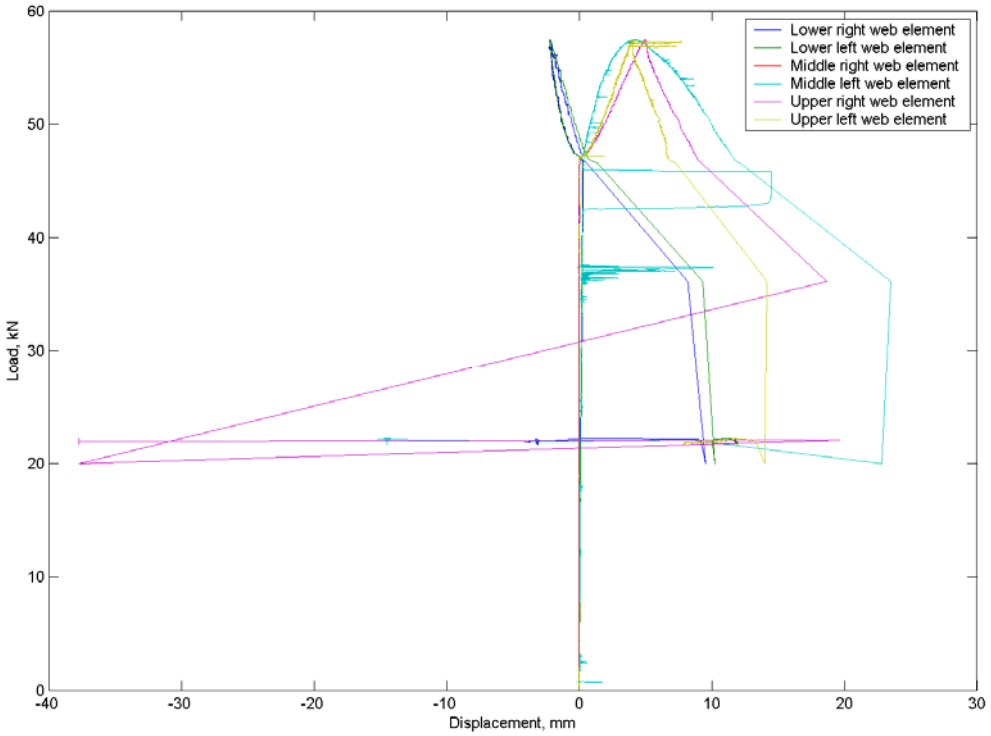

Figure B - 44 Plot of load vs. web LVDT displacements for specimen SWC1300_2

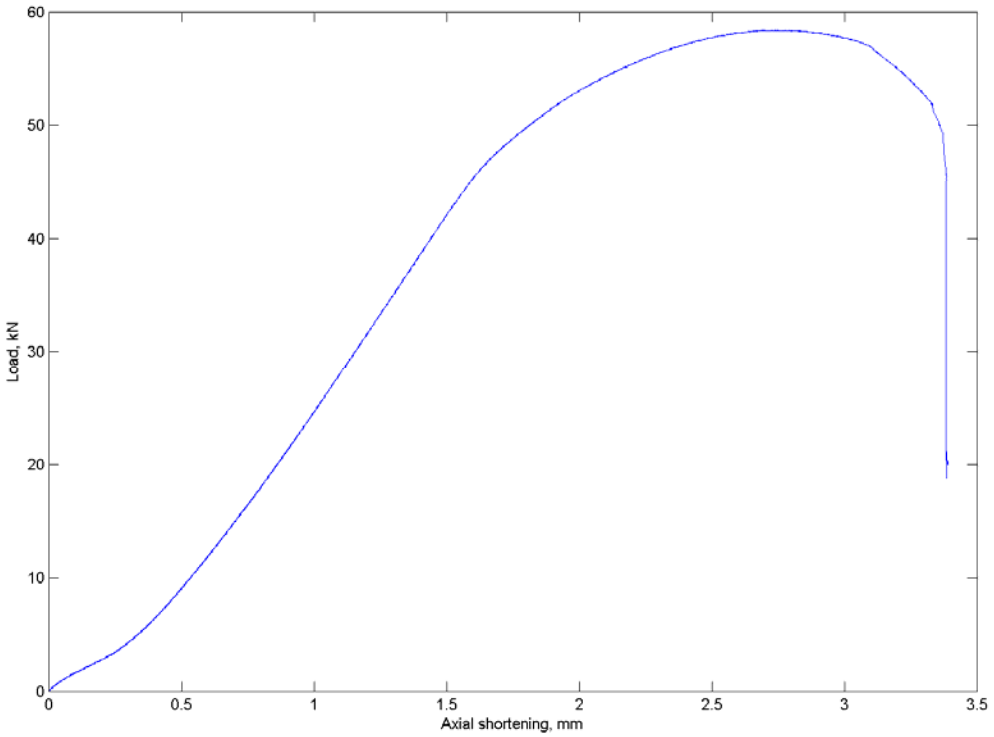

Figure B - 45 Plot of load vs. axial shortening for specimen SWC1300_3

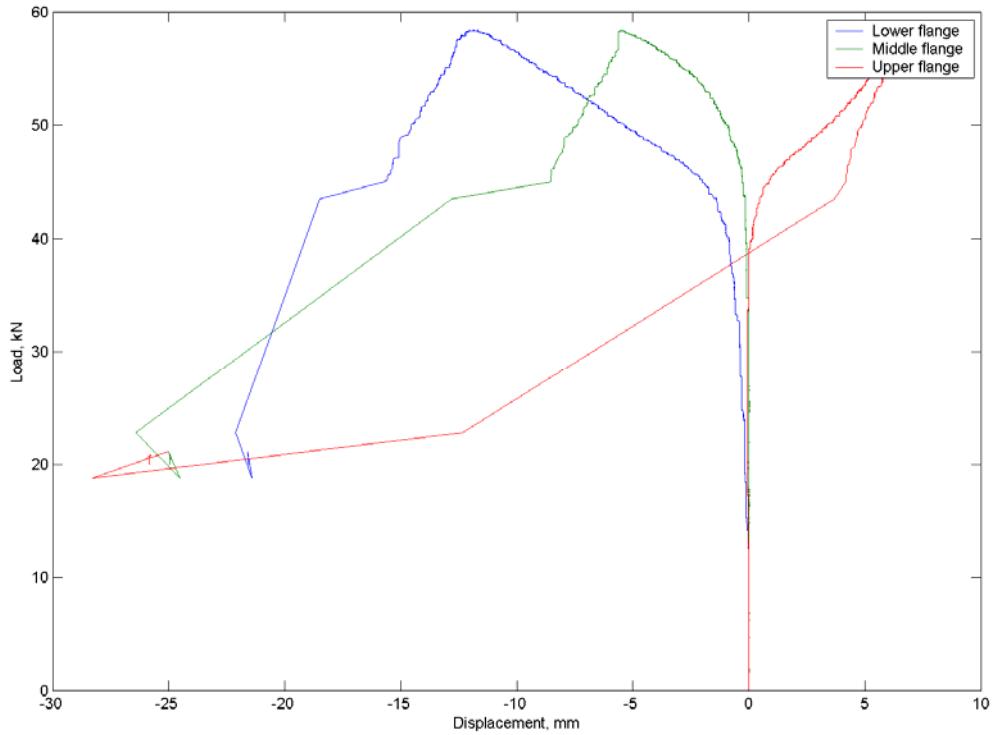

Figure B - 46 Plot of load vs. right flange LVDT displacements for specimen SWC1300_3

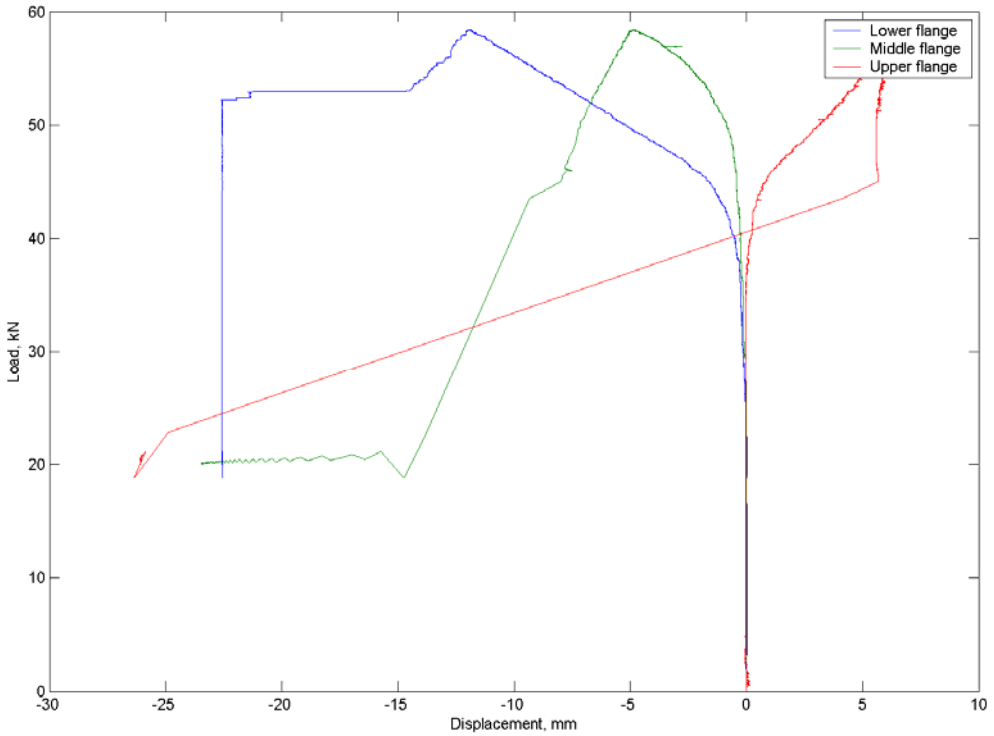

Figure B - 47 Plot of load vs. left flange LVDT displacements for specimen SWC1300_3

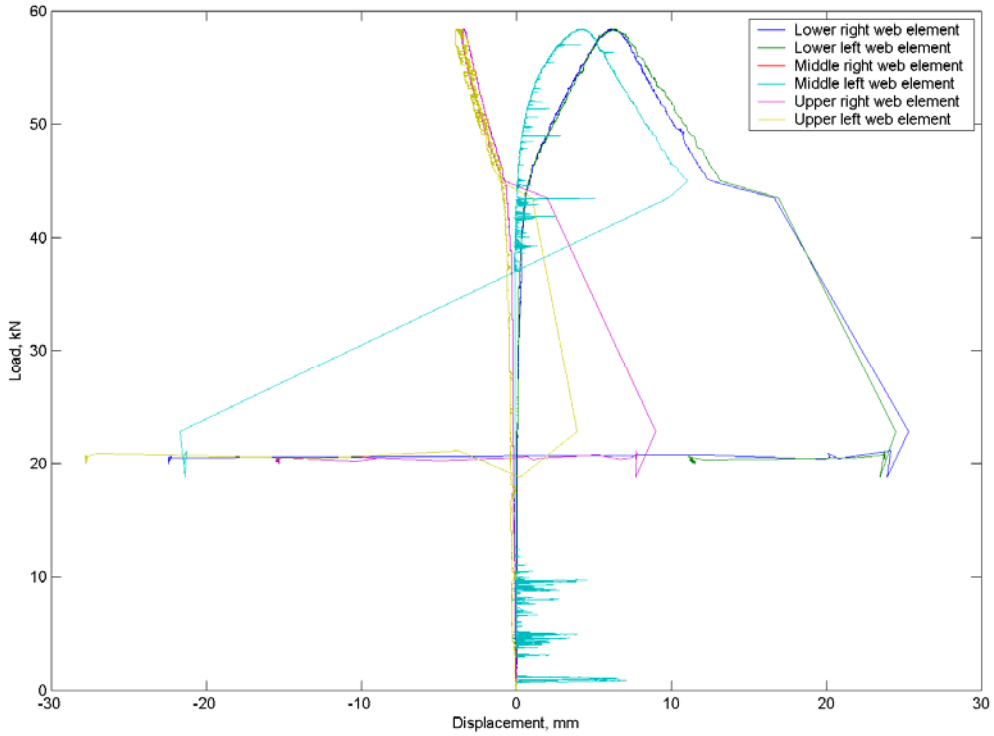

Figure B - 48 Plot of load vs. web LVDT displacements for specimen SWC1300_3

B.5 Stiffened-web channel section with length 2000 mm

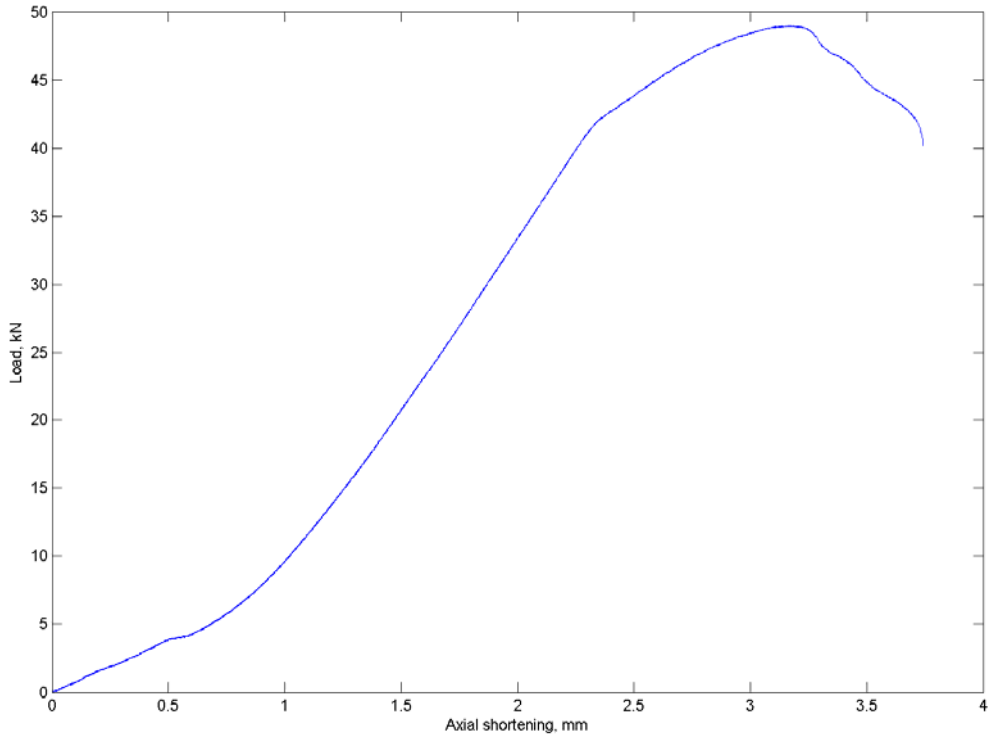

Figure B - 49 Plot of load vs. axial shortening for specimen SWC2000_1

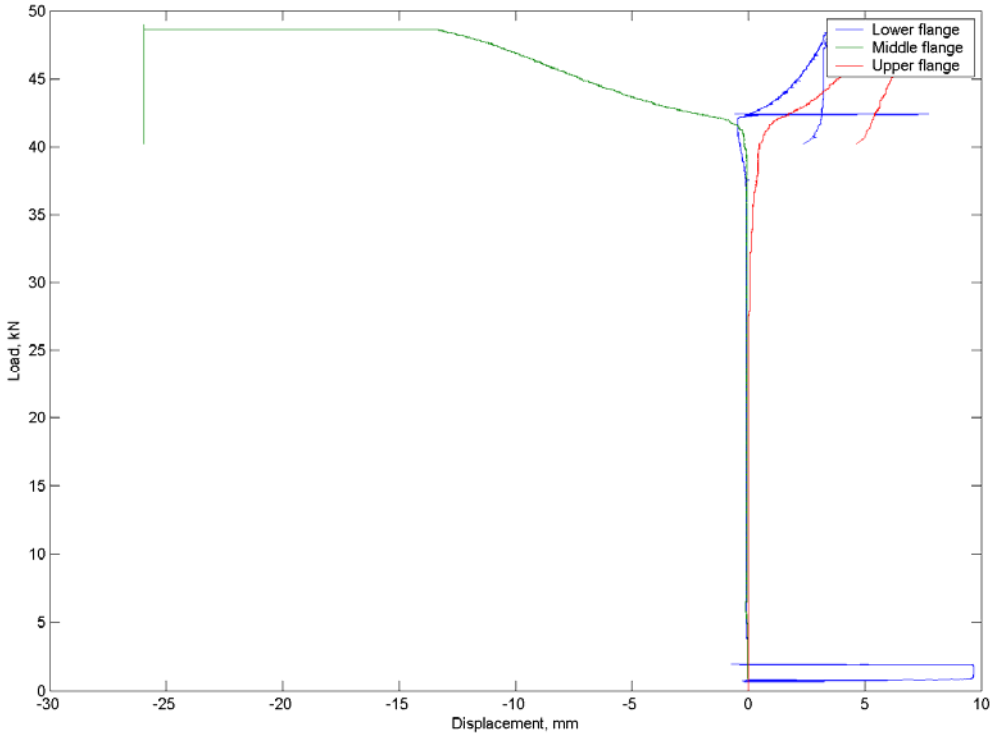

Figure B - 50 Plot of load vs. right flange LVDT displacements for specimen SWC2000_1

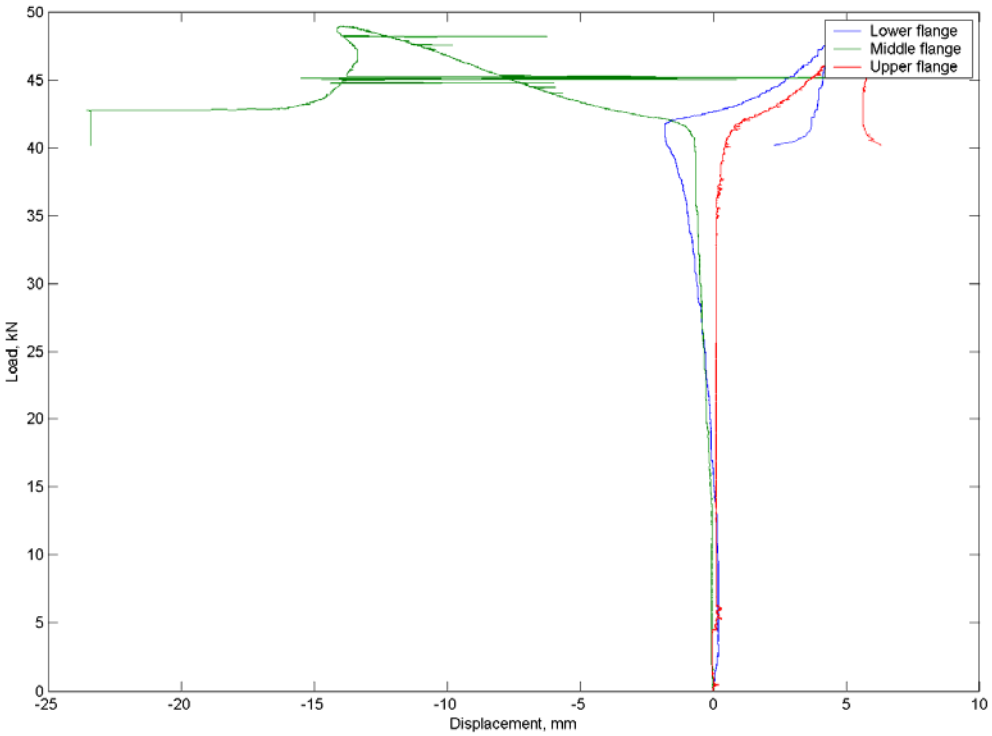

Figure B - 51 Plot of load vs. left flange LVDT displacements for specimen SWC2000_1

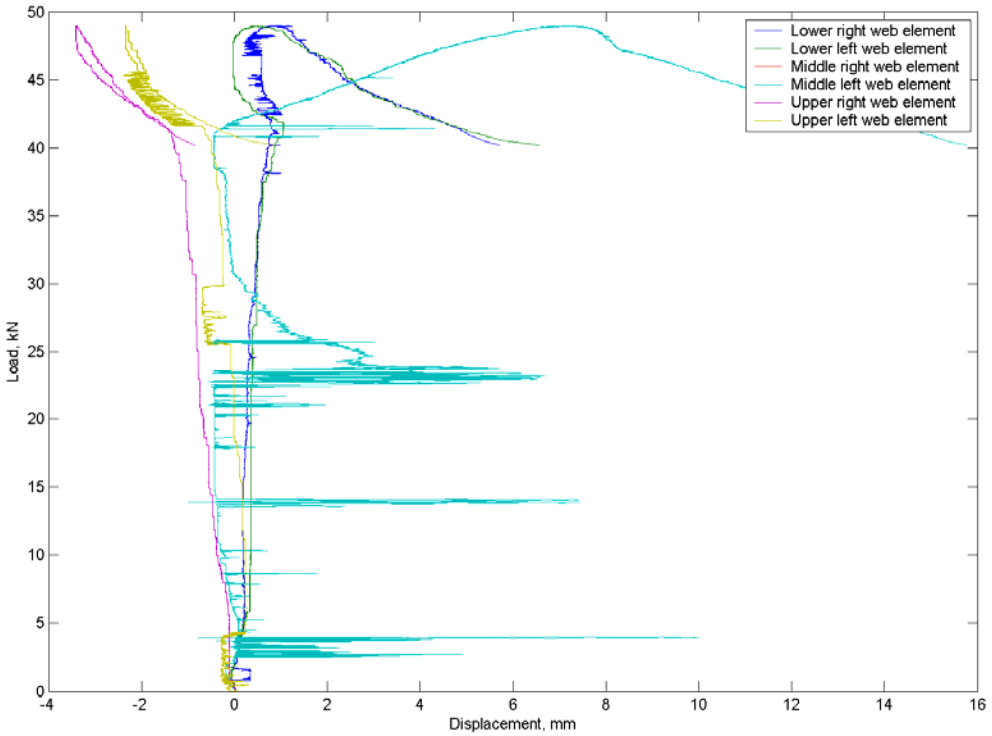

Figure B - 52 Plot of load vs. web LVDT displacements for specimen SWC2000_1

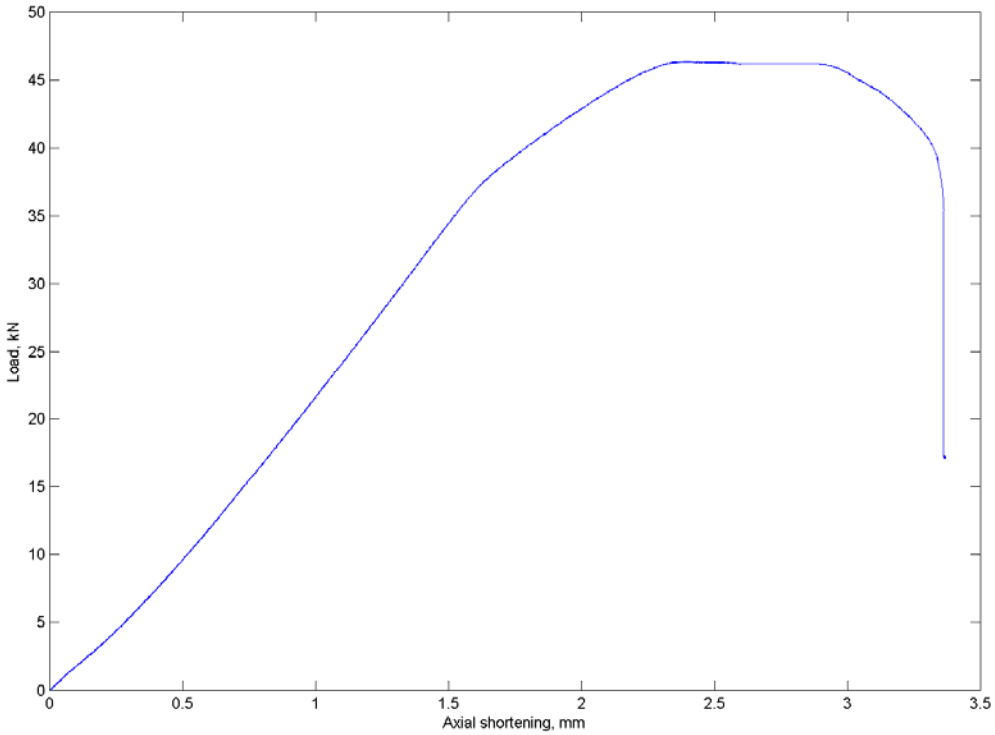

Figure B - 53 Plot of load vs. axial shortening for specimen SWC2000_2

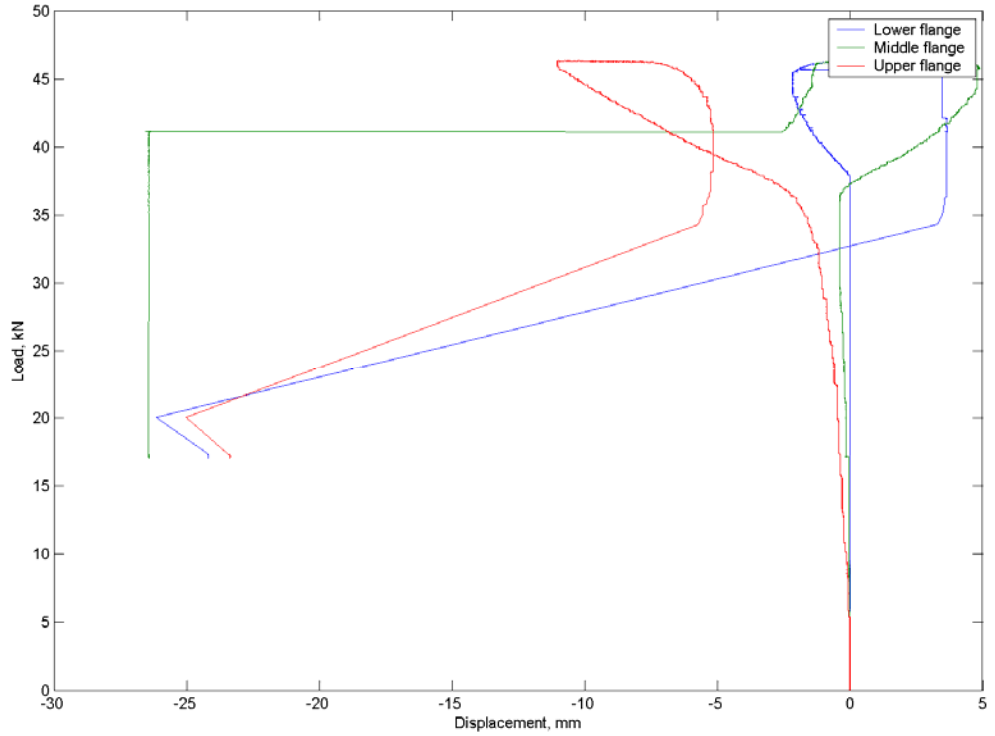

Figure B - 54 Plot of load vs. right flange LVDT displacements for specimen SWC2000_2

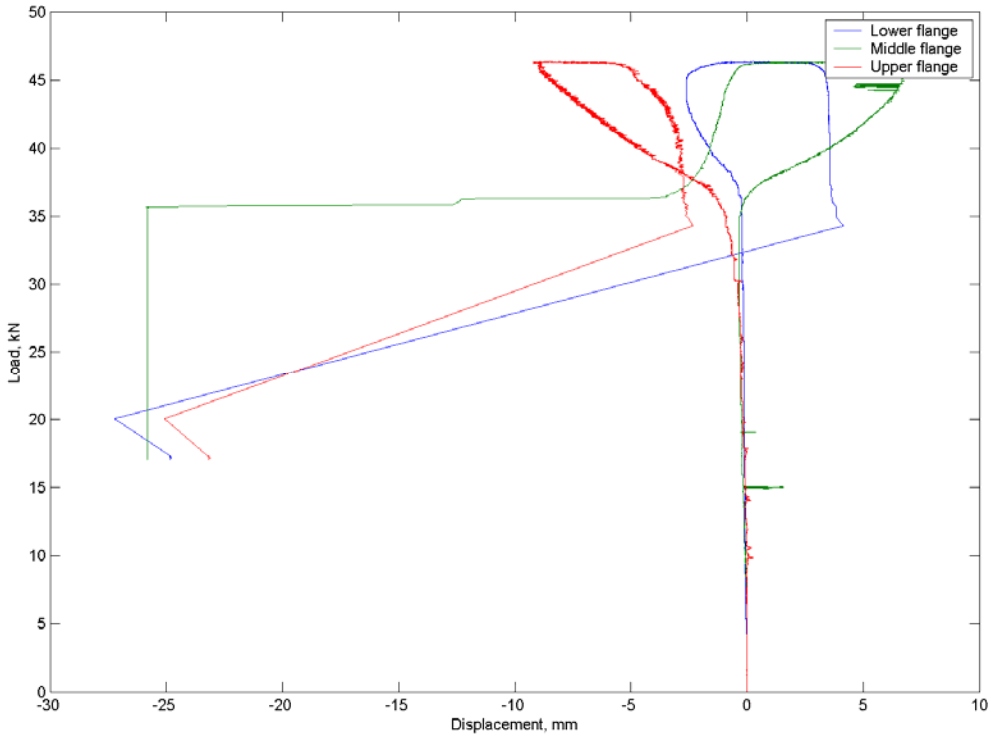

Figure B - 55 Plot of load vs. left flange LVDT displacements for specimen SWC2000_2

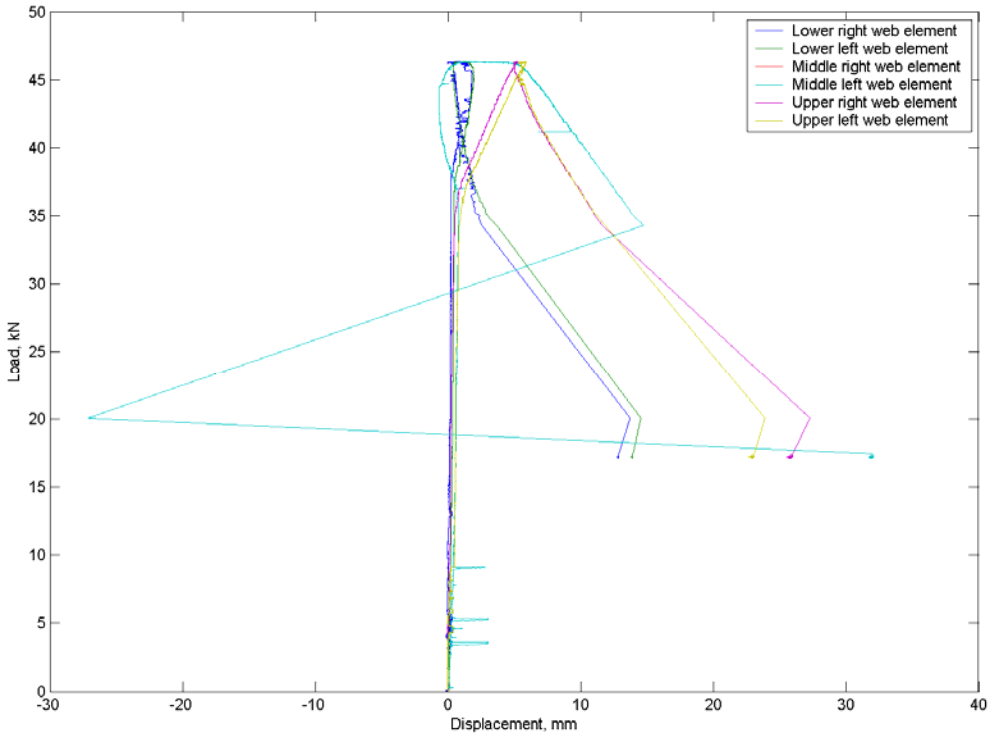

Figure B - 56 Plot of load vs. web LVDT displacements for specimen SWC2000_2